CHARACTERIZATION OF MUSCLE GLYCOGEN SYNTHASE AND ITS ASSOCIATION WITH RNA IN SERTOLI CELLS

DISSERTATION ZUR ERLANGUNG DES DOKTORGRADES DER NATURWISSENSCHAFTEN (DR.RER.NAT)
DER FAKULTÄT FÜR BIOLOGIE UND VORKLINISCHE MEDIZIN
DER UNIVERSITÄT REGENSBURG

Vorgelet von

Rodrigo Maldonado

aus

Valdivia

2013

Promotionsgesuch eingereicht am: 9.12.2013
Die Arbeit wurde angeleitet von: Dr. Ilona Concha
Dr. Gernot Längst

Die vorliegende Dissertation mit dem Titel

CHARACTERIZATION OF MUSCLE GLYCOGEN SYNTHASE AND ITS ASSOCIATION WITH RNA IN SERTOLI CELLS

vorgelegt von Rodrigo Maldonado Aguila

entstand unter der gemeinsamen Betreuung

der Universität Regensburg und
der Universidad Austral de Chile

im Rahmen des bi-nationalen Promotionsprogramms RegenVald
als Doppelpromotion

RegenVald
German-Chilean PhD Program
Programa de Doctorado Alemán-Chileno

PUBLICATIONS AND AWARDS

- Villarroel-Espíndola F., **Maldonado R**., Mancilla H., Vander Stelt K., Acuña A., Covarrubias A., Lopez C., Angulo C., Castro M. A., Slebe J. C., Durán J., Garcia-Rocha M., Guinovart J. J., Concha I. I. **MUSCLE GLYCOGEN SYNTHASE ISOFORM IS RESPONSIBLE FOR TESTICULAR GLYCOGEN SYNTHESIS: GLYCOGEN OVERPRODUCTION INDUCES APOPTOSIS IN MALE GERM CELLS**. J Cell Biochem 2013 Jul; 114(7):1653-64. doi: 10.1002/jcb.24507.

- Villarroel-Espíndola F., Mancilla H., **Maldonado R.**, Covarrubias A., López C., Cereceda K., Vander Stelt K., Castro M. A., Angulo C., Slebe J. C., Concha I. I. **THE MANY FACES OF TESTICULAR SUGAR METABOLISM: FROM CELL VIABILITY TO APOPTOSIS IN MALE GERM CELLS.** Manuscript submitted for review to Reproduction.

- **Maldonado R.**, Villarroel-Espíndola F., Mancilla H., Covarrubias A., López C.,Vander Stelt K., Cereceda K., Angulo C., Slebe J. C., Méndez R., Guinovart J. J., Concha I. I. **NOVEL ROLE FOR MUSCLE GLYCOGEN SYNTHASE AS RNA-BINDING PROTEIN IN SERTOLI CELLS.** Manuscript in preparation.

- Scholarship is awarded for participation in the course "Molecular Biology of the Cell" in the Pasteur Institute in co-tutorial with Institute Curie, January-February 2010, Paris, France.

- Fellowships MECESUP AUS074 and REGENVALD were awarded for an international scientific internship. From December 2010 to March 2011, in

the laboratory of Dr. Gernot Lägnst, Universidad de Regensburg, Regensburg, Germany.

- Fellowship for doctoral thesis development is awarded during 2012 (code: D-2011-09). Dirección de Investigación y Desarrollo, Universidad Austral de Chile.

- Scholarship for international doctoral internships, BECAS CHILE 2011-2012. From May to August 2012, in the laboratory of Dr. Raúl Méndez, Institute for Research in Biomedicine IRB Barcelona, Barcelona, Spain.

- Fellowship MECESUP AUS074 is awarded for international scientific internships. From May to August 2012, in the laboratory of Dr. Raúl Méndez, Institute for Research in Biomedicine IRB Barcelona, Barcelona, Spain.

- CONICYT scholarship is awarded to support doctoral thesis during 2012 (code: AT-24121041).

CONGRESS PRESENTATIONS

- EFECTO DEL LITIO EN CÉLULAS DE SERTOLI: LOCALIZACIÓN DE GLICÓGENO SINTASA. Maldonado, R., Villarroel, F., Torres, C., Cereceda, K., Van der Stelt, K., Castro, M.A., Slebe, J.C., Concha I. I. XXI Reunión Anual Sociedad Chilena de Reproducción y Desarrollo, La Serena, Chile, Septiembre 2010. Presentación póster.

- EFECTO DEL LITIO EN LA LOCALIZACIÓN DE LA GLICÓGENO SINTASA EN CUERPOS P/GW EN CÉLULAS DE SERTOLI. Maldonado , R., Villarroel, F., Torres, C., Karina , C., Karen, V.d.S., Castro, M., Slebe, J.C., Concha, I. I. XXXIII Reunión Anual Sociedad de Bioquímica y Biología Molecular de Chile, Chillán, Chile, Septiembre-Octubre 2010. Presentación oral.

- MOLECULAR EFFECTS OF LITHIUM ON SERTOLI CELLS. Maldonado R., Villarroel-Espíndola F., Torres C., Cereceda K., Van de Stelt K., Lopez C., Salazar, E., Covarrubias A., Angulo, C., Castro M., Slebe J.C., Concha I.I. XXXIV Anual Meeting of Chilean Biochemistry and Molecular Biology Society, Valdivia, Chile, September-October 2011. Oral presentation.

- ACTIVATION OF GLYCOGEN SYNTHASE MODULATES ITS LOCALIZATION AND INTERACTION WITH RNA BINDING PROTEINS IN SERTOLI CELLS. Maldonado R., Burgos J., Villarroel F., Mancilla H., Cereceda K., Vander Stelt K., Salazar E., Cobarrubias A., Angulo C., Castro M., Slebe J. C., Méndez R., Concha I.I. 22nd International Union of Biochemistry and Molecular Biology (IUBMB) and 37th Federation of Societies of Biochemistry and Molecular Biology Congress, Sevilla, Spain, September 2012. Poster Presentation.

- BEYOND GLYCOGEN SYNTHESIS: FUNCTIONAL CHARACTERIZATION OF GLYCOGEN SYNTHASE IN SERTOLI CELLS. Maldonado R., López C., Mancilla H., Villarroel-Espíndola F., Cereceda K., Vander Stelt K., Covarrubias A., Slebe, J.C., Méndez R., Concha I.I. XII Panamerican Association for Biochemistry and Molecular Biology (PABMB), Puerto Varas, Chile, Noviembre 2013. Poster Presentation

FUNDING

Proyecto FONDECYT 1110508 (I.I.C) Y 1090740 (J.C.S)

Proyecto DID-UACh D-2011-09, Dirección de Investigación y Desarrollo, Universidad Austral de Chile.

Dirección de Estudios de Postgrado y Escuela de Graduados, Facultad de Ciencias, Universidad Austral de Chile.

Beca CONICYT for doctoral studies in Chile

Beca CONICYT AT-24121041 for support doctoral thesis.

MECESUP AUS0704 (2011 y 2012) and BECAS CHILE (2012) to funding international scientific stays.

GENERAL INDEX

FIGURE INDEX

ABSTRACT

The metabolism of Sertoli cells is highly active to maintain nutritional needs of germ cells. After glucose incorporation, only 1-3% is converted to glycogen suggesting low levels of glycogen synthase. Additionally, expression levels of muscular glycogen synthase (MGS), isoform present in these cells, do not correlate with the low levels of glycogen. Furthermore, MGS has a predicted Rossmann conformation, indicative of enzyme-RNA interaction. The aim of this work was to functionally characterize and explore a new feature of MGS as RNA binding protein in primary culture of Sertoli cells and the Sertoli 42GPA9 cell line. MGS was detected in the cytoplasm of Sertoli cells as well as in their nucleus. The activity rates of the enzyme were very low indicating that MGS is being expressed but is practically inactive. This correlates with high levels of MGS phosphorylation suggested by phosphatase treatments of Sertoli cells extracts and 2D gel electrophoresis of immunoprecipitated MGS. To revert the low levels of glycogen synthesis in Sertoli cells, Protein Targeting to Glycogen (PTG) overexpression and lithium treatments were performed and confirmed that MGS is present but inactive. Thus, to explore a putative new function of MGS in Sertoli cells, the analysis of enzyme localization and protein interactions revealed that the enzyme co-localized and co-immunoprecipitated with AGO2 and other RNA binding proteins. In addition, after the study of MGS interaction with mRNAs by RNA inmunoprecipitation coupled to a microarray, several mRNAs were pulled down with the enzyme, which was confirmed by mass spectrometry. The identities of those mRNAs were classified by molecular function and biological processes where the main associated categories were nucleic acid binding and transcription, respectively. The results presented in this work indicate that MGS is expressed but inactive, and moreover, reveal a novel

function as the interaction with RNAs and RNA binding proteins, suggesting that MGS could play an unknown role in the regulation of mRNA expression of transcription regulation-related genes in Sertoli cells.

ABBREVIATIONS

AGO2: Argonaute 2

AKT: Protein kinase B

AMP: Adenosine mono-phosphate

AMPK: AMP-activated protein kinase

ATP: Adenosine tri-phosphate

BTB: Blood testis barrier

CAMPKII: calmodulin-dependent protein kinase II

CK1: Casein kinase 1

CK2: Casein kinase 2

CPEB: Cytoplasmic polyadenylation element binding protein

CRM1: Exportin 1

Dcp1: mRNA-decapping enzyme 1

DDX6: DEAD (Asp-Glu-Ala-Asp) Box Helicase 6

FBS: Fetal bovine serum

G6P: Glucose-6-phosphate

GAPDH: Glyceraldehyde 3-phosphate dehydrogenase

GDE: Glycogen debranching enzyme

GFP: Green fluorescent protein

GLUTs: Hexose facilitative transporters

GSK3: Glycogen synthase kinase 3

GW182: Trinucleotide repeat containing 6A

LDH: Lactate dehydrogenase

LGS: Liver isoform of glycogen synthase

MCTs: Monocarboxylate transporters

MGS: Muscle isoform of glycogen synthase

NAD^+: Oxidized nicotinamide adenine dinucleotide

NADH: Reduced nicotinamide adenine dinucleotide

P38MAPK: p38 mitogen-activated protein kinase

PhK: Phosphorylase kinase

PI3K: Phosphoinositide 3-kinase

PKA: c-AMP dependent protein kinse A

PP1: Protein phosphatase 1

PTG: Protein targeting to glycogen

RBPs: RNA binding proteins

RNPs: Ribonuclear particles

SC-35: Serine/arginine-rich splicing factor 2

SOX9: SRY-box 9

SRY: Sex determining region X

UDP-glucose: Uridine diphosphate glucose

Xrn1: 5`-3`exoribonuclease 1

ACKNOWLEDGEMENTS

En primer lugar quiero agradecer a mi familia por su apoyo incondicional durante todo lo que duró este trabajo, a mi esposa Loreto y a mi pequeña hija, Agustina, a mi padre Jorge y a mi madre Erica y a mis hermanos Miguel y Joaquín.

De la misma forma quiero agradecer a toda la gente que de una y otra forma me ayudaron en la formulación, desarrollo y finalización de este trabajo. A la Dra. Ilona Concha Grabinger y todos los integrantes de su laboratorio Dra. Constanza Angulo, Dr. Franz Villarroel, Dr. (c) Antonia Covarrubias, Dr. (c) Héctor Mancilla, Dr. (c) Camila López, Karen Vander Stelt, Karina Cereceda y Esteban Salazar.

También agradecer al Dr. Gernot Laengst por acogerme en su laboratorio en la Universidad de Regensburg y al Dr. Thomas Schubert, Dra. Helen Hoffmeister, Dr. Attila Németh y Elizabeth Silberhorn por su gran ayuda tanto en el laboratorio como fuera de él durante mi pasantía en la ciudad de Regensburg, Alemania.

También quiero agradecer al Dr. Raúl Méndez por recibirme muy amablemente en su laboratorio en el IRB Barcelona, y a los integrantes de su laboratorio Dra. Eulália Belloc, Dra. Laure Weill, Dr. Gonzalo Fernández-Miranda, Dr. Alessio Bava, Carlos Maillo, Judith Martín, Verónica Chanes por su gran apoyo para poder realizar los experimentos relacionados con RNA. Finalmente quiero agradecer al Dr. Joan Guinovart por permitirme realizar los ensayos de actividad enzimática en su laboratorio, a Isabel Saez por su ayuda en la realización de dichos ensayos, y también de manera muy especial a mi amigo Felipe Slebe por todo el tiempo dedicado a la discusión de los resultados del trabajo.

1. Introduction

1.1 Seminiferous epithelium and spermatogenesis.

Testes are organs that essentially achieve two functions: sexual hormone synthesis and sperm production. Seminiferous tubules are the main functional component of the testis, which are organized as a complex stratified epithelium. Fundamentally the epithelium is constituted by two cellular components: the somatic that corresponds to Sertoli cells, and the germinal lineage, where spermatogonia, spermatocytes, spermatids and sperm are found [Figure 1A].

Tight junctions between adjacent Sertoli cells compartmentalize the seminiferous epithelium generating the blood-testis barrier [Figure 1, as BTB]. This barrier restricts the flow of biomolecules, segregates cellular events during spermatogenesis, creates an immunological barrier, and confers cell polarity to the seminiferous epithelium (Cheng & Mruk 2012). Polarity is manifested by the formation of two compartments where spermatogenesis takes place. The basal compartment is in contact with blood vessels, while the apical compartment is isolated from the blood flow and faces to the lumen in the tubule (Russell 1977).

Spermatogenesis is a process controlled by several hormones like oestrogen, testosterone, follicle-stimulating hormone and luteinizing hormone, among others (Alves et al. 2013). Furthermore, the development of germ cells is divided into 4 steps: mitosis, meiosis, spermiogenesis, and spermiation, which takes nearly 35 days to complete in mice (de Kretser et al. 1971, Holstein et al. 2003). Spermatogonia are defined as undifferentiated germ cells localized to the basal compartment and 3 types are distinguishable:

A-singles, known as the germ stem cells; A-paired and A-aligned, which are adjacent to the basal lamina of the tubule (Lie et al. 2009). These germ cells enter mitosis and some of them will eventually originate type A spermatogonia, intermediate and type B spermatogonia (de Rooij & Russell, Hess & Renato de Franca 2008) [Figure 1B]. Later, only type B spermatogonia will differentiate into pre-leptotenic spermatocytes, which cross the blood-testis barrier from the basal to the adluminal compartment (Russell 1977) [Figure 1B]. Then, pre-leptotenic spermatocytes differentiate into leptotenic spermatocytes [diploid germ cells]. Once in this compartment, leptotenic spermatocytes develop into pachytene spermatocytes that exhibit 2 meiotic processes [primary spermatocytes on meiosis I, and secondary spermatocytes on meiosis II], where haploid spermatids are generated (Lie et al. 2009) (Figure 1B). Spermatids reach the seminiferous tubule lumen and undergo several morphologic changes [spermiogenesis] like chromatin condensation, acrosome, tail and residual bodies formation (Lie et al. 2009). At the end of spermiogenesis, elongated spermatids are localized in the tubule lumen, prepared to be released from the seminiferous epithelium as spermatozoa [spermiation] (Lie et al. 2009) [Figure 1B]. In theory, in rodents from each A-single spermatogonium, 4096 spermatids and thus spermatozoa are generated. However, more that 75% of germ cells [spermatogonia, spermatocytes, spermatids] undergo apoptosis and degeneration. Thus, the final number of spermatozoa from a single spermatogonium is considerably smaller (Cheng & Mruk 2012).

Under physiological conditions the success of spermatogenesis relies on several factors, the integrity of Sertoli cell being one of the most important. Sertoli cells support germ cell differentiation meiosis and spermatid

Figure 1. Seminiferous epithelium and spermatogenesis. A) Seminiferous epithelium is composed by Sertoli cells and developing germ cells. Leydig and blood vessels are located outside of the tubule in the interstitium. Sertoli cells span from the base to the lumen of the tubule with its nucleus normally situated at the base. Adjacent Sertoli cells form the blood testis barrier [BTB] by tight junctions generating the basal and luminal compartments. Germ cells in different stages develop through the epithelium crossing the BTB reaching the tubular lumen and detaching as spermatozoa. B) Spermatogenesis scheme where type A spermatogonia divides and generates intermediate and type B spermatogonia in the basal compartment [left and down]. The latter enters mesiosis, where preleptotenic primary spermatocytes cross the BTB, and then secondary spermatocytes suffer a second meiosis generating haploid spermatids [right]. In the luminal compartment, round spermatids undergo spermiogenesis, characterized by the formation of an acrosome, tail and residual body to become elongated spermatids, which are released from the seminiferous epithelium at spermiation [left and up]. In the middle, a cross section of seminiferous epithelium with adjacent Sertoli cells [the nucleus located basally, n] and germ cells at different developmental stages depicted as brown, purple and blue between the Sertoli cells. Both figures are modified from (Lie et al. 2009, Rato et al. 2012b).

A

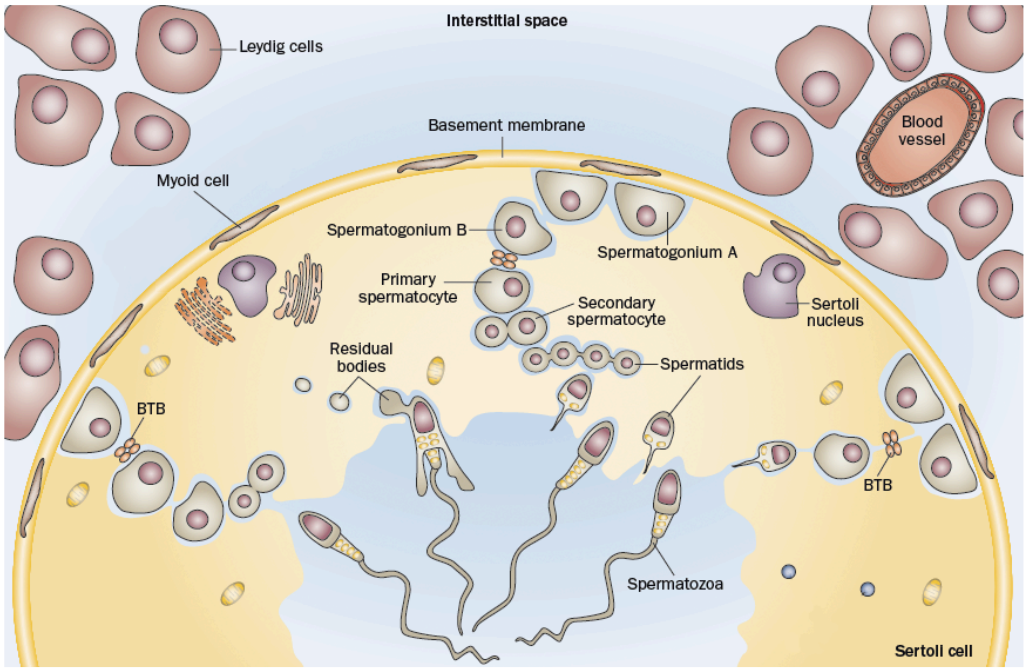
Interstitial space
Leydig cells
Basement membrane
Blood vessel
Myoid cell
Spermatogonium B
Spermatogonium A
Primary spermatocyte
Secondary spermatocyte
Sertoli nucleus
Residual bodies
Spermatids
BTB
BTB
Spermatozoa
Sertoli cell

B

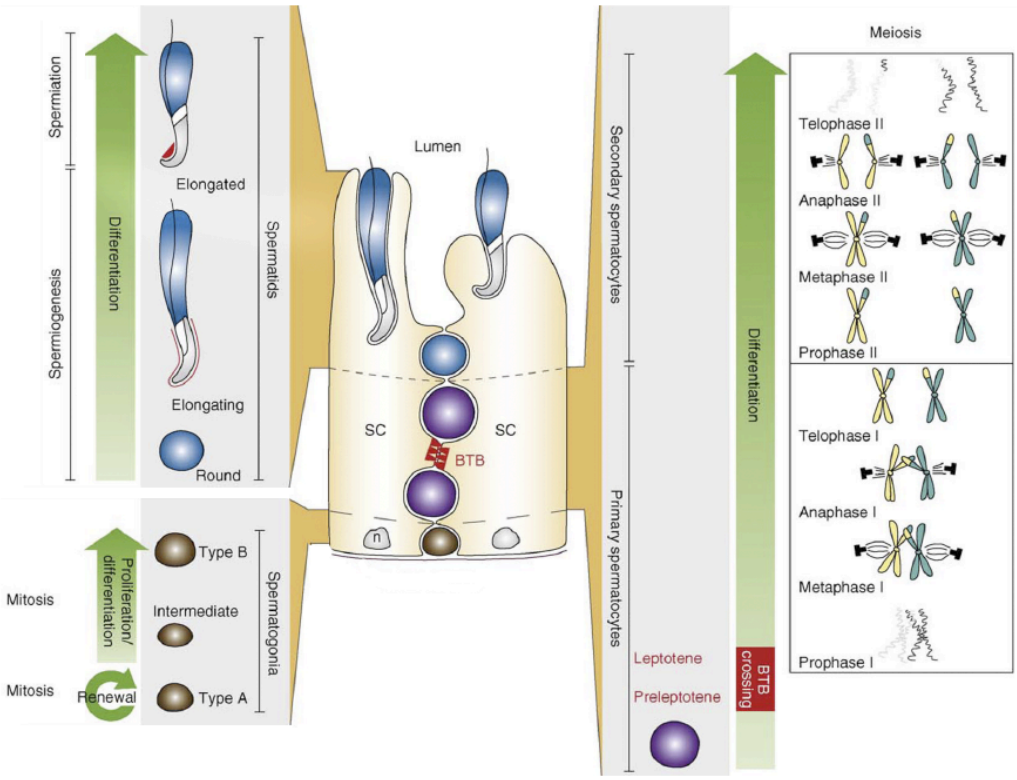
Spermiation
Spermiogenesis
Differentiation
Elongated
Elongating
Round
Spermatids
Lumen
SC
SC
BTB
n
Secondary spermatocytes
Primary spermatocytes
Leptotene
Preleptotene
Differentiation
BTB crossing
Meiosis
Telophase II
Anaphase II
Metaphase II
Prophase II
Telophase I
Anaphase I
Metaphase I
Prophase I
Mitosis
Proliferation/ differentiation
Type B
Intermediate
Mitosis
Renewal
Type A
Spermatogonia

transformation as well as the nutritional needs of developing germ cells (Tarulli et al. 2012; Rato et al. 2012). Structurally, these cells are fixed to the basal membrane, and the apex is extended up to the tubular lumen, while the cytoplasm exhibits numerous prolongations that envelop germ cells (Weber et al. 1983) [Figure 1]. Sertoli cells occupy a volume 17-20% of the seminiferous epithelium of adult men. Its number determinates testis size. Yet remarkably, each one can support up to 30-50 germ cells at different stages of development (Cheng & Mruk 2012, Russell et al. 1990, Sharpe et al. 2003). Moreover, these cells regulate the release of mature spermatozoa from the seminiferous epithelium, the reabsorption of residual bodies, and the phagocytosis of apoptotic germ cells (de Kretser et al. 1971, Nakanishi & Shiratsuchi 2004). In this way, spermatogenesis is a highly complex process regulated by the hypothalamus-pituitary-testis axis and dependent on functional Sertoli cells.

1.2 Glycogen, glycogen synthase, and its regulation

Glycogen is the main form of carbohydrate storage in the human body. It is a highly branched D-glucose polysaccharide where glucose can be released depending on the needs and stimuli. Glycogen metabolism works under a complex regulation involving allosteric factors, covalent modifications, and subcellular compartmentalization of key enzymes. Glycogen synthase and glycogen phosphorylase represent two central elements in this regulation. Different kinases inactivate glycogen synthase by phosphorylation but activate glycogen phosphorylase. They trigger the phosphorolysis of glycogen molecules and the generation of glucose-1-phosphate. The latter subsequently is converted to glucose-6-phosphate. By contrast, dephosphorylation

inactivates glycogen phosphorylase and activates glycogen synthase catalysing the addition of UDP-glucose to growing glycogen molecules (Shulman et al. 1995). Two isoforms of glycogen synthase have been described in mammals: a liver isoform [LGS] that is tissue-specific, and a muscle isoform [MGS] that is not only expressed in muscle, but also in different tissues including adipose tissue, kidney, spleen, nervous system and testis (Halse et al. 2003, Nuttall & Gannon 1993, Villarroel-Espíndola et al. 2013).

Hormone signalling generates diverse responses that depend on the target tissue, where MGS and LGS are phosphorylated on different serine residues. In the case of MGS, Ser7, 10, 640, 644, 648, 652 are phosphorylated by GSK3β, AMPK, PKA, PhK CAMKII and casein kinase I and II, which lead to the inactivation of the enzyme (Halse et al. 2003, Jensen et al. 2006, Palm et al. 2013). From these kinases, GSK3 hierarchically phosphorylates 4 serine residues of MGS [Ser640, 644, 648, 652], where the phosphorylation of Ser640 and Ser644 potently inactivate the enzyme (Skurat et al. 1994).

Furthermore, there are other regulators of glycogen synthase. The allosteric activator glucose-6-phosphate [G6P] activates the enzyme independently of its phosphorylation state (Bouskila et al. 2010). In the carboxy terminal region of MGS, an arginine rich segment is crucial for G6P allosteric activation. Arg to Ala mutations in this region lose the sensitivity of this enzyme to G6P activation (Hanashiro & Roach 2002). Another approach to modulate glycogen synthase activity is the change in its subcellular localization. Glycogen synthase is diffusedly localized in the cytosol of hepatocytes. While in glucose treated cells it accumulates at the cell periphery where glycogen deposition appears (Fernández-Novell et al. 1997).

Likewise, in transfected muscle and hepatic cells with depleted glycogen reserves, muscle glycogen synthase accumulates as a nuclear speckled pattern

Figure 2. MGS Phosphorylation sites. Schematic illustration of MGS phosphorylation sites. The phosphorylatable serines are indicated below the numbered sites that are reported for these residues. The kinases that phosphorylate the serine residues are showed over each residue. Phosphorylation clusters are presented inside dotted lines. Amino and carboxy terminal ends are showed in each extreme. c-AMP dependent protein kinase A [PKA], phosphorylase kinase [PhK], calmodulin-dependent protein kinase II [CAMKII], AMP-activated protein kinase [AMPK], casein kinase 1 [CK1], glycogen synthase kinase 3 [GSK3], casein kinase 2 [CK2]. Figure modified from (Palm et al. 2013)

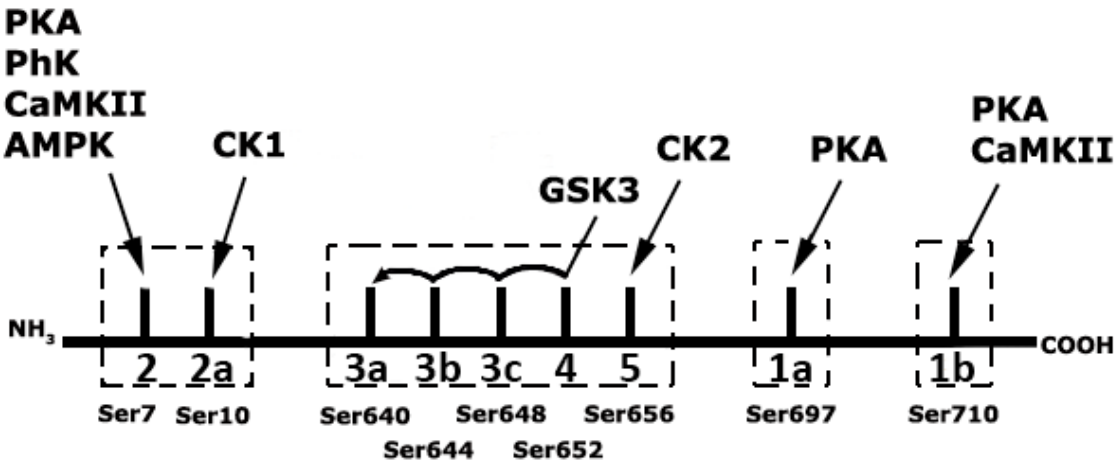
PKA
PhK
CaMKII
AMPK
CK1
GSK3
CK2
PKA
PKA
CaMKII
NH3
COOH
2
2a
3a
3b
3c
4
5
1a
1b
Ser7
Ser10
Ser640
Ser644
Ser648
Ser652
Ser656
Ser697
Ser710

when cultured without glucose, indicating that nuclear accumulation correlates inversely with cellular glycogen content (Cid et al. 2005). On the other hand, dephosphorylation is another manner to regulate glycogen synthase activity. Protein phosphatase 1 [PP1] is the responsible enzyme for the afore mentioned activity. To dephosphorylate glycogen synthase, PP1 must bind to glycogen molecules. G-subunits with glycogen specific binding capacity accomplish this task directing specifically PP1 to glycogen molecules (Hubbard & Cohen 1991). To date, four different G-subunits have been identified: GM exclusively expresses in muscle and heart tissue (Hubbard & Cohen 1991); GL is only described in the liver (Aggen et al. 2000); Human PPP1R5 and its mouse homolog PTG, are found principally in muscle, liver, and adipose tissue (Aggen et al. 2000, Brady et al. 1997); while PPP1R6 is expressed in all human tissues (Brady et al. 1997). PTG has the capacity to direct PP1 to glycogen and also other enzymes involved in glycogen metabolism, including glycogen synthase, glycogen phosphorylase, and phosphorylase kinase among others (Brady et al. 1997, Printen et al. 1997). Thus, PTG acts as a scaffold to assemble the enzymatic machinery of glycogen metabolism, and its overexpression is a suitable target to activate glycogen synthase. (Printen et al. 1997, Vilchez et al. 2007, Zibrova et al. 2008).

Another alternative to activate glycogen synthase by decreasing its phosphorylation state is inhibiting the main kinase that inactivates the enzyme, Glycogen Synthase Kinase-3 [GSK3]. Lithium is one of the most well known inhibitors of GSK3 by competing for magnesium binding site (Ryves & Harwood 2001). In adipocyte cells [3T3-L1] and rat skeletal muscle cells [L6], lithium effectively inhibits GSK3 activity, stimulates glucose incorporation, induces the activation of glycogen synthase, and thus glycogen

storage (MacAulay et al. 2003, Oreña et al. 2000). On the other hand, the role of GSK3 in the spermatogenic process has been associated with the stimulation of DNA synthesis in meiotic preleptotene spermatocytes in mice, and as a pro-apoptotic factor in the basal metazoan *Hydra* (Guo et al. 2003, Rentzsch et al. 2005). In male rat testes, subchronic lithium carbonate treatments induce the reduction of testes, epididymis, and accessory sex organs´ weight, as well as cauda epipidymis and daily sperm count (Thakur et al. 2003). Serum testosterone, intratesticular fluid volume, seminal vesicle and prostate secretions were also reduced in male rats that were treated with lithium (Thakur et al. 2003). Histologically, lithium carbonate treatments caused the loss of spermatogenic cells or desquamation of the tubule, and specifically the vacuolization and detachment from basal lamina of Sertoli cells (Thakur et al. 2003, Zarnescu & Zamfirescu 2006). These effects produce a 50% decrease in the fertility index, showing the toxicity of lithium treatments to the testicular function (Thakur et al. 2003). Similar results were observed in spotted munia [*Lonchura punctulata,* a seasonal breeding subtropical finch], where lithium chloride treatments also produce degenerative changes in tubular epithelium (Banerji et al. 2001). In humans, lithium induces a significant decrease of sperm motility *in vitro* (Raoof et al. 1989).

All these data suggest that testicular injuries observed during lithium treatments could be explained by an indirect activation of muscle glycogen synthase without discarding the effect over other enzymes affected by lithium.

1.3 Glycogen in Testis

During mouse sex determination at embryonic stages, Sertoli cell differentiation is promoted by *Sry* [sex-determining region Y] activation that upregulates *Sox9* in XY gonads resulting in testis formation (Morais da Silva et

al. 1996). Testis morphogenesis is initiated by SRY/SOX9 expression and requires specific events like cell proliferation of the coelomic epithelium of gonads, migration of mesonephric cells, vasculogenesis, cord formation and glycogen storage (Matoba et al. 2005, Schmahl & Capel 2003, Tilmann & Capel 1999). Glycogen accumulation starts, in pre-Sertoli cells of developing mouse XY gonads, shortly after the onset of *Sry* expression and is reported to be necessary for the activation of *Sox9*, indicating that a readily available energy source of glucose is needed for testis morphogenesis (Matoba et al. 2008).

In humans, an ultrastructural analysis showed the presence of glycogen particles in foetal testis (Fukuda et al. 1975). Whereas from infantile to pubertal periods, testicular glycogen content increases (Seilicovich & Pérez Lloret 1973). In pathological conditions like cryptorchid testis and unilateral varicocele, lower amounts were detected in comparison to normal patients (Sultan Sheriff 1984). A detailed study of glycogen content in hamster testicular cells during development revealed that in the first day after birth seminiferous epithelium cells are almost devoid of glycogen and that only the tunica albuginea and arterioles walls were the main source of testicular glycogen (Fouquet & Guha 1969). In the first wave of spermatogenesis [≈ week 6 in hamsters] there is an increase in glycogen content, mainly present in Sertoli cells with respect to germ cells, following a cycle pattern depending in the stage of the tubule (Fouquet & Guha 1969). The activity of glycogen phosphorylase and glycogen synthase reaches their maximum levels during this period. Nevertheless, glycogen phosphorylase activity is always higher than glycogen synthase (Fouquet & Guha 1969). Hamsters aged 2 to 4 months show a small increase of glycogen content, although the activity and

presence of glycogen phosphorylase is very insignificant as is glycogen synthase activity (Fouquet & Guha 1969).

Rat testes from different developmental stages show distinctive glycogen content. From prenatal to the postnatal first day, glycogen amounts are 20 times higher in comparison with incoming days including immature, mature, and aged stages of rat growth (Gunaga et al. 1972). This effect was described precisely in germ cells where glycogen content also declines progressively from the immediate postnatal period to adulthood (Leiderman & Mancini 1969). Nevertheless, as within human pathologic conditions, higher glycogen concentration was observed in adult cryptorchid rat testis in comparison with control animals (Hárkómen & Kormano 1970).

Despite lower glycogen levels observed in postnatal testis, its metabolism must be intact. Mono-2-ethylhexil-phtalates bind and inhibits glycogen debranching enzyme [GDE], interfering with normal degradation rates of glycogen and thus its accumulation, causing germ cell apoptosis and testicular toxicity (Kuramori et al. 2009).

In our laboratory we have determined that only the muscular isoform of glycogen synthase is expressed in testicular cells, and that enzymatic activity/glycogen content is higher during the first postnatal days (Villarroel-Espíndola et al. 2013). Also, we reported that glycogen synthase activity/expression regulation machinery is active in this tissue and that an overproduction of glycogen triggers apoptosis in a germ cell line (Villarroel-Espíndola et al. 2013). These results suggest a negative role of this polysaccharide once its metabolism is altered, or specifically, when an overproduction develops.

1.4 Sertoli Cell Metabolism

Sertoli cells accomplish fundamentally two functions: first, testis formation by regulating gonad cell differentiation during embrionary stages, and second, act as a mechanical and nutritional support of germ cell differentiation being indispensable for spermatogenesis once reached maturity (Tarulli et al. 2012). These cells are the main structural component of the seminiferous epithelium; their number define testis size occupying between 17-20% of an adult seminiferous epithelium volume (Russell et al. 1990, Sharpe et al. 2003). It has been described that Sertoli cells are capable of supporting between 30 and 50 germ cells from different developmental stages (Waites & Gladwell 1982). Germ cells have particular nutritional requirements that change during development and depend on Sertoli cells (Bajpai et al. 1998).

Seminiferous epithelium is highly compartmentalized and oxygen deprived, restricting nutrient availability where only Sertoli cells and spermatogonia are in direct contact with blood vessels derived fluid (Setchell 2004, Wenger & Katschinski 2005). Spermatogonia use glucose for ATP production, while spermatocytes and spermatids depend on lactate offered by Sertoli cells [produced from glucose via glycolysis] (Boussouar & Benahmed 2004). For these reasons spermatogenesis essentially requires glucose, directly as fuel for spermatogonia, or indirectly for lactate production to spermatocytes and spermatids by Sertoli cells (Boussouar & Benahmed 2004, Zysk et al. 1974).

Lactate is the germ cell fuel, stimulates RNA and protein synthesis, and inhibits apoptosis (Erkkilä et al. 2002, Jutte et al. 1981). Moreover, in 1999, intratesticular lactate infusions recovered spermatogenesis in adult cryptorchid rats (Courtens & Plöen 1999). Positive effects of intratubular lactate rely on

Sertoli cell function, because they are capable of converting more than 90% of glucose to lactate and secreting it to the extracellular space (Robinson & Fritz 1981). Sertoli cells are the major source of this anion in testis and its production is regulated by several mechanisms (Rato et al. 2012). Hexose facilitative transporters [GLUTs] incorporate glucose from the extracellular milieu and the presence of at least 4 isoforms [GLUT1, GLUT2, GLUT3 and GLUT4] have been reported in Sertoli cells (Angulo et al. 2008). The enzyme lactate dehydrogenase [LDH] interconverts lactate and pyruvate. Monocarboxylate transporters [MCTs] are responsible for lactate efflux to the extracellular. Both are mainly accountable for lactate provision to developing germ cells from Sertoli cells (Oliveira et al. 2011). Sertoli glycolytic activity is high; nevertheless, under adverse metabolic conditions, they are capable of adapting and safeguarding lactate production for germ cells. In glucose deprived conditions, lactate production practically does not decrease and Sertoli cells adapt by increasing glucose uptake and GLUT1 expression, decreasing GLUT3 expression and activating AMPK, PI3K/AKT and p38MAPK signalling pathways (Riera et al. 2009).

Lactate production from Sertoli cells is highly regulated and numerous factors are responsible. Activation of AMPK by the use of an AMP analog, AICAR [5-aminoimidazole-4-carboxamide-2-b-d-ribonucleoside] or adding adenosine, stimulate glucose internalization and GLUT1, MCT4 mRNA expression, increasing lactate production (Galardo et al. 2007; Galardo et al. 2010). By contrast, treatments with the steroidal sexual hormone 5α-dihidrotestosterone [DHT] generates a significant decrease in lactate secretion and LDH mRNA expression despite high glucose consumption and glucose consumption rate (Oliveira et al. 2011). Moreover, DHT treatments redirect the incorporated glucose to tricarboxylic cycle conducing Sertoli cells to a

more efficient metabolic state (Oliveira et al. 2011; Rato et al. 2012). Follicle stimulating hormone [FSH], basic fibroblast growth factor [BFGF], triiodothyronine hormone [T3], interleukin 1α [IL-1α], insulin and insulin like growth factor I [IGFI] stimulate lactate production. FSH activates PI3K/AKT signalling, glucose incorporation and synergistically with BFGF induces lactate production (Meroni et al. 2004, Schteingart et al. 1999). T3 increases lactate levels regulating GLUT1, MCT1 and 4 expressions, while IL-1α stimulating glucose transport and the expression and activity of LDH (Carosa et al. 2005, Fugassa et al. 1987, Nehar et al. 1998). Insulin and IGFI stimulate lactate production by means of an increment of glucose transport, observed as an increase in a glucose analog (2-deoxyglucose) incorporation (Oonk et al. 1989). By contrast, cultured cells in the absence of insulin present altered glucose consumption and lactate production, a decrease in GLUT3, LDHA and MCT4 expression while GLUT1 expression increases as an adaptive response (Oliveira et al. 2012).

Despite glucose being principal source for lactate production, it is not the main metabolite for ATP production because Sertoli cells stay viable in the absence of glucose (Xiong et al. 2009). Other proposed ways to obtain energy are catabolism of glycogen and aminoacids. Glycogen and enzymes involved in their synthesis and degradation have been described in Sertoli cells (Slaughter & Means 1983, Villarroel-Espíndola et al. 2013). In embryonic stages, pre-Sertoli cells use glycogen as an energy source to maintain SOX9 expression, a fundamental process for testiculogenesis (Matoba et al. 2005, 2008). During postnatal stages, there is only one report about glycogen metabolism in rat Sertoli cells, which described that less than 2% of incorporated glucose is converted to glycogen (Robinson & Fritz 1981). In mice testis, glycogen synthase is more active during the first 5 postnatal days,

where mostly Sertoli cells compose seminiferous tubules (Villarroel-Espíndola et al. 2013). Likewise, in immature rat testis FSH activates glycogen phosphorylase that immunolocalized to cytoskeletal associated structures in Sertoli cells (Slaughter & Means 1983). On the other hand, rat Sertoli cells can oxidize alanine, leucine, valine and glutamine to CO_2 to obtain energy, where glucose and palmitic acid are capable to regulate their metabolism (Kaiser et al. 2005).

From all the cells that compose the testis, Sertoli cells are the ones that produce more ATP (Xiong et al. 2009). ATP production comes principally from phagocytosis of apoptotic germ cells and residual bodies to obtain lipids, which are the source for ATP via beta-oxidation (Xiong et al. 2009). This process was demonstrated by blocking glycolysis with 2-DOG, where ATP levels are maintained. When blocking beta-oxidation with an inhibitor of the long chain acyl-CoA dehydrogenase (2-mercaptoacetate), ATP levels decrease drastically (Xiong et al. 2009). In addition, rat Sertoli cells cultured in presence of different palmitate concentrations, show that they can oxidize it to CO_2, ketonic bodies, and fatty acids, the last ones being the main energy source for these cells (Jutte et al. 1985). This indicates that in this biological context beta-oxidation of lipids acquired from phagocytosed apoptotic germ cells and residual bodies is the main pathway to obtain ATP by Sertoli cells.

Thereby, Sertoli cell metabolism is highly regulated by several hormones and growth factors, is focused in lactate production through glycolysis as energetic fuel for developing germ cells, and generates its own energy from apoptotic germ cells and residual bodies to obtain ATP via beta-oxidation, without discarding glycogen and aminoacid metabolism contribution.

1.5 Metabolic Enzymes as RNA Binding Proteins.

Metabolic enzymes are classically described to have specifics roles related to different anabolic or catabolic processes, which are useful for cell survival and function. In many studies they are referred to as "housekeeping genes", but in the last decades new roles have been reported that link the intermediary metabolism and the regulation of gene expression (Cieśla 2006, Hentze & Preiss 2010). Enzymes involved in different processes like tricarboxylic acid cycle, glycolysis, pentose phosphate cycle, fatty acid metabolism, and pyrimidine synthesis, have been shown to bind RNA, and leading edge technology is being used to demonstrate this relationship (Castello et al. 2012a, Cieśla 2006, Kim & Dang 2005).

The most studied enzyme that binds RNA is the cytosolic aconitase, also known as iron responsive protein 1 [IRP-1]. This enzyme catalyses the isomerization of citrate to isocitrate in the tricarboxylic acid cycle and binds to iron responsive RNA elements [IREs] located in mRNA untranslated regions [UTRs] of iron metabolism related genes (Beinert & Kennedy 1993, Kaptain et al. 1991). In iron-replete cells, a 4Fe-4S cluster inserts to the bifunctional enzyme allowing its catalytic activation, being inactive as an IRE binding protein (Hentze & Kuhnt 1996). While in iron-deficient cells, the enzyme without the cluster leaves the IRE-binding site accessible allowing the binding to IREs. This permits the regulation and stability of mRNAs encoding functions in iron homeostasis and related processes (Hentze & Kuhnt 1996, Wallander et al. 2006). In the same way, all three enzymes of the thymidylate synthesis cycle [thymidylate synthase [TS], serine hydroxymethyl-transferase [SHMT] and dihydrofolate reductase [DHFR]] regulate the translation of their own mRNAs among others (Chu & Allegra 1996, Chu et al. 1991, 1993; Liu et al. 2000). These enzymes bind to 5`UTR or coding regions and the binding is

negatively regulated by their substrates, for the case of TS, deoxyuridyn-monophosphate [dUMP] and dihydrofolate [DHFP] (Chu et al. 1993, Liu et al. 2002). Another enzyme described to bind RNAs is glyceraldehyde-3-phosphate dehydrogenase [GAPDH], which metabolically catalyses the conversion of glyceraldehyde-3-phosphate to 1,3-biphosphoglycerate using NAD^+ as cofactor. Non-glycolytic activities have been attributed to GAPDH including DNA binding, helicase activity, and DNA repair, showing that this enzyme has broad features regarding nucleic acid interaction (Karpel & Burchard 1981, Meyer-Siegler et al. 1991, Perucho et al. 1977). AU-rich elements [AREs] are involved in the turnover and translation of numerous mRNAS and GAPDH was discovered as a new AREs binding protein [ARBP]. GAPDH/RNA interaction rely specifically in its NAD^+ binding region [Rossman Fold], thus depending on NAD^+ concentrations to act as a glycolytic enzyme or an ARBP (Nagy & Rigby 1995, Nagy et al. 2000). Also, *in vivo* studies have shown that GAPDH interacts with RNAs, as part of ribonucleoprotein particles in human parainfluenza virus-infected cells (De et al. 1996).

Another glycolytic enzyme like lactate dehydrogenase [LDH], which catalyses the interconvertion of pyruvate and lactate with concomitant oxidation of NADH to NAD^+, have been identified to bind mRNAs. LDH acts as an ARBP interacting with granulocyte-macrophage colony-stimulating factor [GMCSF] mRNA 3`UTR regulating its translation (Pioli et al. 2002). The binding occurs in the NAD^+-binding region and the localization in translationally active polysomes depends on the RNA binding capacity, which is supported by the complex with the RNA binding proteins AUF1 and Hsp70 (Pioli et al. 2002). In addition to GAPDH and LDH, glucose-6-phosphate dehydrogenase [G6PDH] binds specifically to various regions of

the GLUT1 mRNA, indicating the relevance of this mechanism to control the rate-limiting step in glucose utilization (McGowan & Pekala 1996). Similarly, phosphoglycerate kinase [PGK] binds to the coding region of urokinase-type plasminogen activator receptor [uPAR] mRNA, downregulating its expression affecting the proliferation and migration of human bronchial epithelial cells (Shetty et al. 2004).

Glycogen synthase can be associated to RNAs because few studies have shed light on this connection. A proteomic survey of endoplasmic reticulum [ER] function in the liver shows the differences between rough and smooth ER protein components. The hepatic isoform of glycogen synthase [LGS] was found as an enriched component of rough endoplasmic reticulum but not in the smooth endoplasmic reticulum (Song et al. 2010). In another approximation, using a proteomic multidimensional protein identification technology, muscle isoform of glycogen synthase [MGS] was identified as a component of ribosomes (Fuchs et al. 2011). As a non-ribosomal protein, MGS was associated with translationally active ribosomes in HeLa cells, and specifically the phosphorylated form in Serine640 [pSer640-MGS] (Fuchs et al. 2011). MGS depletion in HeLa cells resulted in a loss of polysomes, corroborated by a small, but not significant, decrease in [^{35}S]methionine incorporation on global cellular translation (Fuchs et al. 2011). This suggests that the enzyme might regulate the translation of only a subset of mRNAs.

Our laboratory described the functional presence of malin, an E3 ubiquitin ligase, and laforin, a dual phosphatase, promoting the polyubiquitination of MGS in Sertoli cells through the interaction with malin-ring domain in the Sertoli cell line 42GPA9 (Villarroel-Espíndola et al. 2013). Malin has been described to be recruited to processing bodies, co-localizing with different markers like AGO2, Dcp1, Xrn1, and GW182 in HeLa cells

(Singh et al. 2012). Malin regulates the recruitment of the mRNA decapping enzyme Dcp1 by promoting its polyubiquitination and degradation, and playing a pivotal role in microRNA-mediated gene silencing by processing bodies (Singh et al. 2012). Additionally, laforin, which interacts indirectly with MGS through malin-ring domain, was reported to be a ribosome-associated protein, being immunoprecipitated in polyribosomes fractions (Ganesh et al. 2000).

1.6 Problem statement

The present data indicates that glycogen content in mature mice testis is scarce. Nevertheless, the amount of detected glycogen synthase does not correlate with glycogen content in Sertoli cells [unpublished results from our laboratory]. Additionally, it was observed that in lithium treated Sertoli cells MGS is accumulated in only one or two cytoplasmic granules. This behaviour is very different in muscle and adipose tissue, where lithium produces many glycogen particles, indicating that MGS acts differently in Sertoli cells. Furthermore, the reported interaction of the hepatic isoform with rough ER, the cosedimentation of pSer640MGS with elongating ribosomes, and the interaction of Malin and Laforin, which in turn interact with MGS, with ribonucleoprotein complexes, indicate that MGS could effectively interact directly or indirectly with ribonucleoprotein complexes and regulate, by some unknown mechanism, the expression of several mRNAs. These antecedents constitute a motivating challenge to demonstrate that MGS acts as an RNA binding protein. By the analysis of MGS relationship with mRNA expression regulation, it is possible to unveil a putative novel function of this enzyme in mice Sertoli cells.

2. Hypothesis

Muscle glycogen synthase is predominantly inactive and has a new role as an RNA binding protein in mice Sertoli cells

2.1 General Objectives

1. To demonstrate the activity state of muscle glycogen synthase in Sertoli cells.
2. To demonstrate glycogen synthase interaction with RNAs in Sertoli cells

2.1.1 Specific Objective for General Objective 1

- To evaluate muscle glycogen synthase expression, localization, phosphorylation state and function in Sertoli cells obtained from primary cell cultures and cell line 42GPA9.

2.1.2 Specific Objective for General Objective 2

- To evaluate the interaction of muscle glycogen synthase with RNAs and different RNA binding proteins.

3. Materials and Methods

3.1 Materials

3.1.1 Reagents

The following reagents were acquired from Winkler Ltda.: Tris [hydroximethyl] aminomethane, sodium dodecyl sulfate [SDS], ammonium persulfate, glycerol, sodium bicarbonate, phenylmethanesulfonylfluoride [PMSF], lithium chloride, lithium carbonate, glycine, dimethylsulfoxide [DMSO], bromophenol blue, sodium chloride and sodium fluoride. Calbiochem: ß-mercaptoethanol. Merck, Darmstadt, Germany: sodium hydroxide, potassium chloride, formaldehyde solution 37%, agar-agar, hydrogen chloride, methanol, ethanol, tetramethylethylenediamine [TEMED], acrylamide, bis-acrylamide, isopropanol and chloroform. US biological, Swampscott, MA, USA: Ehylenediaminetetraacetic acid [EDTA], ampicillin sodium salt. Thermo Fisher Scientific: Hyclone classical powdered media DMEM F12 [SH30004.04], Hyclone fetal bovine serum FBS [SH30396.03], Hyclone trypsin [SH30236.01], dimethyl pimelimidate*2HCl [21666], pageruler plus prestained protein ladder [26619], Halt protease inhibitor cocktail 100X [87786], ECL Western blotting substrate. Sigma-Aldrich: Sodium deoxycholate, D-glucose, 2-mercaptoethanol, tween-20, triethanolamine, sucrose, collagenase crude type IA [C2674], Hyaluronidase type V [H6254], deoxyribonuclease I [DN25], Hanks` balanced salt solution, monoclonal anti-α-tubulin antibody produced in mouse [T5168]. Life Technologies, Carlsbad, USA: Trizol reagent [15596018], RNAseout recombinant RNAse inhibitor [10777019], dynabeads protein A [10002D],

Gibco antibiotic-antimycotic 100X [15240-062], Opti-MEM I® reduced serum media [31985-062], Lipofectamine® 2000 transfection reagent [11668-019], SYBR ® SAFE DNA stain, alexa fluor 488 donkey anti-mouse IgG [A-21202], alexa fluor 488 donkey anti-rabbit IgG [A-21206], alexa fluor 568 goat anti-mouse IgG [A-11004], alexa fluor 633 goat anti-rabbit IgG [A-21070] and 4`,6-diamidino-2-phenylindole, dihydrochloride [DAPI]. MO BIO Laboratories: LB Broth powder growth media. Dako: Fluorescent mounting medium. Promega: RQ1 RNase-free DNase [#M6101], 1 kb DNA ladder. Bio-Rad: Bio-Rad protein Assay, IPG strips 7 cm. pH range 4-7. New England Biotechnologies: Lambda protein phosphatase [NEB.P0753S]. Cell Signaling: anti-phospho-glycogen synthase [Ser640] antibody produced in rabbit [#3891], anti-glycogen synthase 15B1 produced in rabbit [#3886], pS640MGS and MGS 3886 respectively in this work. Abcam: anti-Ago2/eIF2C2 antibody produced in rabbit [ab32381]. Santa Cruz Biotechnology: normal rabbit IgG [sc-2027], anti-glycogen synthase 1 GS-7H5 antibody produced in mouse [sc-81173], puromycin [sc-108071], Polybrene® [sc-134220]. Millipore: anti-glycogen synthase CT antibody produced in rabbit [04-357], ctMGS in this work. GeneON: Maximo Taq DNA Polymerase, MMLV Reverse Transcriptase, 4 dNTP´s set.

3.1.2 Animals used for experimentation

Experimental procedures were performed using C57BL6 mice, maintained (housing, handling, care and processing) in accordance with the "Rules for animal investigation" dictated by the Animal Usage in Research Committee of the Universidad Austral de Chile. The sleep and wakefulness cycles, as well as, alimentation and *ad libitum* drinking water were always maintained. Animal slaughtering was also performed under the rules of the

Animal Usage in Research Committee of the Universidad Austral de Chile avoiding animal suffering and pain. Animal remains were eliminated under biosafety instructions of the aforementioned committee.

3.1.3 Equipment

Laboratory pH meter inoLab pH720; microfuge Sigma 1-14; centrifuge Sigma 2-16PK; ultra turrax IKA T10 basic; revolver rotator Labnet; waving plataform Heidolph polymax 1040; magnetic stirrer IKA rh basic 2; precision balance Sartorius TE612; analytical balance A&D GR-200; rocking incubator Zhicheng ZHWY-100B; thermoregulated bath Oilbath ONE; chemiluminiscence documentation system Syngene G:BOX chemi; gradient thermocycler Eppendorf Mastercycler gradient; CO_2 incubator Nuaire DH Autoflow; biological safety cabinet class II, type A2 Nuaire UN-425-600-E; UV-Vis spectrophotometer NanoDrop 2000; confocal microscope OLYMPUS Fluoview FV1000; inverted microscope OLYMPUS CKX41; ultrasonic bath Elmasonic S30H; sonicator Bioruptor®; electrophoresis system mini-protean® tetra cell; electrophoretic transfer cell system mini trans-blot®; fluorescence UV transiluminator InGenius Syngene; magnetic rack for microcentrofuge tubes MagnaRack TM Invitrogen; Hitachi high-speed refrigerated centrifuge CR22 GIII.

3.2 Methods

3.2.1 Cell cultures

3.2.1.1 Sertoli 42GPA9 cell line culture

Sertoli 42GPA9 cell line was widely validated by the group that isolated them, Georges Pontis and Dominique Segretain at the Université Paris 5, Paris, France (Bourdon et al. 1998). Cells were grown on supplemented DMEM-F12 with 10% (v/v) fetal bovine serum [FBS], L-glutamine 2mM, penicillin 50 U/mL, streptomicyn 50 mg/mL and fungizone 50ng/mL at 37ºC and 5% CO_2 (Bourdon et al. 1998). Cells at 80% confluence were detached using 0.25% trypsin-5 mM EDTA.

3.2.1.2 Mice primary Sertoli cell cultures

Sertoli cells were obtained from 30-40 days old C57BL6 male mice as described previously (Anway et al. 2002), with modifications. Testis were removed, decapsulated and placed in 1X Hanks. The seminiferous tubules were dispersed, not fragmented, in a collagenase solution [10mL, 0.5 mg/mL] in Hanks 1X at 34ºC for 15 minutes, shaken at 80 oscillations/min, and allowed to settle. The supernatant was decanted and the tubules were washed three times with Hanks 1X. The tubules were further incubated in a trypsin solution [10 mL, 0.5 mg/mL] in Hanks 1X at 37ºC without shaking. Next, tubules were washed two times with Hanks 1X, and the third wash was made with Hanks 10% [v/v] FBS to inhibit trypsin and allowed to settle for 2 minutes. To separate Sertoli and germ cells, tubules were incubated with a mix of enzymes [10 mL, 1 mg/mL collagenase, 2 mg/mL hyaluronidase and 0.4

mg/mL DNAse I] and 1% FBS in Hanks 1X at 34ºC for 40 minutes, shaken at 80 oscillation/min. Sertoli cell preparation was centrifuged to pellet the cells at 500 Xg for 3 minutes, and then washed 3 times with Hanks. It was important to disperse cell clumps to separate the cells. The last wash was made with supplemented DMEM-F12 [as is described in **3.2.1.1]** in the same conditions. Other protocols were not used because they comprise more steps, including hypotonic treatments to destroy germ cells that decrease the number of isolated Sertoli cells. Finally, the cell mixture to the plate and washed them 10 times per day with sterile PBS. Only Sertoli cells were found attached to the plate, while remaining dead germ cells were discarded during daily washes.

3.2.2 Protein extraction

Both for polyacrylamide gel electrophoresis and inmunoprecipitation assays, protein extracts were obtained in RIPA buffer [150 mM NaCl, 1% Triton-X100, 0.5% sodium deoxycholate, 0.1% SDS, 50 mM Tris-HCl, pH 8.0] supplemented with a cocktail of proteases, phosphatase inhibitors [10mM NaF, 1mM inorganic pyrophosphate, 25 nM okadaic acid, 2 mM sodium orthovanadate]. RNAse inhibitor was added only for RNA inmunoprecipitations. For tissue protein extraction, 5 mg of tissue was homogenised with ultra-turrax in supplemented RIPA buffer. In the case of cell cultures, the supplemented buffer was directly added to the plates, which were scraped to detach the cells. Next, the cell suspension was sonicated twice for 5 minutes on ice, vortexing between each sonication, and then the extracts were passed 8 times through a 25G needle. Protein concentration was quantified using Bio-Rad protein Assay based on the method of Bradford.

3.2.3 Protein immunodetection and cellular immunolocalization

3.2.3.1 Polyacrylamide gel electrophoresis (SDS-PAGE)

Protein extracts were resuspended in sample buffer [62.5 mM Tris-HCl pH 6.8, 25% glycerol, 12.5% ß-mercaptoethanol, 0.025% bromophenol blue] and heated at 95ºC for 5 minutes and then loaded into the gel. All the preparations were run in 8% polyacrylamide gels. The stacking and spacer gel was prepared from a 29.2:0.8 acrylamyde:bis-acrylamide stock solution. The spacer gel was prepared to a final concentration of 8% containing 375 mM Tris-HCl [pH 8.8], 0.1% SDS, 0.04% ammonium persulfate and 0.03% TEMED. The stacking gel was prepared to a final concentration of 5% containing 125 mM Tris-HCl [pH 6.8], 0.1% SDS, 0.09% ammonium persulfate and 0.06% TEMED. Gel electrophoresis was performed at 100 Volts during approximately 3 hours in running buffer [25 mM Tris-HCl, 190 mM glycine, 0.1% SDS) until the dye front reached the bottom of the gel.

3.2.3.2 Western Blot

Electrophoretically separated proteins were transferred to a PVDF membrane previously activated for 30 second with 100% methanol. The membranes were blocked with 5% non-fat dry milk in TBS-T for at least 45 minutes. Then, the blocked membranes were incubated with a primary antibody overnight at 4ºC with constant rotation. Dilution of all the primary antibodies was 1:1000, except for tubulin that was used in 1:5000. Next, the membranes were washed 3 times with TBS-T and incubated with the secondary antibody, conjugated to peroxidase, for 1 hour at room temperature. Finally, luminescent signal was detected using the chemiluminescent substrate for peroxidase, ECL, and visualized by

chemiluminescence documentation system, Syngene G:BOX chemi. The secondary antibodies were diluted 1:5000 in TBS-T. The obtained bands were statistically evaluated by Student's t-test or non-parametric statistical analyses using Prism version 5.0 for Mac OS X.

3.2.3.3 Indirect immunofluorescence in Sertoli cells

Cultured Sertoli cells, from the cell line 42GPA9 and primary cultures, were grown in circular coverslips to 50% confluence and prior to fixation were washed 3 times with ice cold PBS to discard any rest of culture media, and fixed with 4% formaldehyde in PBS for 15 minutes with moderate shaking. To permeabilise Sertoli cells, formaldehyde was discarded and immediately -20ºC methanol was added for 10 minutes with shaking at room temperature. Next, 5% bovine serum albumin in TBS was used to block for 1 hour with soft agitation at room temperature. Primary antibodies were prepared in the same blocking solution at different concentrations, incubated overnight at 4ºC and then washed 3 times with TBS-T. Fluorescent secondary antibodies, in addition with the nuclear dye [DAPI or propidium iodide], were also prepared in TBS in a concentration of 1:300, incubated 2 hours at room temperature and washed 3 times with TBS-T. Finally, the cells in coverslips were mounted in glass slides using 5 uL of DAKO fluorescent mounting medium per cover. The immunofluorescence signals were analysed using the confocal microscope OLYMPUS Fluoview FV1000.

3.2.4 Electronic microscopy

Transmission electronic microscopy analyses were performed with the collaboration of Gernot Längst in the University of Regensburg, Regensburg, Germany. Cultured 42GPA9 cells on 12 well plates were fixed with

glutaraldehyde 2.4% in 100 mM phosphate buffer at pH 7.0, for 2 hours at 4ºC, and then washed 2 times for 15 minutes with the same buffer. The samples were post-fixated with 1% osmium tetroxide in 100 mM phosphate buffer at pH 7.0, for 2 hours at 4ºC, and then washed again 3 times with the same buffer. Next, the cells were dehydrated as follows: 50% [v/v] ethanol for 10 minutes, 70% [v/v] ethanol for 10 minutes, 90% [v/v] ethanol for 10 minutes, 96% [v/v] ethanol for 10 minutes, 100% [v/v] ethanol 2 times for 5 and 10 minutes, and 100% [v/v] acetone 2 times for 5 and 10 minutes. After dehydration, cells were included in Araldite by incubating with acetone/Araldite 1:1 [v/v] for 1 hour, and then only with the resin for 4 hours. To polymerise the resin, cells were baked at 56ºC for 12 hours in the 12 well plates. Finally, the resin blocks with the cells were ultra-sectioned and collected in grids to stain the anionic and cationic components with 5% uranyl acetate during 15 minutes, and 0.4% lead citrate for 3 minutes.

3.2.5 Glycogen synthase activity

Glycogen synthase activity and glycogen quantification assays were performed in the Laboratory of Metabolic Engineering and Diabetes directed by Joan Guinovart PhD, in the Institute for Research in Biomedicine IRB Barcelona, Barcelona, Spain. The assays were done in AdGFP and AdPTG transduced Sertoli cells as was described in Vilchez et. al. 2007, and in 24 hours treated Sertoli cells with 90 mM lithium chloride.

3.2.5.1 Measurement of Glycogen synthase activity

Determination of glycogen synthase activity was assayed as described previously (Thomas et al. 1968, Vilchez et al. 2007). Frozen Sertoli cells grown in 100 mm diameter plates were scraped and homogenised with a 25G needle

in a buffer containing protease and phosphatase inhibitors. To normalize the activity values, protein concentration of each sample was determined following Bradford method using the Bio-Rad protein assay reagent. The activity was measured in the absence or presence of the allosteric activator G6P [6.6 mM]. In the presence of G6P, the measured activity represents the total activity of the enzyme, while the measured activity in the absence of G6P represents only the intrinsically active enzyme. For this reason, the –G6P/+G6P activity ratio represents the activation state of the enzyme, where values below 0.1 indicate a fully inactive enzyme whereas those above 0.7 are equivalent to complete activation (Guinovart et al. 1979).

3.2.5.2 Glycogen quantification

Glycogen content quantification was performed as described previously (Chan & Exton 1976). Sertoli cells grown on 100 mm diameter plates were frozen with liquid nitrogen, scrapped on ice with 200 uL of 30% KOH, and transferred to a 1.5 mL tube. Then, cell extracts were heated 15 minutes at 100ºC and all the volume was added over a Whatman filter paper. Each sample volume was annotated for calculations and 5-10 uL of each extract was used for protein quantification. Once the samples were absorbed in the filter paper, they were washed with 66% cold ethanol [stored at -20ºC] for 10 minutes shaking. At this concentration only glycogen precipitates in the paper. Two more washes were made with 66% cold ethanol for 30 minutes each with shaking. Next, the papers were incubated in acetone for 5 minutes to eliminate ethanol and then dried at room temperature. Dried papers were transferred to a 1.5 mL tube with 1 mL of 0.5 mg/mL amyloglucosidase in 100 mM sodium acetate buffer pH 4.8, and incubated at 37ºC for 90 minutes. During this step amyloglucosidase hydrolyse glycogen to glucose molecules.

Finally, glucose quantity was determined spectrophotometrically by measuring the absorbance [340 nm] of reduced NADH generated from the coupled reaction hexokinase/G6PDH that is directly proportional to glucose amounts.

Reaction:

$$\text{D-Glucose + ATP} \xrightarrow{\text{Hexokinase}} \text{Glucose-6-P + ADP}$$

$$\text{Glucose-6-P + } NAD^+ \xrightarrow{\text{G6PDH}} \text{gluconate-6-P+ NADH+ } H^+$$

Calculation:

$$\frac{\text{glucose concentration (mg/dL) * 9000}}{\text{sample volume (uL) * protein concentration (ug/uL)}} = \text{ug glycogen/mg protein}$$

9000= factor from conversion of 1 ug of glycogen to glucose [0.9], and the conversion from the other units to get to ug glycogen/mg protein.

3.2.6 RNA immunoprecipitation and microarray profiling

The experiments were performed in the Laboratory of Translational Control of Cell Cycle and Differentiation directed by Raúl Mendez PhD, while the Biostatistics/Bioinformatic Unit achieved the bioinformatics analysis, both at the Institute for Research in Biomedicine, IRB Barcelona, Barcelona, Spain.

3.2.6.1 Crosslinking

Sertoli cells were grown until 80% confluence in 100 mm diameter plates and washed twice with cold PBS to eliminate any remain of culture medium. For crosslinking, the cells were incubated for 10 minutes with 1% formaldehyde in PBS at room temperature with gentle agitation. Then, 1 M glycine was added to the plates to obtain a final concentration of 0.25 M glycine and incubated for 5 minutes with soft agitation at room temperature to stop the crosslinking. Cells were washed twice with PBS and then the extracts were obtained as described in **3.2.2.**

3.2.6.2 Antibody covalent binding to Dynabeads

Dynabeads [50 uL] were transferred to a 1.5 mL tube, washed twice with and resuspended in 600 uL PBS. The same amount of each antibody used [rabbit IgG, anti-ctMGS, anti-pSer640MGS, anti-Ago2] was added to dynabeads suspension and incubated for 2 hours on a wheel rotator at room temperature. Next, the suspension was washed once with PBS, twice with 0.2 M triethanolamine pH 8.2, and then incubated with 1 mL of 20 mM dimethyl pimelimidate*2HCl [DMP] in triethanolamine for 30 minutes on a wheel rotator at room temperature. DMP was used to induce the covalent binding of the antibodies to the protein A Dynabeads. The reaction was stopped with 2 washes with 0.05 M glycine for 5 minutes at room temperature. The preparation was washed 3 times with PBS and then incubated with 600 uL of 0.1 M citric acid pH 3.0 for 2 minutes on a wheel rotator at room temperature to remove free antibodies. Finally, coupled antibodies to protein A Dynabeads were washed twice with lysis buffer [RIPA] and resuspended with 500 uL of the same buffer supplemented with protease inhibitors.

3.2.6.3 Immunoprecipitation

Dynabeads protein A [25 uL] were washed twice with PBS and then used for pre-clearing approximately 500-600 uL of cellular extract [from **3.2.2**]. Pre-clearing was performed by incubating the mixture for 30 minutes at 4ºC on a wheel rotator. An aliquot of 50 uL of the cellular extract was taken before making the pre-clear as an input for the Western blot, while 200 uL of the input were saved for total RNA extraction. The antibodies conjugated to protein A Dynabeads were incubated with the pre-cleared cellular extracts during 4 hours on a wheel rotator at 4ºC, to immunoprecipitate the desired proteins depending on the used antibody. After the 4 hours, magnetic protein A Dynabeads were concentrated using a magnetic rack [MagnaRack] for 1.5 mL tubes, and an aliquot of 50 uL of the unbounded extract was taken from each sample as "unbound" for the Western blot. The rest of the unbounded extract was discarded and the magnetic beads were washed 10 times with RIPA buffer. After the last wash, the immunoprecipitated extract with the magnetic beads was resuspended with 1 mL of RIPA, where 300 uL were used to verify if the immunoprecipitation was successful by Western blot. The remaining 700 uL were used for RNA extraction. The immunoprecipitated fraction for Western blot, as well as, input and unbound extracts were resuspended in 30 uL of sample buffer. Heated at 95ºC for 5 minutes, briefly pelleted by a spin down, and then only the aqueous portion was loaded on the gel, while the magnetically concentred beads were discarded.

3.2.6.4 Crosslinking reversion, RNA extraction and mRNA expression profiling

Input and immunoprecipitated extracts for RNA purification were firstly treated with 70 ug of proteinase K for 1 hour at 37ºC. Next, to revert

the crosslink, samples were heated to 65ºC for 1 hour. Then, RNA extraction was performed by the phenol-chloroform method using the Trizol reagent as described in http://www.dnaarrays.org/D_SmallTrizol.pdf. Briefly, the RNA was precipitated with isopropanol, washed with 75% ethanol, re-precipitated with ethanol at -20ºC to remove remaining phenol, and washed again with 75% ethanol. The extracts were finally treated with RNAse free DNAse and quantified to assess the concentration and quality of the RNAs with a NanoDrop 2000. Purified RNAs were used to perform an mRNA profiling by using an Affymetrix expression array for mouse genome.

3.2.6.5 Profiling data analysis

Data for microarray analysis was obtained from a single RNA inmunoprecipitation assay. For this reason it was necessary to normalize probe intensities, because probes with minor intensities tend to produce higher fold changes. To produce corrected fold changes, the Bioconductor (Gentleman et al. 2004) function "rma" from the oligo package was used to perform an RMA normalization (Irizarry et al. 2003). The background was corrected, and a quantile normalization and median polish summarization was performed. The summarization was done from the probe level to the probe set level. Fold changes were corrected for probe intensity biases. Gam approximation was used to estimate and remove biases in mean and deviation.

A bayesian posterior probability model was fitted to the adjusted fold changes to compute posterior probabilities in order to identify significantly differentially expressed genes with a false discovery rate of 5% (Rossell et al. 2008).

3.2.7 Amplification of studied sequences

3.2.7.1 RNA extraction and complementary DNA synthesis

Total RNA extraction from tissue and cultured Sertoli cells was made using the Trizol reagent according to the manufacturer instructions. Next, the preparations were treated with the RQ1 RNAse-free DNAse and quantified using NanoDrop 2000. For cDNA synthesis, 1 ug of RNA was retrotranscribed following the MMLV reverse transcriptase [GeneOn 105-100] instructions, to a single strand of complementary DNA [cDNA]. A negative control, to verify any contamination for retrotranscription, a reaction mix without template was used.

3.2.7.2 Polymerase chain reaction PCR

Encoded fragments of genes of interest were obtained from previously synthesised cDNAs from tissue and cell RNA as described in the afore mentioned point. The protocol indicated by the manufacturer of Maximo Taq DNA polymerase was used to amplify the fragments of interest from the cDNA. The amplification program consisted in an initial denaturation for 5 minutes at 94 ºC, 25 cycles of denaturation for 15 seconds at 94º C, annealing for 15 seconds at 55-65 ºC depending of the primers used, and extension for 1 minute at 72º C, and a final extension of 5 minutes at 72 ºC. A negative control was prepared in the absence of template. The amplicons were analysed by 1.5% agarose gel electrophoresis in TAE buffer.

3.2.8 Mass spectrometry analysis

This assay was performed in the Laboratory of Translational Control of Cell Cycle and Differentiation directed by Raúl Mendez PhD, and in the Mass

Spectrometry Core Facility in the Institute for Research in Biomedicine, IRB Barcelona, Barcelona, Spain.

Protein extracts of Sertoli cells, obtained as described on **3.2.2**, were used for corroborate the inmunoprecipitation of glycogen synthase. The enzyme was immunoprecipitated with 3 different antibodies [pSMGS, MGS 3886 and ctMGS] as described in **3.2.6.3**, and the immunoprecipitated extracts were run on a PAGE-SDS gel. The corresponding band for glycogen synthase, by size [≈ 85 kDa], was excised and samples were digested in-gel with trypsin and resuspended in 50 uL 1% formic acid. 4 uL of each sample were loaded to a 180 μm x 2 cm C18 Symmetry trap column [Waters] at a flow rate of 15 μl/min using a nanoAcquity Ultra Performance LC™ chromatographic system [Waters Corp., Milford, MA]. Peptides were separated using a C18 analytical column [BEH130™ 75 mm x 10 cm, 1.7 μm, Waters Corp.] with a 80 min run, comprising three consecutive steps with linear gradients from 1 to 35% B in 60 min, from 35 to 50% B in 5 min, and from 50 % to 85 % B in 3 min, followed by isocratic elution at 85 % B in 10 min and stabilization to initial conditions [A= 0.1% FA in water, B= 0.1% FA in CH3CN]. The column outlet was directly connected to an Advion TriVersa NanoMate [Advion] fitted on an LTQ-FT Ultra mass spectrometer [Thermo]. The mass spectrometer was operated in a data-dependent acquisition [DDA] mode. Survey MS scans were acquired in the FT with the resolution [defined at 400 m/z] set to 100,000. Up to six of the most intense ions per scan were fragmented and detected in the linear ion trap. The ion count target value was 1,000,000 for the survey scan and 50,000 for the MS/MS scan. Target ions already selected for MS/MS were dynamically excluded for 30s. Spray voltage in the NanoMate source was set to 1.70 kV. Capillary voltage and tube lens on the LTQ-FT were tuned to 40 V and 120 V. Minimal signal required to trigger

MS to MS/MS switch was set to 1000 and activation Q was 0.250. The spectrometer was working in positive polarity mode and singly charge state precursors were rejected for fragmentation. At least one blank run before each analysis was performed in order to ensure the absence of cross contamination from previous samples.

A database search was performed with Proteome Discoverer software v1.3 [Thermo] using Sequest search engine and SwissProt database [rodent release 12_05]. Search parameters included trypsin enzyme specificity, allowing for two missed cleavage sites, carbamidomethyl in cysteine as static modification and methionine oxidation as dynamic modifications. Peptide mass tolerance was 10 ppm and the MS/MS tolerance was 0.8 Da. Peptides with a q-value lower than 0.1 were considered as positive identifications with a high confidence level.

3.2.9 Two-dimensional gel electrophoresis of immunoprecipitated MGS

Protein extracts of muscular, brain and Sertoli 42GPA9 cells were obtained using homogenization buffer [10 mM Tris-HCl pH 7.0, 150 mM KF, 15 mM EDTA, 0.6 M sucrose, 15 mM 2-mercaptoethanol, 10 μg/ml leupeptin, 10 μg/ml aprotinin, 10 μg/ml pepstatin, 1 mM benzamidine, 1 mM sodium orthovanadate, 25 nM okadaic acid and 1 mM phenylmethylsulfonyl fluoride] as was described in **3.2.5.1**. From total protein extracts, MGS was immunoprecipitated using the antibody against the C-terminal end of the enzyme as was described in **3.2.6.3**. The pulled down proteins were precipitated overnight with acetone [4:1 acetone:sample] at -20ºC, and then rehydrated with 2D buffer [8M urea, 20mM DTT, 0,5% IPG buffer]. Each sample was loaded on 7 cm IPG strips pH 4-7. The program for isoelectric focusing [IEF] was the following: active re-hydratation 15 hours/50 Volts,

clean I 0,25 hours/250 Volts, clean II 1 hour/1000 Volts, pre-focus 1 hour/4000 Volts, focus 20000 Volts/hour for 8 hours and a stop phase of 500 Volts for 2 hours. After the IEF, the strips were equilibrated for 15 minutes in equilibration buffer [75mM Tris-HCl pH 8.8, 6M urea, 30% v/v glycerol, 2% w/v SDS and 0.002% bromophenol blue] supplemented with fresh DTT to reach a concentration of 65 mM, with a final rinse of the strips with the SDS/Tris-glycine running buffer. Finally, the strips were loaded and run in a 10% SDS-PAGE to finally visualize the immunoprecipitated proteins separated by IEF and molecular weight by silver staining.

4.Results

4.1 Muscle glycogen synthase characterization in Sertoli cells

We have recently reported the expression of the glycogen synthase muscle isoform in testis and that Sertoli cells are the main source for testicular glycogen production (Villarroel-Espíndola et al. 2013). The present work is focused on the characterization of MGS specifically in Sertoli cells, using primary cell cultures and Sertoli 42GPA9 cells as biological models.

MGS mRNA expression was detected by semi quantitative RT-PCR, amplifying the complete transcript of the enzyme [≈ 1 Kb] in testis, primary Sertoli cells, and 42GPA9 Sertoli cells, using muscle extract as a positive control. The detection of MGS mRNA differs among Sertoli cells and testicular extracts. In testicular extracts the enzyme mRNA was barely detected [Figure 3A]. While in primary Sertoli and 42GPA9 Sertoli cells, the identification of MGS mRNA was positive. In the Sertoli cell line, the enzyme messenger was amplified in comparable levels with respect to the positive control [Figure 3A]. Likewise, Western blot analysis of MGS protein expression shows similar band intensities among Sertoli cells and testicular tissue. In testes the enzyme is hardly detectable despite the higher loading observed for tubulin [Figure 3B]. While both Sertoli cell models express similar, but not equal, levels of MGS [Figure 3B]. Apparently more enzyme was detected in Sertoli 42GPA9 cells in comparison with primary Sertoli cells.

These results show that in testes, MGS is concentrated in Sertoli cells. Which is in line with the fact that Sertoli cells contain higher levels of glycogen synthase that results in larger amounts of glycogen with respect to germ cells (Villarroel-Espíndola et al. 2013). Thus, RT-PCR results correlate with Western blot where the MGS signal is almost undetectable in testes and

Figure 3. Sertoli cells express muscle glycogen synthase. A) RT-PCR analysis of cDNAs synthesized from 1 ug of RNA extracted from Muscle, Testis, Primary Sertoli cells and Sertoli 42GPA9 cells. Specific primers for the complete transcript of the MGS were designed to amplify ≈1 Kb region. GAPDH was used as loading control obtaining an amplicon of 104 pair bases. The negative control (-), was made by replacing the template for nuclease-free water in the reaction mix. **B)** Immunodetection by Western blot of MGS, using protein extracts of Muscle, Testis, primary Sertoli cells and Sertoli 42GPA9 cells. A specific antibody against the C-terminal region of glycogen synthase [ctMGS] was used to detect a band of approximately 85 KDa that corresponds to the enzyme. Tubulin detection was used as loading control obtaining a 55 KDa band. For A) and B) Muscle RNA and protein extracts were used as positive controls. **C)** MGS localization by indirect immunofluorescence assay in testicular slides [left], primary Sertoli cells [middle] and Sertoli 42GPA9 cells [left]. MGS detection was performed using the same antibody as in B) in a dilution of 1:200 and a secondary Alexa-488 donkey anti rabbit IgG in a dilution of 1:300. Nuclei were stained with TO-PRO-3 ®. Scale bars: 20 um.

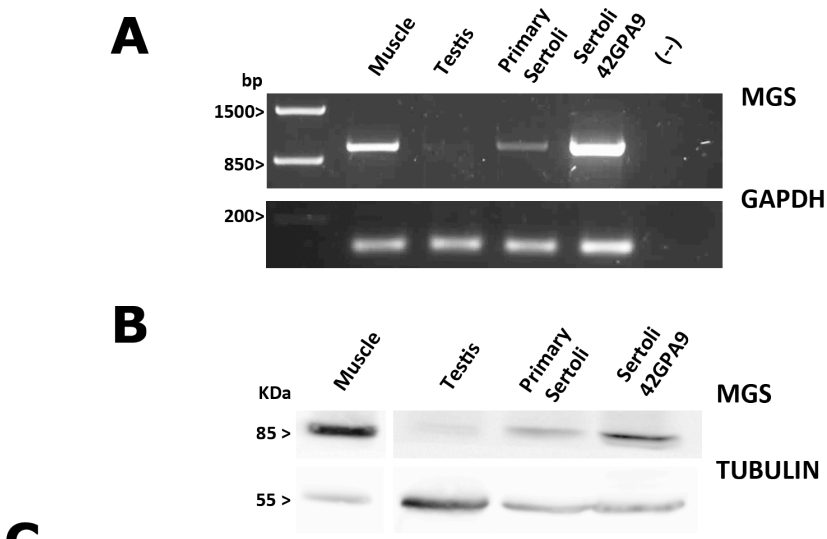
A
Muscle
Testis
Primary Sertoli
Sertoli 42GPA9
(--)
bp
1500>
850>
200>
MGS
GAPDH
B
Muscle
Testis
Primary Sertoli
Sertoli 42GPA9
KDa
85 >
55 >
MGS
TUBULIN

C

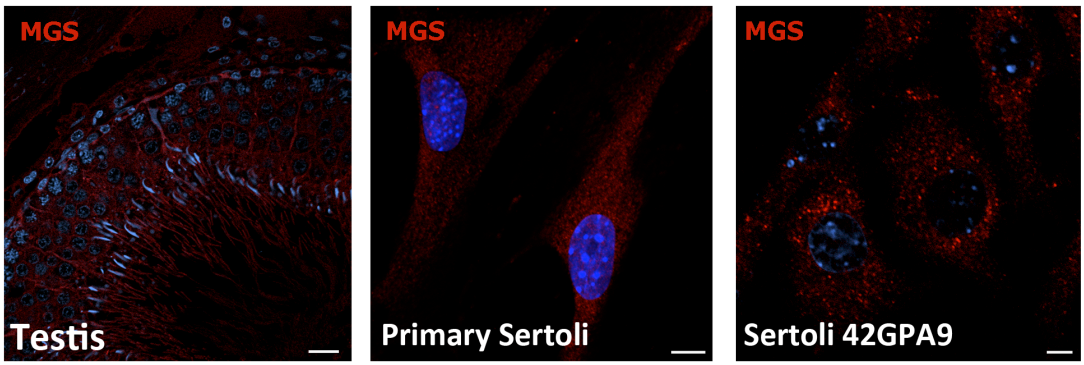
MGS
Testis
MGS
Primary Sertoli
MGS
Sertoli 42GPA9

is higher in Sertoli 42GPA9 cells than in primary Sertoli cells [Figure 3A and 3B]. However, it is important to notice that the expression levels of the enzyme in Sertoli cells and testicular extracts are considerably lower than in muscle.

Next, MGS localization was analysed by confocal immunofluorescence. In testicular slices a dotted pattern of MGS signals across the seminiferous tubule was observed [Figure 3C, left]. This indicates the presence of MGS in all the cellular components of the tubule, from spermatogonia to spermatids and in Sertoli cells, in the same way as was described in (Villarroel-Espíndola et al. 2013). Likewise, the punctuated pattern of MGS immunofluorescent signals was observed homogenously distributed over the cytoplasm of primary and 42GPA9 Sertoli cells [Figure 3C, center and right, respectively].

Transduced human muscle glycogen synthase fused to GFP was described in a nuclear speckled pattern of muscle and adipose cells, which were deprived of glucose and depleted of glycogen reserves (Cid et al. 2005). The same report suggested MGS participation in nuclear processes. This was achieved by blocking MGS nuclear export to the cytoplasm with Leptomicyn B, co-localizing MGS nuclear speckles with a marker of Cajal bodies [p80-coilin], and inhibiting the nuclear localization with transcription inhibitors (Cid et al. 2005). However, there are no reports about the nuclear localization of endogenous MGS in any cell type.

Cellular fractionation of 42GPA9 Sertoli cell was performed to separate nuclear and cytosolic extracts [Figure 4A]. Western blot analysis incubating with two antibodies against MGS, were used to detect the enzyme in both cellular compartments. The first antibody recognizes the C-terminal region of MGS [ctMGS] and detects total unphosphorylated and phosphorylated forms of the enzyme. Meanwhile the second specifically identifies the

phosphorylated form in serine640 [pS640MGS]. Cellular fractionation was verified with tubulin and SC-35 as markers for cytosolic and nuclear extracts, respectively [Figure 4A]. Both MGS antibodies detected the enzyme in cytosolic as in nuclear extracts of Sertoli cells with different levels of intensity [Figure 4A]. In the cytoplasm as in the nucleus, pS640MGS detection was stronger in comparison with the ctMGS signal [Figure 4A], revealing that the phosphorylated form of the enzyme in Ser640 is present in Sertoli cell nuclei. Thus, for the first time, the endogenous enzyme was identified in nuclear extracts with two different antibodies, besides its presence in the cytoplasm.

To confirm the results of cellular fractionation with both MGS antibodies, co-immunofluorescence assays were performed in primary and Sertoli 42GPA9 cells [Figure 4B]. Detection of total and phosphorylated MGS were similar in primary Sertoli cells and Sertoli 42GPA9 cells. For both Sertoli cell types, ctMGS fluorescent signals were homogenously distributed over the cytoplasm, while the nuclear localization was almost undetectable [Figure 4B, upper left, and lower left]. Likewise, pS640MGS was homogenously distributed in the cytoplasm and also in a nuclear speckled pattern [Figure 4B, upper right, and lower center]. For Sertoli 42GPA9 cells, the nuclear localization of pS640MGS was confirmed by the co-localization with the splicing factor SC-35 [Figure 4B, right]. Therefore, these results indicate that endogenous MGS, and specifically the phosphorylated form in Ser640, is present in both, the cytoplasm and in the nuclei of Sertoli cells.

After the analysis of MGS expression and cellular localization, and to continue with the characterization of MGS, the activity rates of the enzyme were analysed in both Sertoli cell types. Different reports about glycogen content in testes describe that glycogen amounts decrease after the first post-

Figure 4. pS640MGS is located in the cytoplasm and nucleus of Sertoli cells. A) Cytoplasmic [C] and nuclear [N] extracts that were obtained by cellular fractionation and analysed by Western blot to detect total MGS and the phosphorylated form of the enzyme in Serine 640 with the ctMGS and pS640MGS antibodies, respectively. Tubulin detection was used as a cytoplasmic control, while the splicing factor SC-35 was the control for purified nuclear extracts. Representative images of three independent assays are shown. In **B)**, MGS immunolocalization was performed in primary Sertoli cells [upper panels] and Sertoli 42GPA9 cells [lower panels], by using the same antibodies than in A). ctMGS and pS640MGS antibodies were used in a dilution of 1:200, while the secondary antibody Alexa-488 donkey anti rabbit IgG in a dilution of 1:300. SC35 was detected with an antibody dilution of 1:250 and conjugated with an Alexa-568 donkey anti mouse IgG secondary antibody. Nuclei were stained with DAPI ®. Scale bars: 20um.

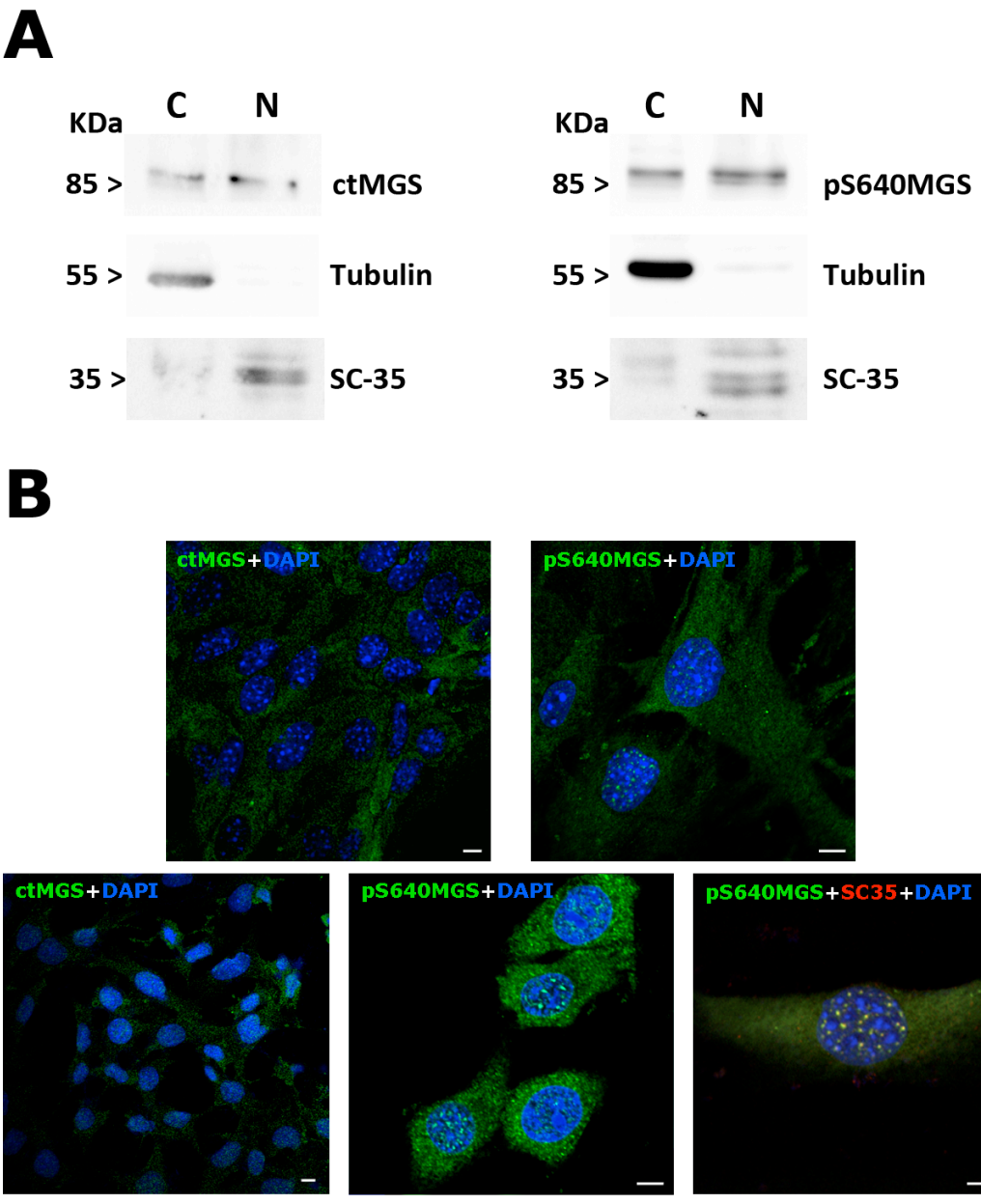
A
KDa
C
N
85 >
ctMGS
55 >
Tubulin
35 >
SC-35
KDa
C
N
85 >
pS640MGS
55 >
Tubulin
35 >
SC-35
B
ctMGS+DAPI
pS640MGS+DAPI
ctMGS+DAPI
pS640MGS+DAPI
pS640MGS+SC35+DAPI

natal day (Gunaga et al. 1972, Leiderman & Mancini 1969). Additionally, other authors show that activity rates of glycogen synthase in testes are very low, while glycogen phosphorylase is much higher, concluding that glycogen amounts in testes of sexually mature animals are scarce. There are two important points to consider about this evidence: first, those studies used experimental techniques based on testicular polysaccharide staining, which is not specific for glycogen and the quantification is difficult; second, all of these studies were focused on the whole tissue without discriminating each cellular component of the testes. For these reasons and to functionally characterize the enzyme in these biological models, the activity rate of MGS was studied.

Glycogen synthase activity was measured as mUnits of glycogen synthase per milligram of proteins [umol UDP-^{14}C-glucose/min*mg protein] in the absence and presence of the allosteric activator glucose-6-phosphate [G6P]. The obtained activity values in the absence of G6P correspond to the enzyme that is intrinsically active. Meanwhile, the values acquired in the presence of the allosteric activator represent the total activity, which corresponds to the whole amount of the enzyme present in the cell extract. A very good approach to determine the proportion of the enzyme that is effectively active from the complete amount is the activity ratio -G6P/+G6P, where values below 0.1 indicate a fully inactive enzyme, and those above 0.7 are equivalent to a complete activation (Guinovart et al. 1979). In primary Sertoli cell extracts, intrinsic glycogen synthase activity was 0.146±0.019 mU/mg protein, while the total activity reached 5.101±0.446 mU/mg protein, and the activity ratio –G6P/+G6P was 0.0287±0.0043 [Figure 5, up]. Similar results where obtained in the Sertoli 42GPA9 cell line, where the activity rates in the absence of G6P was 0.176±0.023 mU/mg protein, in the presence of G6P 7.308±0.382 mU/mg protein and the activity ratio –G6P/+G6P,

Figure 5. MGS is almost inactive in Sertoli cells. Activity rates of primary Sertoli cell and Sertoli 42GPA9 cell extracts. Both were measured as mUnits of glycogen synthase per milligram of proteins [umol UDP-^{14}C-glucose/min*mg protein] in the absence [graphs in left, black bars] and presence [graphs in left, white bars] of the allosteric activator glucose-6-phosphate [G6P]. The graphs on the right represent the ratio between –G6P/+G6P activity rates, obtained for both Sertoli cell types and shown in the left graphs. Each graph indicates the mean and standard deviation of three independent experiments.

Primary Sertoli cells

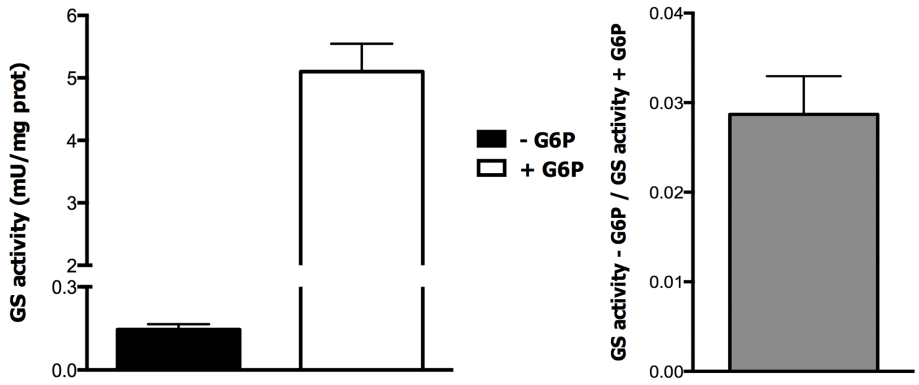

Sertoli 42GPA9 cells

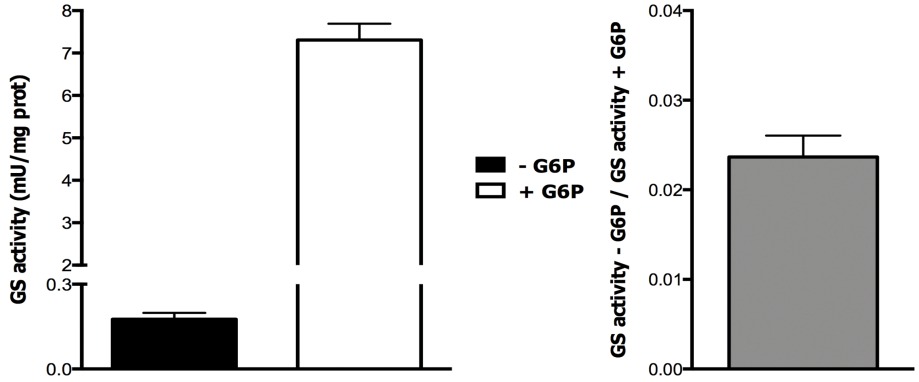

0.0237±0.0024 [Figure 5, down]. Intrinsic activity values in both Sertoli cell types were very low, indicating that MGS is almost inactive. Sertoli cell line 42GPA9 showed higher values for total activity than the primary cells, corroborating the higher levels of the enzyme observed in the Figure 3. Total activity rates reached values 40 times higher in comparison with the intrinsic ones [Figure 5], demonstrating that MGS is effectively present but almost inactive in primary and 42GPA9 Sertoli cell extracts. For both Sertoli cell types, -G6P/+G6P activity ratios were no more than 0.03, confirming that only a very small part from the total MGS is active MGS and that almost all of the enzyme present is inactive.

Another way to evaluate the MGS activity in Sertoli cells is analysing the phosphorylation state of the enzyme. Casein kinase II phosphorylates MGS Ser-656 [site 5, Figure 2], which is needed as a priming site for the GSK3 hierarchical phosphorylation of Ser-652, Ser-648, Ser-644 and Ser-640 [sites 4, 3c, 3b and 3a, respectively, Figure 2] (Roach 1990, Skurat et al. 1994). This indicates that Ser-640 residue is the last site for GSK3 phosphorylation once casein kinase II begins to phosphorylate MGS. It has been reported, by Ser to Ala mutations, that sites 3b and 3a together with site 2 [Ser-7], were the most effective to promote the activation of MGS (Friedman & Larner 1963, Skurat et al. 1994). For this reason, the phosphorylation state of MGS in Sertoli cells was evaluated.

Levels of total and phosphorylated MGS were compared previous and after phosphatase treatment. Total MGS was detected with the ct-MGS and the 3886 antibodies, while the phosphorylated enzyme was detected with the pS640MGS antibody, both in the presence and the absence of a wide range phosphatase in Sertoli cells [Figure 6]. Comparable results were obtained in primary and 42GPA9 Sertoli cells, corroborating the utilization of the cell line

Figure 6. Muscle glycogen synthase presents a highly phosphorylated state in Sertoli cells. Western blot analysis of primary Sertoli cell [up] and Sertoli 42GPA9 cell [down] extracts were treated [+] or not [-] with 200 units of λ Phosphatase, and then incubated with antibodies against total MGS [ctMGS] and its phosphorylated form in Serine 640 [pSer640MGS]. Graphs on right represent the quantification of band intensities as relative abundance for both MGS detections, taking as control the bands in the absence of λ Phosphatase and normalizing them with tubulin signal. Each graph indicates the mean and standard deviation of three independent experiments.

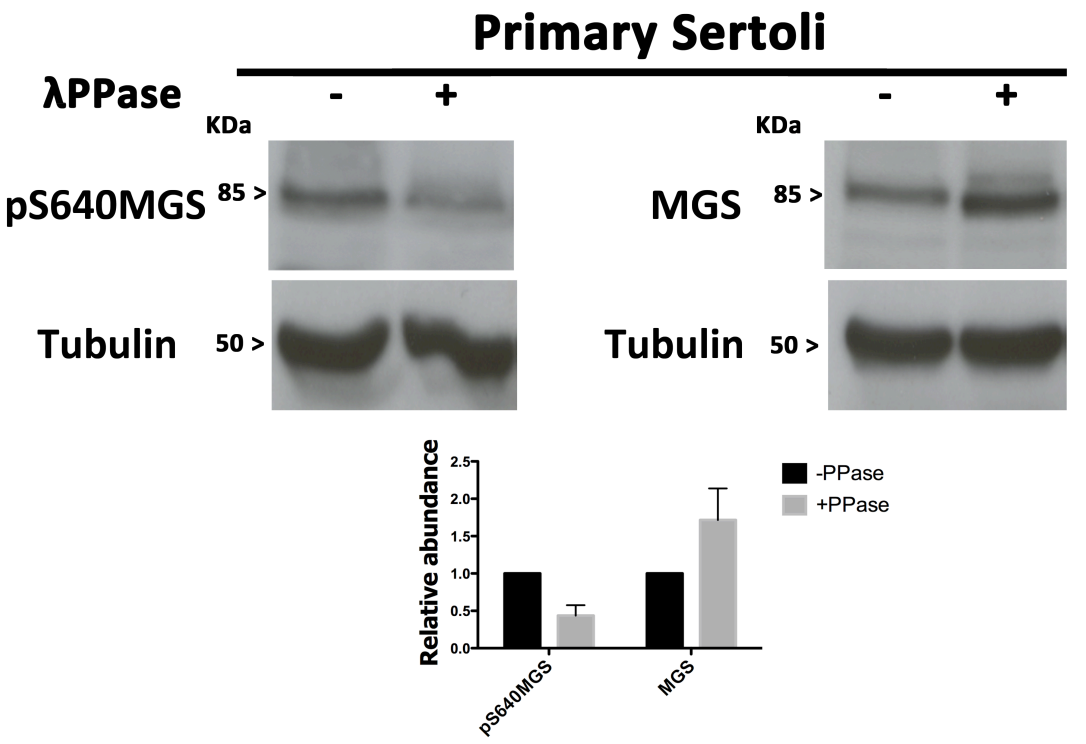
Primary Sertoli
λPPase
-
+
-
+
KDa
KDa
pS640MGS
85 >
MGS
85 >
Tubulin
50 >
Tubulin
50 >
Relative abundance
2.5
2.0
1.5
1.0
0.5
0.0
-PPase
+PPase
pS640MGS
MGS

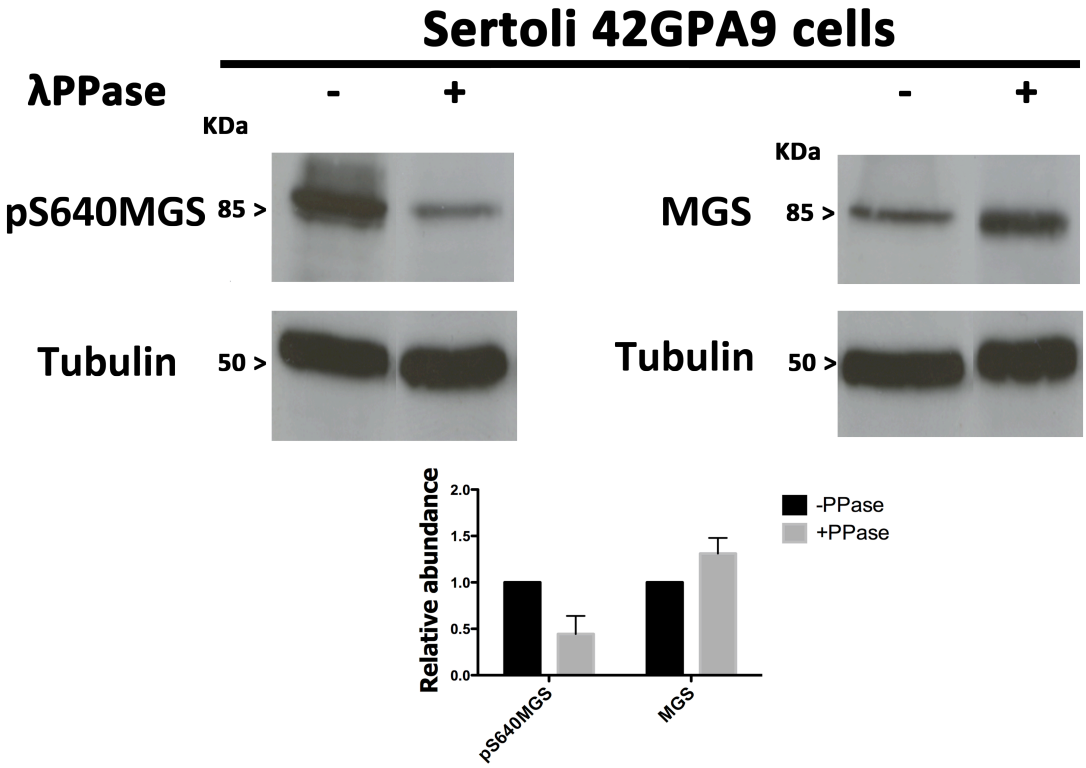
Sertoli 42GPA9 cells
λPPase
-
+
-
+
KDa
KDa
pS640MGS
85 >
MGS
85 >
Tubulin
50 >
Tubulin
50 >
Relative abundance
2.0
1.5
1.0
0.5
0.0
-PPase
+PPase
pS640MGS
MGS

as a model for this study. Treatments with λ phosphatase successfully produced a decrease in the pS640MGS signals in comparison with non-treated cells [Figure 6]. This decrease in the phosphorylation signal for pS640MGS does not correspond to a difference in protein loading, because tubulin signals are similar in each line [Figure 6]. After quantifying the pS640MGS signals in treated and non-treated extracts, and normalizing them with tubulin, we determined that treatments produced a decrease in nearly half of the levels of pS640MGS [Figure 6]. On the other hand, after phosphatase treatments total MGS detection showed a band that runs faster in comparison with the total MGS band of non-treated extracts [Figure 6]. This reveals that MGS could be present in a highly phosphorylated state. Moreover, λ phosphatase treatments do not produce a decrease in the signals of total MGS as was observed for pS640MGS, proving that the enzyme is being dephosphorylated and not degraded [Figure 6]. Additionally, the use of antibodies against total MGS in the presence of λ phosphatase seemed to make the enzyme more immunoreactive in comparison to non-treated cells [Figure 6]. In turn, the intensification of the quantified total MGS signals after λ phosphatase treatments corresponds to a 50% increase of the observed signal in non-treated Sertoli cell extracts [Figure 6]. These results suggest that MGS could be present in a high phosphorylation state, and that the antibodies against the total MGS are able to detect the enzyme more easily when it is dephosphorylated. The suggested high phosphorylation state for MGS reinforces the idea that this enzyme is almost inactive in Sertoli cells.

Reported post-translational modifications of MGS are exclusively related to phosphorylation of different serine residues (Poulter et al. 1988). The enzyme has been described to be phosphorylated by several kinases on 9 serine residues that are grouped into 4 phosphorylation clusters modulating

the MGS activity [see Figure 2 dotted lines], but always depending on G6P concentrations (Bouskila et al. 2010, Palm et al. 2013). The importance of these clusters is that single residue phosphorylation does not affect the MGS activity. While during a combinational or clustering phosphorylation, the enzyme activity decreases (Roach 1990, Skurat et al. 1994). These effects add relevance to the phosphorylation pattern of MGS, because its activity can be modulated by the combination of different phosphorylation sites, and this is directly associated to the activation of the different kinases. For these reasons, two dimensional gel electrophoresis was performed to elucidate the pattern of MGS post-translational modifications.

Immunoprecipitated MGS, with the ct-MGS antibody, was obtained from muscle, brain, and Sertoli 42GPA9 cell extracts. The immunoprecipitated extracts were loaded and separated firstly by isoelectric focusing. Then, the separated proteins by their isoelectric point were run and separated by molecular weight in an SDS-PAGE gel and visualized by silver staining [Figure 7]. Muscle immunoprecipitated MGS was observed in a four spot pattern between pH 6,36-6,77 [Figure 7, upper gel]. In the case of brain immunoprecipitated MGS, 3 spots between pH 6,30-6,67 were observed, and another set localized more in the middle of the gel approximately to pH 5.8 [Figure 7, middle gel]. Meanwhile, Sertoli immunoprecipitated MGS was spotted in two different forms: one more basic localized in pH 7; and another set of eight spots more acidic ranging to the pH 5.55-6.35 [Figure 7 bottom gel].

MGS separation by 2D gel electrophoresis of muscle and brain MGS showed a similar pattern in the more basic MGS forms [pH 6,3-6,7]. However, only the brain and not the muscle MGS was spotted in the more acidic pH [5,8]. In contrast, Sertoli MGS presented a clearly different pattern

Figure 7. Sertoli muscle glycogen synthase presents a different two-dimensional gel electrophoresis pattern in comparison with muscle and brain. Five hundred micrograms of muscular, brain and Sertoli cell extracts were used to immunoprecipitate the MGS. Each pulled down extract was precipitated overnight with acetone and then solubilized with solubilisation buffer supplemented with 8M urea, 20 mM DTT and 0.5% IPG buffer. Samples were separated firstly by isoelectric focusing between pH 4-7, and subsequently by molecular weight in a 10% SDS-PAGE. Finally, immunoprecipitated proteins were visualized by silver stain. Black squares indicate the different patterns of MGS forms in each gel.

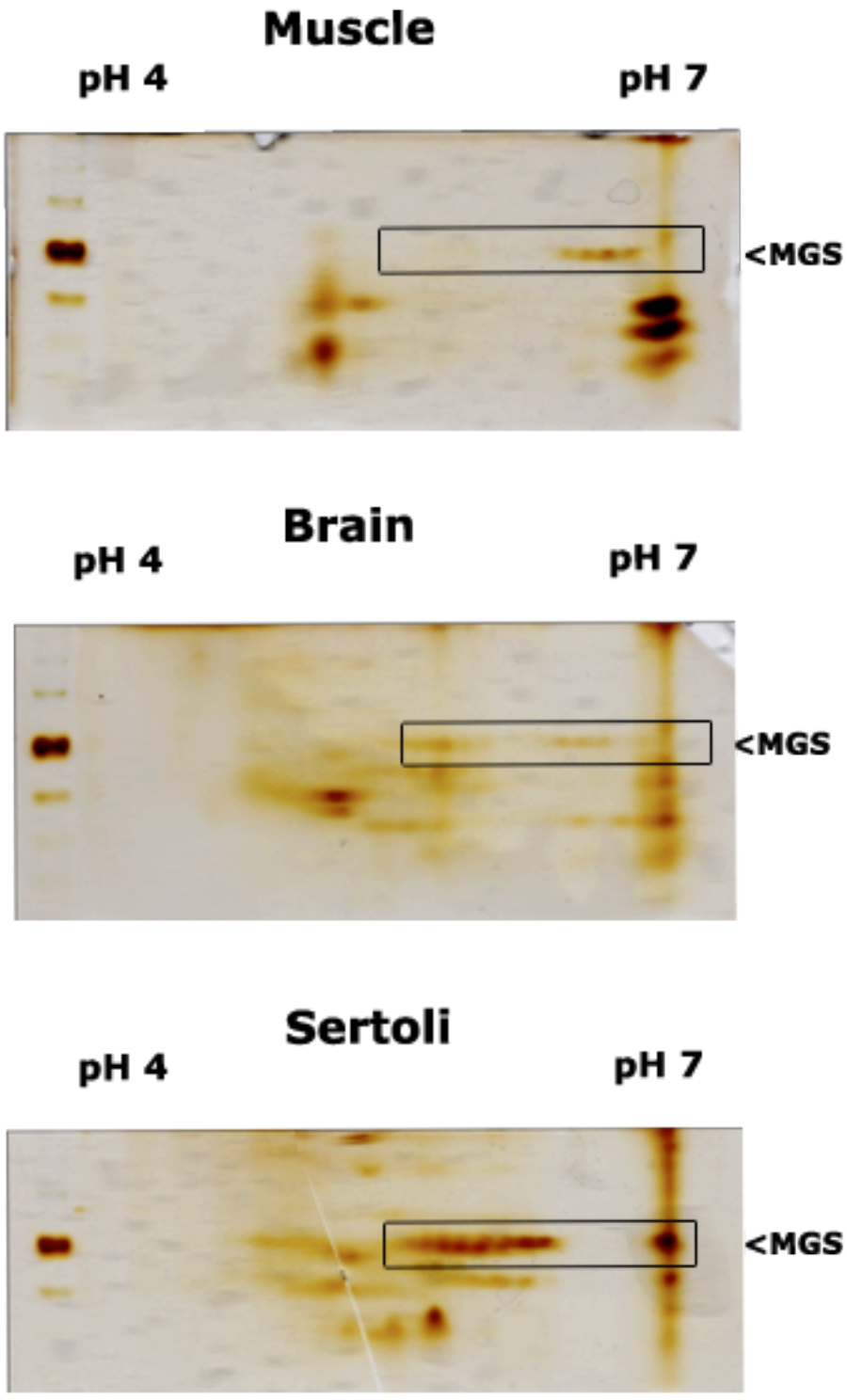
Muscle
pH 4
pH 7
<MGS
Brain
pH 4
pH 7
<MGS
Sertoli
pH 4
pH 7
<MGS

when compared with the muscle and brain forms. The basic spot in pH 7 was not present in muscle nor in the brain. Also the more acidic eight spot pattern between the pH 5,55-6,35 was not observed for the muscle form, but could be similar to the more positive spots visualized for the brain MGS form. Thus, these results showed that Sertoli cells present a different form of the enzyme in comparison with muscle and brain. Also an important point to highlight is the presence of two populations of the enzyme. The MGS spots localized to more acidic pH of the 2D gel electrophoresis agrees with the activity and phosphatase assays, because they can also be associated with the high levels of MGS phosphorylation and inactivity.

Overexpression of PTG [Protein Targeting to Glycogen] is a valuable approach to induce glycogen synthase activity. This scaffold protein is responsible to drive the Protein Phosphatase 1 [PP1] to glycogen, where glycogen synthase is situated. Once situated in glycogen, PP1 is able to dephosphorylate and activate the enzyme stimulating the accumulation of glycogen. This experimental methodology was used in this work to evaluate how susceptible is MGS to dephosphorylation when PTG is overexpressed. Since this should activate the total amount of the expressed enzyme even in the absence of the allosteric activator G6P.

PTG overexpression was achieved through the infection with adenoviral particles that encode GFP, as a control, and GFP-PTG in both Sertoli cell models. After 48 hours of infection, Sertoli cells expressed both GFP and GFP-PTG, so all the adenoviral infection related experiments were made in this time lapse [data not shown]. In the absence of the allosteric activator G6P very low activity rates of MGS were described, 0.146±0.019 mU/mg protein and 0.176±0.013 f mU/mg protein for primary and 42GPA9 Sertoli cells, respectively [Figure 5 and 8A]. However, when PTG is

Figure 8. Muscle glycogen synthase is susceptible to activation by Protein Targeting [PTG] overexpression in Sertoli cells. Primary Sertoli cells and Sertoli 42GPA9 cells were transduced with adenoviral particles to overexpress GFP [Ad GFP], as an infection control, and PTG-GFP [Ad PTG] to activate the enzyme. The overexpression of GFP and PTG-GFP was corroborated by fluorescent microscopy. Maximal fluorescent signals were detected after 48 hours post infection for both, AdGFP and AdPTG. The MGS activity rates of primary Sertoli cells [black bars], Sertoli 42GPA9 cells [white bars] and PTG-transduced Sertoli 42GPA9 cells [grey bars] in the absence, **A)**, and presence, **B)**, of the allosteric activator glucose-6-phosphate [G6P] are shown. **C)** These values were used to determine the ratio between the activity rates –G6P/+G6P. Each graph indicates the mean and standard deviation of three independent experiments. **D)** Glycogen content measurement of non-infected, AdGFP transduced [GFP] and AdPTG-GFP transduced primary Sertoli cells [black bars] and Sertoli 42GPA9 cells [white bars]. The values are shown as fold change over the AdGFP transduced Sertoli cells of a single experiment.

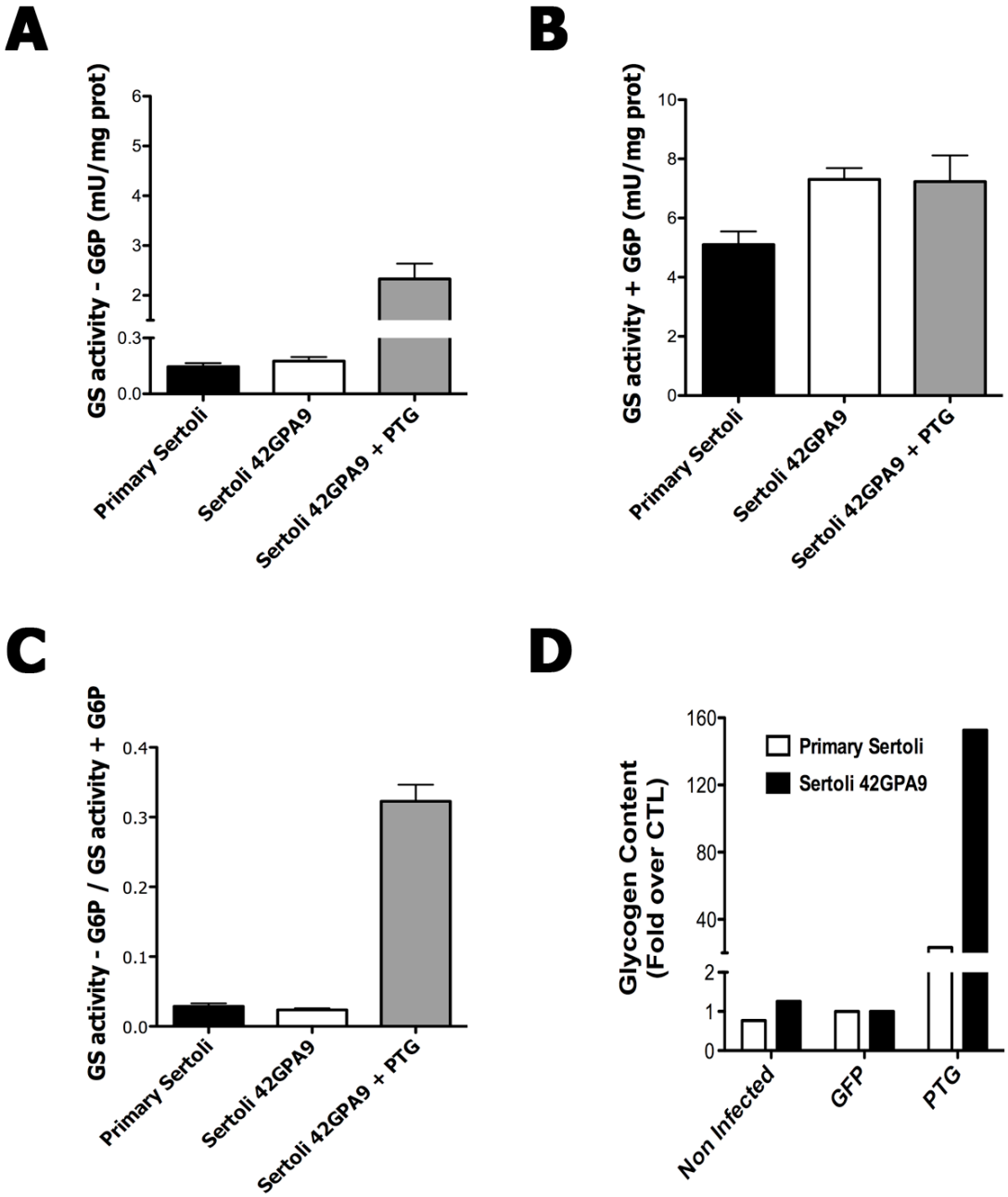
A
GS activity - G6P (mU/mg prot)
6
5
4
3
2
0.3
0.0
Primary Sertoli
Sertoli 42GPA9
Sertoli 42GPA9 + PTG
B
GS activity + G6P (mU/mg prot)
10
8
6
4
2
0
Primary Sertoli
Sertoli 42GPA9
Sertoli 42GPA9 + PTG
C
GS activity - G6P / GS activity + G6P
0.4
0.3
0.2
0.1
0.0
Primary Sertoli
Sertoli 42GPA9
Sertoli 42GPA9 + PTG
D
Glycogen Content
(Fold over CTL)
160
120
80
40
2
1
0
Primary Sertoli
Sertoli 42GPA9
Non Infected
GFP
PTG

overexpressed, the enzyme activity increased approximately 15 times, reaching 2.331±0.178 mU/mg protein [Figure 8A, grey bar]. This means that PTG overexpression effectively induced the activation of MGS in Sertoli cells. Nevertheless, the activation magnitude is not total nor affects the whole amount of the expressed enzyme because it does not reach total activity values. This was demonstrated in the same activity assays but in the presence of the allosteric activator, where similar levels of activation were observed in non infected [7.308±0.382 mU/mg protein], and in PTG infected 42GPA9 cells [7.231±0.512 mU/mg protein] [Figure 8B, white and gray bars], proving that higher glycogen synthase activity rates during PTG overexpression were not due to an increase in MGS expression. Similarly, activity ratio –G6P/+G6P analyses indicated that in Sertoli cells that overexpress PTG this ratio rises to 0.323±0.0136, from the observed 0.0287±0.0043 and 0.0237±0.0024 in non-infected primary and 42GPA9 Sertoli cells, respectively [Figure 8C].

All the obtained activity data reveals that PTG overexpression was unable to induce a complete activation of MGS, because in the absence of external G6P, the activity values increased only to one third with respect to what was observed in the presence of the allosteric activator. Also, this is reinforced by the activity ratio –G6P/+G6P value in PTG infected cells [≈0.323], which did not reveal total activation of the enzyme that is described to be 0.7 or more (Guinovart et al. 1979).

To validate the activation of the enzyme, glycogen content measuring was performed in AdPTG infected Sertoli cells using AdGFP infection as a control [Figure 8D]. Glycogen amounts of non-infected primary and 42GPA9 Sertoli cells were very similar in comparison with the control of infection [GFP, Figure 8D]. Meanwhile in AdPTG infected cells, glycogen content

increased ≈30 times and ≈150 times, in primary and 42GPA9 Sertoli cells, respectively [Figure 8D]. This reveals that despite the partial activation of MGS in AdPTG infected Sertoli cells, the fraction of activated enzyme is capable of synthesizing larger amounts of glycogen. No statistical analysis was made because the large differences of the obtained values for intrinsic activity and glycogen content between control [AdGFP] and AdPTG infected cells.

Another experimental methodology described to activate glycogen synthesis is the treatment with lithium salts. Lithium indirectly activates glycogen synthesis through the inhibition of Glycogen Synthase Kinase 3 [GSK3], which is constitutively active and phosphorylates key residues that regulate glycogen synthase activity [Ser640]. This ion acts as an inhibitor of mammalian GSK3 by competing for Magnesium [Mg^{2+}], but not for the substrate or ATP sites (Ryves & Harwood 2001). In 3T3-L1 adipocytes and L6 myotubes, lithium chloride treatments induce glucose incorporation and glycogen synthesis, exhibiting an insulin-like behaviour, without preventing the desensitization of glycogen synthase activity after chronic insulin treatments (MacAulay et al. 2003, Oreña et al. 2000). In these reports, lithium treatments were performed using millimolar concentrations [50 mM]. Therefore, to study the activation of MGS by lithium treatments, 90mM LiCl was used considering the low levels of intrinsic activity and higher level of phosphorylation in both Sertoli cell types.

In the absence of G6P, intrinsic activity of MGS in 42GPA9 Sertoli cells [0.176±0.023 mU/mg protein] was slightly increased during lithium chloride treatments [0.246±0.019 mU/mg protein] [Figure 9A]. By contrast, in the presence of G6P total activity of the enzyme suffered a decrease from 7.308±0.382 mU/mg protein to 4.460±0.395 mU/mg protein after lithium chloride was added [Figure 8A]. This suggests that lithium treatments cause a

Figure 9. Muscle glycogen synthase is weakly activated by lithium treatment in Sertoli cells. A) MGS activity rates in the absence [-G6P] and presence [+G6P] of the allosteric activator glucose-6-phosphate, in non-treated [CTL, black bars] and 90 mM lithium chloride treated [Li, grey bars] Sertoli 42GPA9 cells. **B)** The values in A) were used to calculate the ratio –G6P/+G6P of the activity rates, in non-treated [CTL, black bars] and 90 mM lithium chloride treated [Li, grey bars] Sertoli 42GPA9 cells. Each graph indicates the mean and standard deviation of three independent experiments. **C)** Glycogen content quantification in non-treated [CTL] and 90mM lithium chloride treated primary Sertoli cells [black bars] and Sertoli 42GPA9 cells [white bars]. Values of single experiment are expressed as the fold change over the non-treated cells.

A

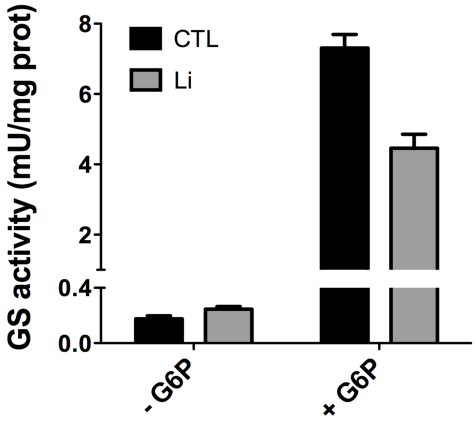
GS activity (mU/mg prot)
CTL
Li
8
6
4
2
0.4
0.0
- G6P
+ G6P

B

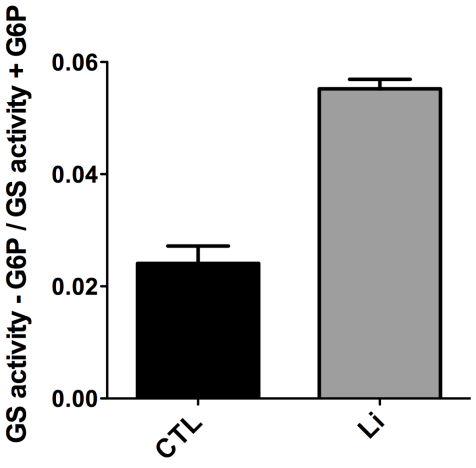
GS activity - G6P / GS activity + G6P
0.06
0.04
0.02
0.00
CTL
Li

C

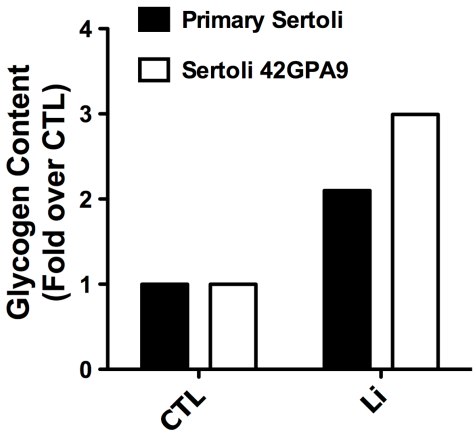
Glycogen Content
(Fold over CTL)
Primary Sertoli
Sertoli 42GPA9
4
3
2
1
0
CTL
Li

decline in the expression of MGS in Sertoli cells. Then, by analysing the activity ratio –G6P/+G6P, lithium treated cells showed a 2-fold increase compared to non-treated cells [0.0241±0.0018 to 0.0552±0.001] [Figure 9B].

This increase is still not sufficient to activate the enzyme, and this was corroborated by glycogen accumulation measurements. For both Sertoli cell types, lithium produced a small increment in glycogen content comparable to the one observed in non-treated control. The rise in the glycogen content was approximately 2.1 and 3 times in primary and 42GPA9 Sertoli cells, respectively [Figure 9C]. Thus, these results revealed that lithium treatments caused a decrease in the total activity of MGS, which in turn, affects the total levels of functional MGS in Sertoli cells. Additionally, the small portion of MGS that is activated was capable only of duplicating and triplicating the glycogen content for primary and 42GPA9 Sertoli cells, respectively.

In muscular, fibroblast, and hepatic cells, GFP-MGS fusion protein was described to translocate from the nucleus to the cortex of the cells, near the membrane, where glycogen synthesis starts in response to glucose treatments (Cid et al. 2005, Fernández-Novell et al. 1997, Ferrer et al. 1997). This behaviour denotes that MGS is an enzyme that can change its subcellular localization in response to external stimulus.

For this reason and for the observed effects of lithium in the enzyme activity, MGS localization analyses during lithium treatments of Sertoli cells were carried out. By confocal immunofluorescence of Sertoli 42GPA9 cells, total MGS and pS640MGS localization was analysed in non-treated [control] cells versus lithium chloride treated cells [30mM and 90mM]. In control cells, total MGS was homogenously distributed in a dotted pattern over the cytoplasm [Figure 10A, up and left]. During lithium treatments with 30 and 90 millimolar, MGS was accumulated in cytoplasmic granules that were no more

Figure 10. Lihtium treatments induce the formation of cytosolic granules of glycogen synthase in Sertoli cells. A) and **B)**, confocal immunofluorescent images of fixed and permeabilized cells that were incubated with antibodies against total MGS [MGS] and its phosphorylated form in Serine 640 [pS640MGS] in a dilution of 1:200. The secondary antibody Alexa-488 donkey anti rabbit IgG was used in a dilution of 1:300. Nuclei were stained with propidium iodide [PI]. Scale bars 20 um. In **A),** non-treated [Control], 30mM lithium chloride treated [30mM Li^+] and 90mM lithium chloride treated [90mM Li^+] Sertoli 42GPA9 cells were used to detect total MGS [up] and pS640MGS [down]. In **B),** primary Sertoli cells of mice treated with 6 umol Li_2CO_3 per day during 30 days were assessed. These primary cultures were mantained for two [left] and 8 days [rigth] before the fixation. Then total MGS [left] and pS640MGS [rigth] were detected. Phase contrast is shown to visualize the shape and vacuolization of the cells. [both images up]. **C)** Transmission electronic microscopy analysis of 90mM lithium chloride treated Sertoli 42GPA9 cells. Scale bar, 250 nm. A zoom-in of the interested region of Sertoli cell cytoplasm is shown in the lower image. Scale bar, 50 nm.

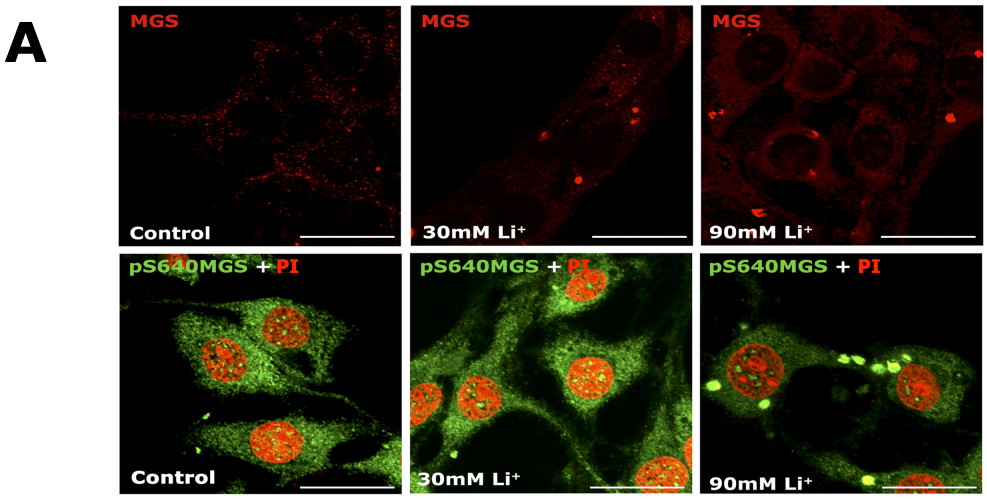
A
MGS
MGS
MGS
Control
30mM Li+
90mM Li+
pS640MGS + PI
pS640MGS + PI
pS640MGS + PI
Control
30mM Li+
90mM Li+

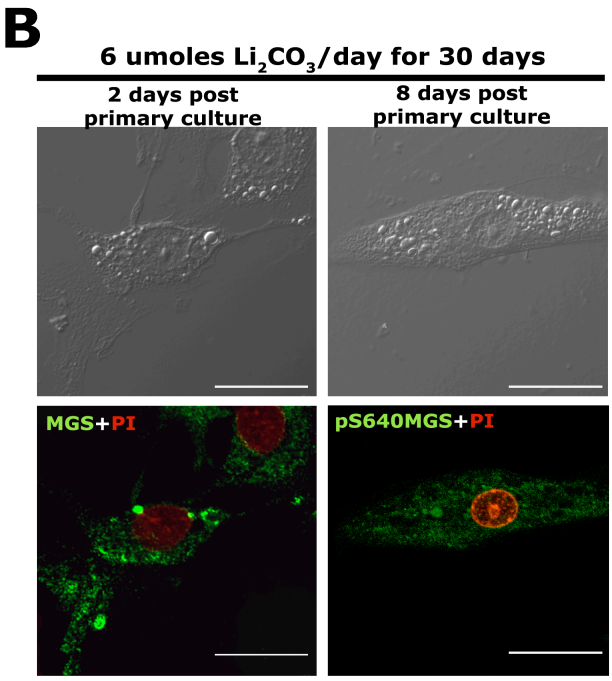
B
6 umoles Li2CO3/day for 30 days
2 days post primary culture
8 days post primary culture
MGS+PI
pS640MGS+PI

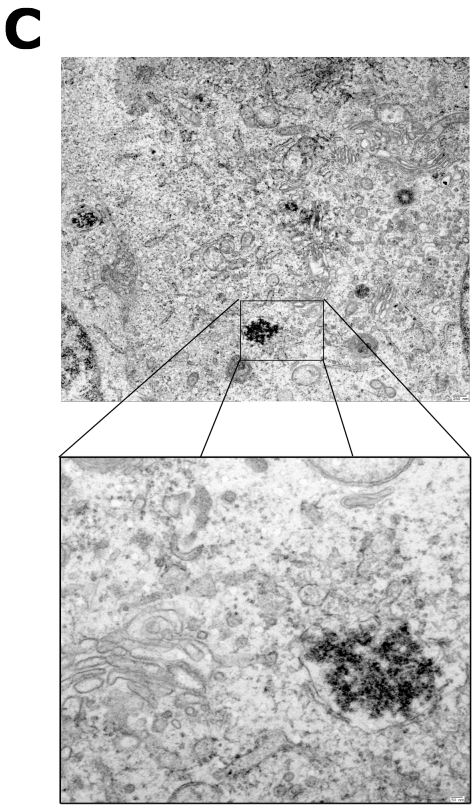
C

than two or three per cell [Figure 10A, up center and right]. The pS640MGS was found dispersed in the cytoplasm with a nuclear-speckled pattern [Figure 10A, down and left]. Corresponding to what was observed with the total MGS immunolocalization, a cytoplasmic granule accumulation of the phosphorylated enzyme was visualized during lithium treatments [Figure 10A, down center and right]. Any MGS granule was observed by treating Sertoli cells with NaCl, proving that lithium was the responsible for the MGS granule formation and to discard the influence of the hyperosmotic effect [data not shown].

Lithium effects on testicular cells have been reported to be ambiguous. Some of them refer to lithium as a toxic agent for testicular cells, thus causing deleterious effects on the seminiferous epithelium. By contrast, others have shown that this ion has positive effects by protecting testes from the damage caused by cadmium (Al-Azemi et al. 2010, Banerji et al. 2001, Thakur et al. 2003, Zarnescu & Zamfirescu 2006). All these studies have focused their experimental procedures on histological and ultra-structural analysis of the seminiferous tubule, without investigating the molecular events where lithium takes place. In the present work, we decided to corroborate *in vivo* the observed effects in the cell line 42GPA9 regarding MGS re-localization [Figure 10A]. To prove this, mice were treated with therapeutic doses of 6 umoles per day of lithium carbonate [Li_2CO_3] for 30 days. Then, primary cell cultures of Sertoli cells from treated mice were maintained for two and eight days post-primary culture. After this time interval, cells were fixed and assayed by confocal immunofluorescence, confirming the cytosolic accumulation in a granule like structure of the MGS at both days [Figure 10B, down]. Additionally, primary Sertoli cells presented numerous vacuoles in the cytoplasm, which is an evident sign of stress [Figure 10B, up].

To elucidate the ultra-structural characteristics of these cytoplasmic granules, the samples were assessed by transmission electron microscopy [TEM]. Sertoli 42GPA9 cells were treated with 90mM LiCl for 24 hours before fixation, and TEM analysis showed the formation of an electrodense structure in the cytoplasm [Figure 10B, zoom out]. Interestingly, this electrodense structure viewed in a higher zoom has a glycogen like shape [Figure 10C, zoom in]. When compared with non-treated cells it is important to highlight that none of these structures or something similar was observed, indicating that lithium was responsible for the formation of these granules and those could be related to the observed small increase of glycogen content in Figure 9C.

These results show the effect of lithium on the Sertoli 42GPA9 cell line and reinforce the idea that this ion barely induces MGS activity. However, the small activation is able to provoke the re-localization of the enzyme in the cytosol, possibly to glycogen particles, which apparently causes stress to Sertoli cells.

4.2 Muscle Glycogen Synthase and RNA binding proteins

Several metabolic enzymes have been reported to bind RNA molecules, and moreover, to regulate the expression of different mRNAs, including their own (Castello et al. 2012b, Cieśla 2006). In the case of MGS, it has been related directly and indirectly to RNA binding proteins, ribonuclear particles, and thus RNA molecules. MGS interacts with many proteins including laforin and malin, which regulate its degradation through the ubiquitin proteasome system, and both of them are functionally expressed in Sertoli cells (Vilchez et al. 2007, Villarroel-Espíndola et al. 2013). Both proteins have been connected to RNA metabolism, providing indirect associations of MGS and RNAs. In

HeLa cells, Laforin, a dual phosphatase of tyrosine and serine/threonine residues, was found in the cytoplasm associated with polyribosomes (Ganesh et al. 2000), while Malin, an E3 ubiquitin ligase, was discovered to be recruited to processing bodies co-localizing with different markers like AGO2, Dcp1, Xrn1, and GW182 (Singh et al. 2012). In the case of MGS, it has been directly related to ribonuclear particles. The enzyme, and specifically pS640MGS, was found to be associated to translationally active polyribosomes, not with the inactive ones, suggesting a role in the modulation of ribosome activity in HeLa cells (Fuchs et al. 2011). These reports, in addition to the presence of an almost inactive enzyme, led us to propose the existence of some association between MGS and RNA and RNA binding proteins in Sertoli cells.

RNA interference [RNAi] works as a gene silencing pathway and has been described in Sertoli cells as a vital process for spermatogenesis (Papaioannou et al. 2009). This process is achieved by many conserved elements, including RNAseIII enzymes and components of the RNA-induced silencing complex [RISC]. One of the main components of the RISC complex is the protein Argonaute2 [AGO2], because it is responsible for the cleavage activity of RISC (Liu et al. 2004, Meister et al. 2004). AGO2 belongs to a family of proteins that interact with small interfering RNAs [siRNAs], micro RNAs [miRNAs] and Piwi RNAs [piRNAs] regulating gene expression at the level of transcription, mRNA stability and translation (Rüdel et al. 2008, Younger & Corey 2011). Interestingly, elevated expression levels of this endonuclease have been reported in testes and specifically in the somatic Sertoli cells when compared with germ cells (González-González et al. 2008). For these reasons, and keeping in mind the indirect associations of MGS with RNAi, the idea that MGS could interact with some RNA binding proteins like AGO2 was developed. The interaction was assessed by performing co-

immunofluorescence and co-inmunoprecipitation assays using specific antibodies against the enzyme and Argonaute-2 [AGO2].

Confocal co-immunofluorescence analysis in primary Sertoli cells showed the aforementioned localization of total MGS homogenously over the cytoplasm [Figure 11, left MGS in green]. Similarly, AGO2 immunolocalization was also distributed in the cytoplasm in a dotted pattern, including the nucleus [Figure 11, left AGO2]. Co-localization of both MGS and AGO2 immunodetections was evident in numerous regions of the cytoplasm and also in the perinuclear area, creating a ring like pattern [Figure 11, left MERGE]. It is important to emphasize that despite high levels of MGS and AGO2 co-localization not all the fluorescent signals co-localize between them, as observed in some peripheral zones of the Sertoli cell cytoplasm [Figure, 11, left MERGE].

RNAi-mediated gene silencing by AGO2 requires the presence of several components that are described to be present in different ribonuclear particles [RNPs] like processing bodies, stress granules and chromatoid bodies among others (Moser & Fritzler 2010). From a single cell, the spatiotemporal localization of these components varies from being present in all the RNPs, like AGO2, to being part of some percentage of some RNPs, a fact that demonstrates the dynamism of proteins and RNAs that interchange between different RNPs (Moser & Fritzler 2010). These components include proteins involved in mRNA degradation, stabilization, processing and transport where Dicer, AGO2, GW182, CCR4, XRN1, DDX6, Staufen and CPEB among others, have been described (Eulalio et al. 2007).

In Sertoli 42GPA9 cells, co-immunofluorescence analyses between MGS, AGO2 and CPEB1 showed that each immunofluorescent signal is localized throughout the cytoplasm [Figure 11, right]. For the case of CPEB1,

Figure 11. MGS co-localize with two RNA binding proteins, AGO2 and CPEB1, in Sertoli cells. Co-immunofluorescence studies of fixed and permeabilized primary Sertoli cells [left] and Sertoli 42GPA9 cells [right]. Primary Sertoli cells were incubated with antibodies against total MGS [green] and AGO2 [red] in a dilution of 1:200, and then with the secondary antibodies Alexa-488 donkey anti rabbit IgG and Alexa-568 donkey anti mouse IgG in a dilution of 1:300. Co-localization of the immunofluorescent signals in yellow are shown in MERGE. Nuclei were stained with DAPI®. Sertoli 42GPA9 cells were treated as primary Sertoli cells, but adding an antibody against CPEB1, without staining the nuclei, and revealing the immunodetection with the secondary antibodies: Alexa-488 donkey anti mouse IgG, Alexa-568 donkey anti goat IgG and Alexa-633 donkey anti rabbit IgG. The co-localization of the immunofluorescent signals are shown in MERGE, where triple co-localization is signed with a large arrow, and double co-localization between MGS and AGO2 is indicated with small white arrows. Scale bars, 20 um.

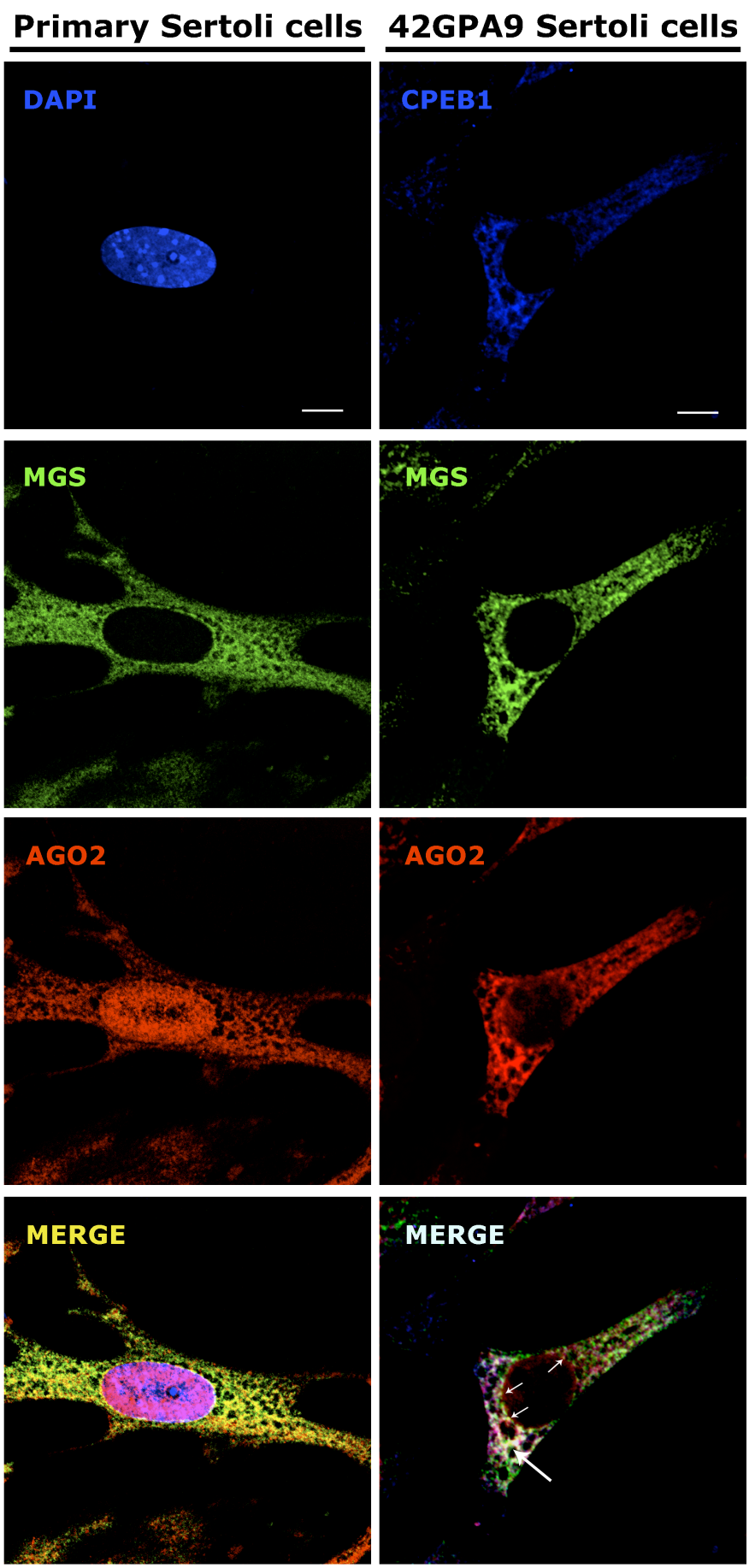
Primary Sertoli cells
42GPA9 Sertoli cells
DAPI
CPEB1
MGS
MGS
AGO2
AGO2
MERGE
MERGE

it is particularly accumulated in certain zones of the cytoplasm, in a well defined pattern near the nucleus [Figure 11, right CPEB1 in blue]. Moreover, MGS and AGO2 presented a homogenous distribution of their immunofluorescent signals in the whole cytoplasm, in a bigger dotted pattern with respect to the primary cells, and AGO2 was barely detected in the nucleus [Figure 11, right MGS in green and AGO2 in red]. MGS and AGO2 co-localization was observed in specific points of the cytoplasm and also in some perinuclear zones [Figure 11, right, MERGE small arrows]. The co-localization analysis of the three signals revealed that MGS, AGO2 and CPEB1 co-localize in specific areas of the cytoplasm, but principally in a zone near the nucleus where CPEB1 is mainly located [Figure 11, right, MERGE big arrow].

To further validate the possible interaction of MGS and AGO2 observed by immunofluorescence co-localization, co-inmunoprecipitation of both proteins was carried out. In order to perform these assays, it was firstly analysed the best conditions and which antibodies worked better to immunoprecipitate the enzyme. Until now there are no reports about the detection of MGS in testes, only glycogen measurements. Therefore, there is no information about the specificity of the antibodies to detect the enzyme in Sertoli cells. To accomplish that, MGS was immunoprecipitated using the three antibodies used in this work [Figure 12]. The first against the C-terminal region of the MGS [ctMGS] that should detect total, phosphorylated and unphosphorylated, forms of the enzyme, another, that was described to distinguish also both enzyme states [3886], and a third antibody specifically against the phospho-Ser640 [pS640MGS].

MGS immunoprecipitation was assayed with Sertoli 42GPA9 cell extracts, where a strong band was observed for the case of the ctMGS -

Figure 12. The antibody against the carboxy terminal region is the most effective to immunoprecipitate muscle glycogen synthase in Sertoli cells. Formaldehyde crosslinked Sertoli 42GPA9 cell extracts were used to immunoprecipitate MGS by using three different antibodies. Total MGS was immunoprecipitated with the ctMGS and 3886 antibodies, while the phosphorylated form of the enzyme in serine640 was pulled down with the pSMGS antibody. Each immunoprecipitated extract was loaded and separated in an SDS polyacrylamide gel electrophoresis and stained with Coomassie blue. The bands that correspond to MGS by size [≈85 KDa] were excised from the gel [red squares] and analysed by mass spectrometry. The proteins identified in all three immunoprecipitations are listed below the gel. The size of the name reflects the abundance of the proteins in the pulled down extracts. At the right of the list the number of MGS peptides identified for each antibody are summarized. Muscle glycogen synthase [Gys1], Heat shock protein 90-beta [HSP90-b], Polyubiquitin-B [PoliUb-B], Heat shock protein 90-alpha [HSP90-a], DNA replication licensing factor MCM5 [MCM5], Putative pre-mRNA-splicing factor ATP-dependent RNA helicase DHX15 [DHX15]

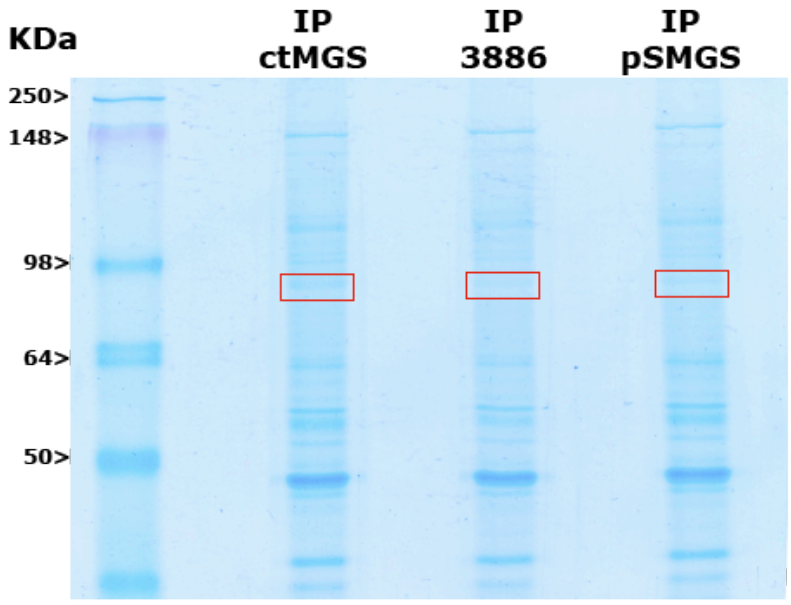

Nano LC-MS/MS

	nº peptides
GYS1	
HSP90-b	
PoliUb-B	
HSP90-a	
MCM5	
DHX15	
ctMGS	28
3886	2
pSMGS	3

immunoprecipitation in comparison with the other two antibodies [Figure 12, red squares]. Then, the selected bands by size [≈80-90 KDa] were excised and digested with trypsin to analyse them by nanoscaled liquid chromatography coupled to tandem mass spectrometry [nano LC-MS/MS]. The nano LC-MS/MS analysis revealed that the antibodies effectively identified MGS in Sertoli cells [GYS1], with a size that has been described for this enzyme, 85 KDa. Additionally to MGS, other proteins were co-immunoprecipitated, where cytosolic [heat shock protein 90, HSP90, and polyubiquitin-B, PoliUb-B] and nuclear proteins [DNA replication licensing factor MCM5, and putative pre-mRNA-splicing factor ATP-dependent RNA helicase DHX15] were found [Figure 12]. Additionally, this study revealed a clear difference between ctMGS, 3886 and pS64MGS antibodies, showing that the best one to immunoprecipitate the enzyme was ctMGS. The immunoprecipitation [IP] with this antibody detected 28 unique peptides of the enzyme, while the 3886 and pS640MGS antibodies only detected two and three peptides, respectively [Figure 12]. Thus, the antibody against the C-terminal region was used to co-immunoprecipitate MGS and AGO2 to validate the co-localization assays.

Sertoli 42GPA9 cell extracts were used to detect AGO2 by Western blot after the immunoprecipitation of the MGS and vice versa, using a rabbit IgG [Rb IgG] as a control of co-IP [Figure 13]. The AGO2 immunoreactive signal was described to be near 90 KDa, but this band was not evidenced after the immunoprecipitation of ctMGS as in the control [Figure 13A, up]. Despite this, and as was predicted by mass spectrometry analysis, an effective IP of the MGS with the ctMGS antibody was observed [Figure 13A, down]. This was visualized as a strong band for the MGS in the ctMGS IP lane, when compared with the control, and a decrease in the signal for the unbound [UB]

Figure 13. pS640MGS co-immunoprecipitates with AGO2 in Sertoli cells. Co-inmunoprecipitation analyses were carried out in Sertoli 42GPA9 extracts. **A)** Western blot detection of AGO2 [up] after the immunoprecipitation of the MGS with the antibody against the carboxy terminal region of the enzyme. The pull down of MGS was corroborated by the detection of ctMGS [down]. **B)** Western blot detection of pS640MGS [up] after the immunoprecipitation of AGO2. The pull down of AGO2 was corroborated by it own detection [down]. For both co-inmunoprecipitation assays a rabbit IgG was used as negative control. Lanes labelled unbound [UB] correspond to the fraction of the extracts that did not immunoprecipitate, while IP corresponds to the immunoprecipitated fraction.

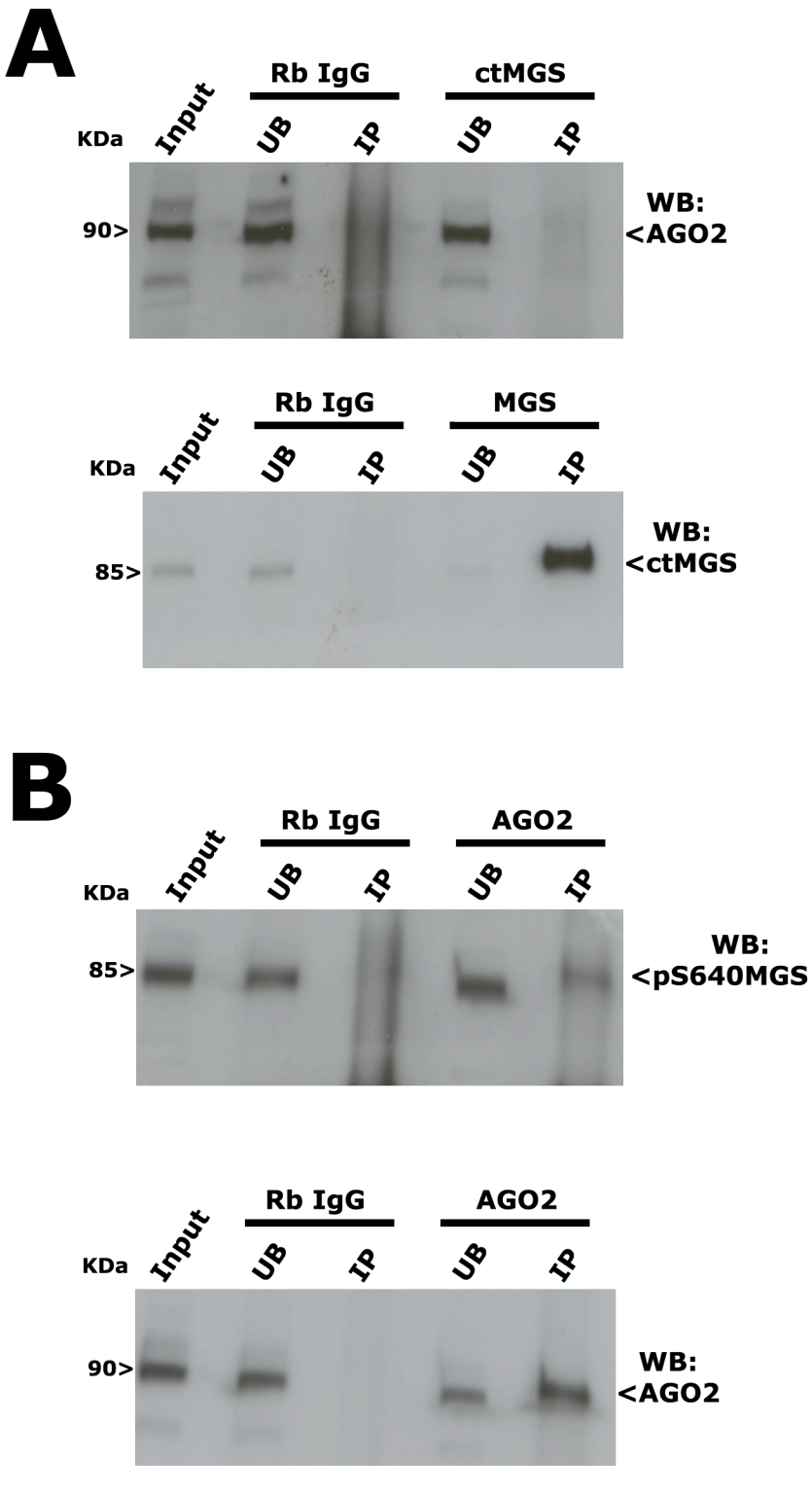
A
Rb IgG
ctMGS
Input
UB
IP
UB
IP
KDa
90>
WB:
<AGO2
Rb IgG
MGS
Input
UB
IP
UB
IP
KDa
85>
WB:
<ctMGS
B
Rb IgG
AGO2
Input
UB
IP
UB
IP
KDa
85>
WB:
<pS640MGS
Rb IgG
AGO2
Input
UB
IP
UB
IP
KDa
90>
WB:
<AGO2

when compared with the INPUT, although the same protein amount was loaded [Figure 13A, down].

On the other hand, when AGO2 was immunoprecipitated, the phosphorylated form of the enzyme [pS640MGS] was detected, demonstrating the co-inmunoprecipitation. This was done because previous results showed that phosphorylated MGS was the main form of the enzyme present in Sertoli cells, making it more detectable by Western blot. This phenomenon was observed in the PPase experiments where total MGS detection was more efficient only in cases when the enzyme was dephosphorylated in both Sertoli cell models [Figure 6]. Thus, when pS640MGS was evaluated by Western blot in AGO2 IP extracts, a positive band appeared for the phosphorylated enzyme in the AGO2 IP lane and not in the negative control of the IP [Figure 13B, up]. Next, to corroborate AGO2 IP, the same protein was blotted, indicating that AGO2 was effectively immunoprecipitated, while no signal was observed in the control [Figure 13B, down]. In summary, these results showed that part of the phosphorylated form of the enzyme [pS640MGS] is interacting with AGO2, and this cannot be observed when the total enzyme [ctMGS IP] is immunoprecipitated. Also, these co-IP experiments revealed a different performance of the MGS antibodies, where the ctMGS antibody works better for MGS IP, while the pS640MGS works better for Western blot detection.

To strengthen the proposal that MGS could interact with different RBPs, and given that these proteins are always interacting in the RNPs, the interaction of MGS with other RBPs was examined [Figure 14]. Those RBPs, include AGO2, and the cytoplasmic polyadenylation element-binding proteins, CPEB1 and 4, together with the ATP-dependent RNA helicase, DDX6. In primary Sertoli and Sertoli 42GPA9 cell extracts, the pS640MGS

Figure 14. pS640MGS co-immunoprecipitates with different RNA binding proteins in Sertoli cells. Co-inmunoprecipitation assays were performed in primary Sertoli cell [up] and Sertoli 42GPA9 cell [down] extracts. For both cases, pS640MGS was detected by Western blot after the inmunoprecipitation of AGO2, CPEB1, CPEB4 and DDX6. In the UB lanes were loaded the unbound extracts that do not immunoprecipitate, while the immunoprecipitated are shown in the IP lanes. Unbound [UB], immunoprecipitated [IP].

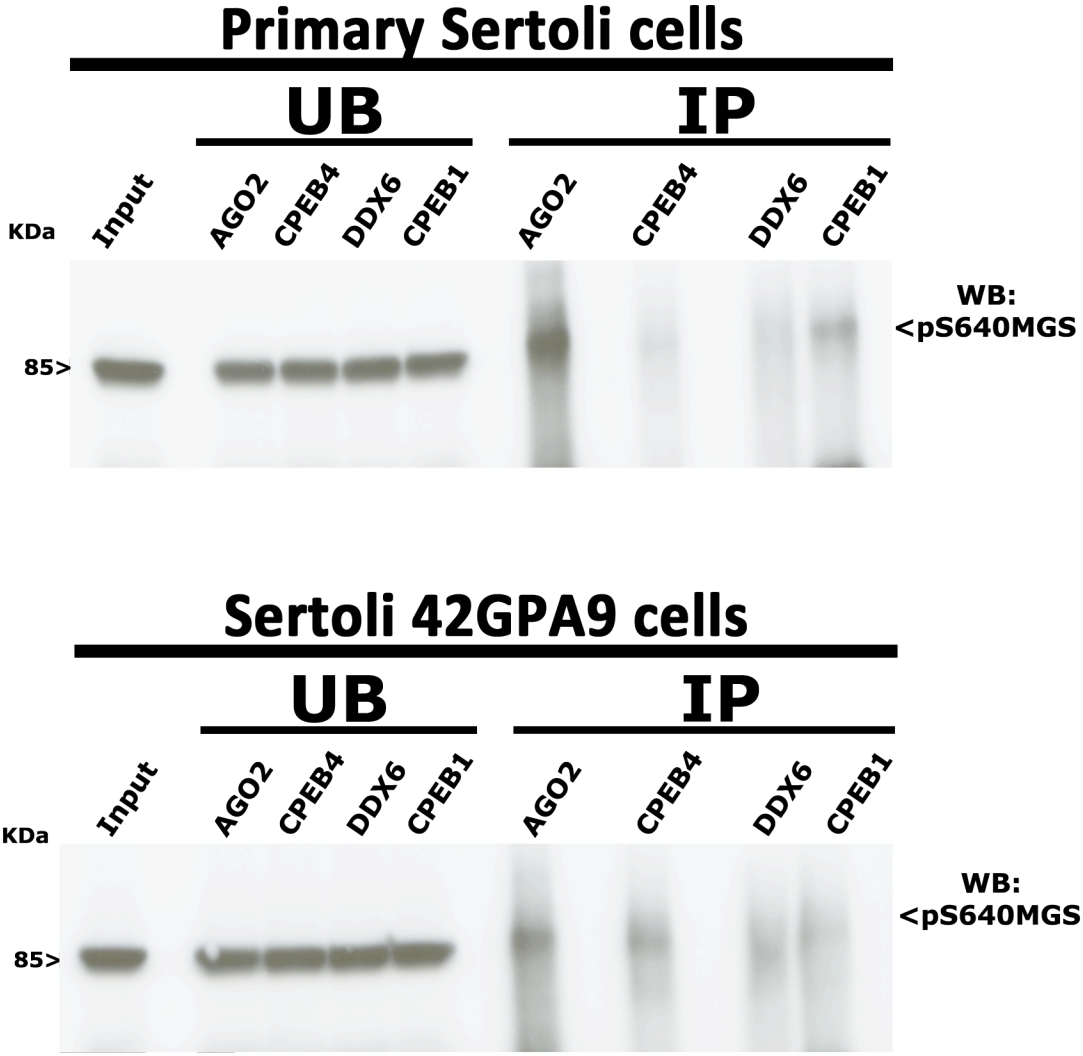
Primary Sertoli cells
UB
IP
KDa
Input
AGO2
CPEB4
DDX6
CPEB1
AGO2
CPEB4
DDX6
CPEB1
85>
WB:
<pS640MGS
Sertoli 42GPA9 cells
UB
IP
KDa
Input
AGO2
CPEB4
DDX6
CPEB1
AGO2
CPEB4
DDX6
CPEB1
85>
WB:
<pS640MGS

was detected after the IP of AGO2, CPEB4, CPEB1 and DDX6. The same band with different intensities was observed in the IP lanes for the phosphorylated form of the enzyme in both Sertoli cell types [Figure 14]. In primary Sertoli cells, pSMGS640 immunoreactive signal was more intense for AGO2 and CPEB1 IPs, in comparison with CPEB4 and DDX6 IPs [Figure 14, up]. Whereas in Sertoli 42GPA9 cells, the most intense bands for pS640MGS were observed in AGO2 and CPEB4 IPs, rather than in DDX6 and CPEB1 IPs. [Figure 14, down]. Consequently, pS640MGS coIPs with different RBPs including AGO2 in both Sertoli cell types supporting the idea that MGS could interact with some RNPs components in Sertoli cells.

Remarkably, despite different signals observed in all the IPs for both Sertoli cell types, higher intensities for pS640MGS were always detected during AGO2 IPs. For this reason, and given the relevance of AGO2 for the RNAi process in concordance with the high levels of this endonuclease founded specifically in Sertoli cells, the pS640MGS-AGO2 interaction was studied. At this point it is unknown if this interaction is direct, or if it depends on other components or the state of those components. To test some of the possible features of the pS640MGS-AGO2 interaction, the coIPs were performed in the presence of an RNAse or changing the activity and phosphorylation state of the MGS [Figure 15].

To analyse if the interaction depends on an RNA molecule, primary and 42GPA9 Sertoli cells extracts were treated [or not] with RNAse A, prior to AGO2 immunoprecipitation. In both cell types, pS640MGS was detected to similar extend in AGO2 IP from RNAse treated or non-treated extracts [Figure 15A and C]. Although a more intense band for pS640MGS was observed in the absence of RNAse treatment in primary Sertoli cells [Figure

Figure 15. Co-immunoprecipitation of pS640MS with AGO2 does not require the presence of RNA molecules and is not affected by PTG overexpression. Western blot analysis for pS640MGS after the inmunoprecipitation of AGO2 in primary Sertoli cell [left] and Sertoli 42GPA9 cell [rigt] extracts. **A)** and **C)**, before the immunoprecipitation, both Sertoli cell extracts were treated [+] or not [-] with RNAse A. In **B)** and **D)**, both Sertoli cell types were transduced with AdGFP alone and AdPTG-GFP, as described in Figure 7. For all the cases, in the UB lanes were loaded the unbound extracts that do not immunoprecipitate, while the immunoprecipitated are shown in the IP lanes. Unbound [UB], immunoprecipitated [IP].

Primary Sertoli cells

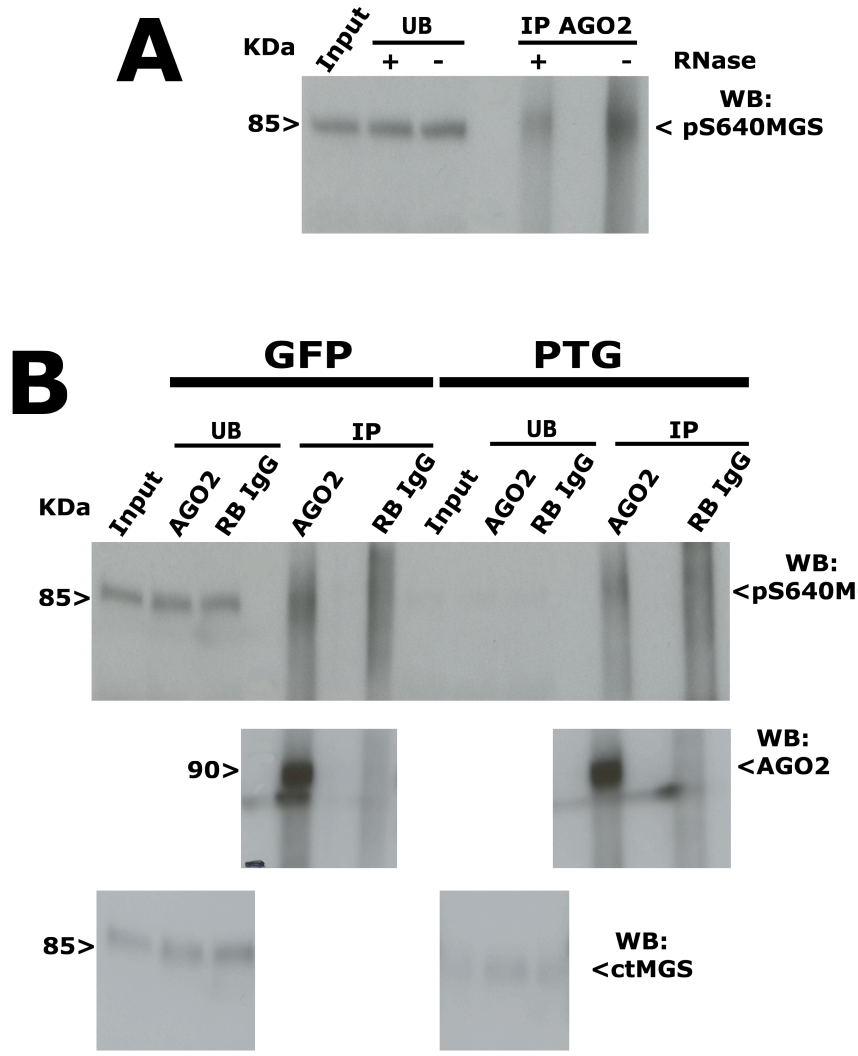

Sertoli 42GPA9 cells

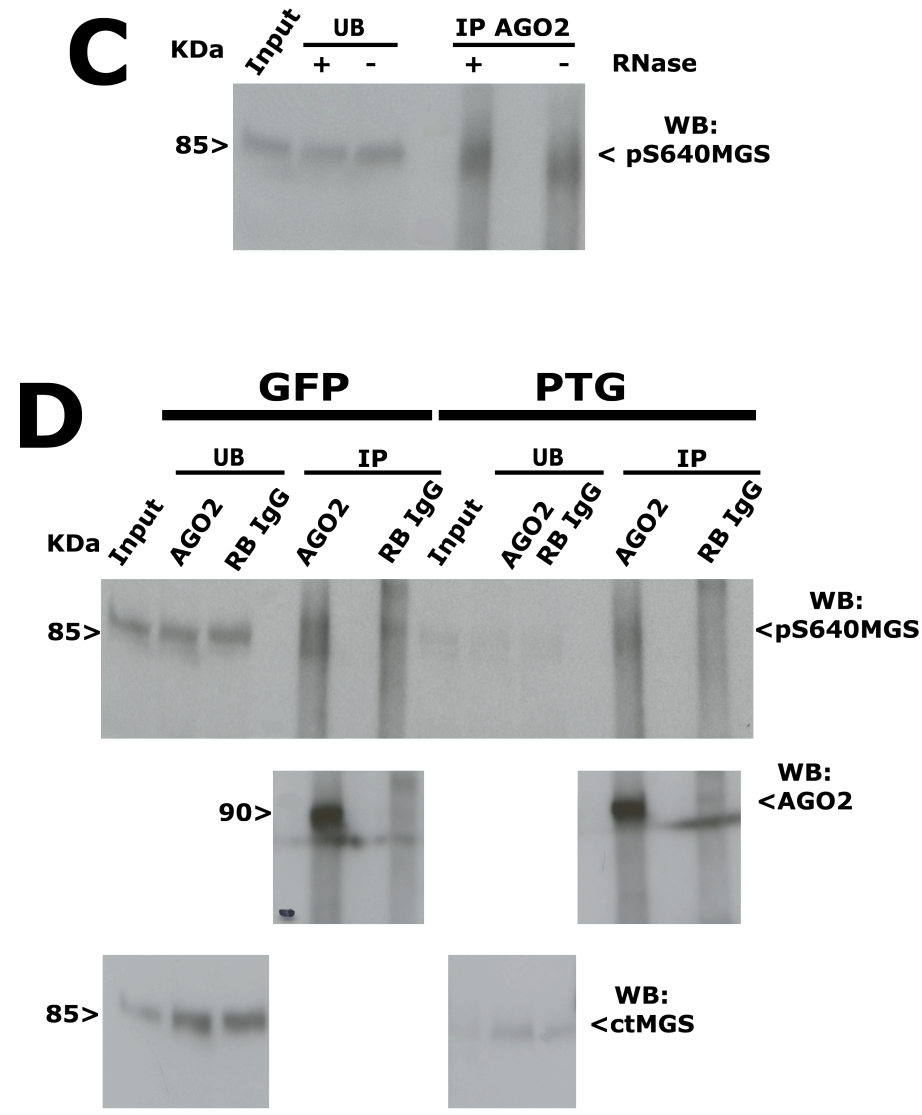

15A]. While in Sertoli 42GPA9 cell extracts, equivalent intensity signals for pS640MGS were detected in treated and non-treated extracts [Figure 15C].

On the other hand, to study if the activity state of the enzyme is crucial for the interaction of pS640MGS and AGO2, the inactive state of the enzyme was partially reverted. To accomplish that, both Sertoli cell types were infected with adenoviral particles that encode for GFP-PTG, and GFP alone as a control, to activate the MGS as was described in the Figure 8. In both Sertoli cell types pS640MGS detection after the IP of AGO2 was undoubtedly positive in AdGFP infected cells, whereas in AdPTG infected cells, pS640MGS detection in the input and unbound [UB], was substantially reduced [Figure 15B and D]. Despite this, ctMGS detection revealed the presence of the enzyme in the input and UB lanes [Figure 15B and D, WB ctMGS]. The reduction in the pS640MGS signal in AdPTG infected cells was most probably due to the overexpression of PTG, which promotes MGS activation by its dephosphorylation. Interestingly, however one portion of the remaining phosphorylated enzyme in Ser640 was still co-immunoprecipitating with AGO2 in both Sertoli cell types [Figure 15B and D]. These results indicate two features of the [direct/indirect] interaction of pS640MGS and AGO2. First, that this interaction was not dependent on the presence of RNA molecules. Second, that despite the enzyme activation by dephosphorylation, a fraction of the phosphorylated enzyme still immunoprecipitates with AGO2.

After observing that pS640MGS interacts with RNPs components and specifically with AGO2, it was reasoned that if the enzyme was interacting with RBPs it should also associate directly or indirectly with RNA molecules. To test this idea, RNA purification after the immunoprecipitation of the

Figure 16. Schematic illustration of the RNA inmunoprecipitation [RIP] protocol. Sertoli cells in approximately 80% confluence were crosslinked with 1% formaldehyde for 15 minutes. Then, they were washed and lysed mechanically by soft sonication and syringe passages. The obtained protein extract and the glycogen synthase antibodies coupled to Dynabeads ® Protein A, were incubated together during 4 hours to immunoprecipitate the enzyme. Next, one third of the immunoprecipitated extracts was used to confirm the immunoprecipitation by Western blot analysis. The other two thirds were heated to revert the crosslinking, and then treated with proteinase K to eliminate proteins. Afterwards, RNA molecules were purified, and treated with DNAse, for a subsequent analysis by a microarray of the immunoprecipitated RNAs with the glycogen synthase.

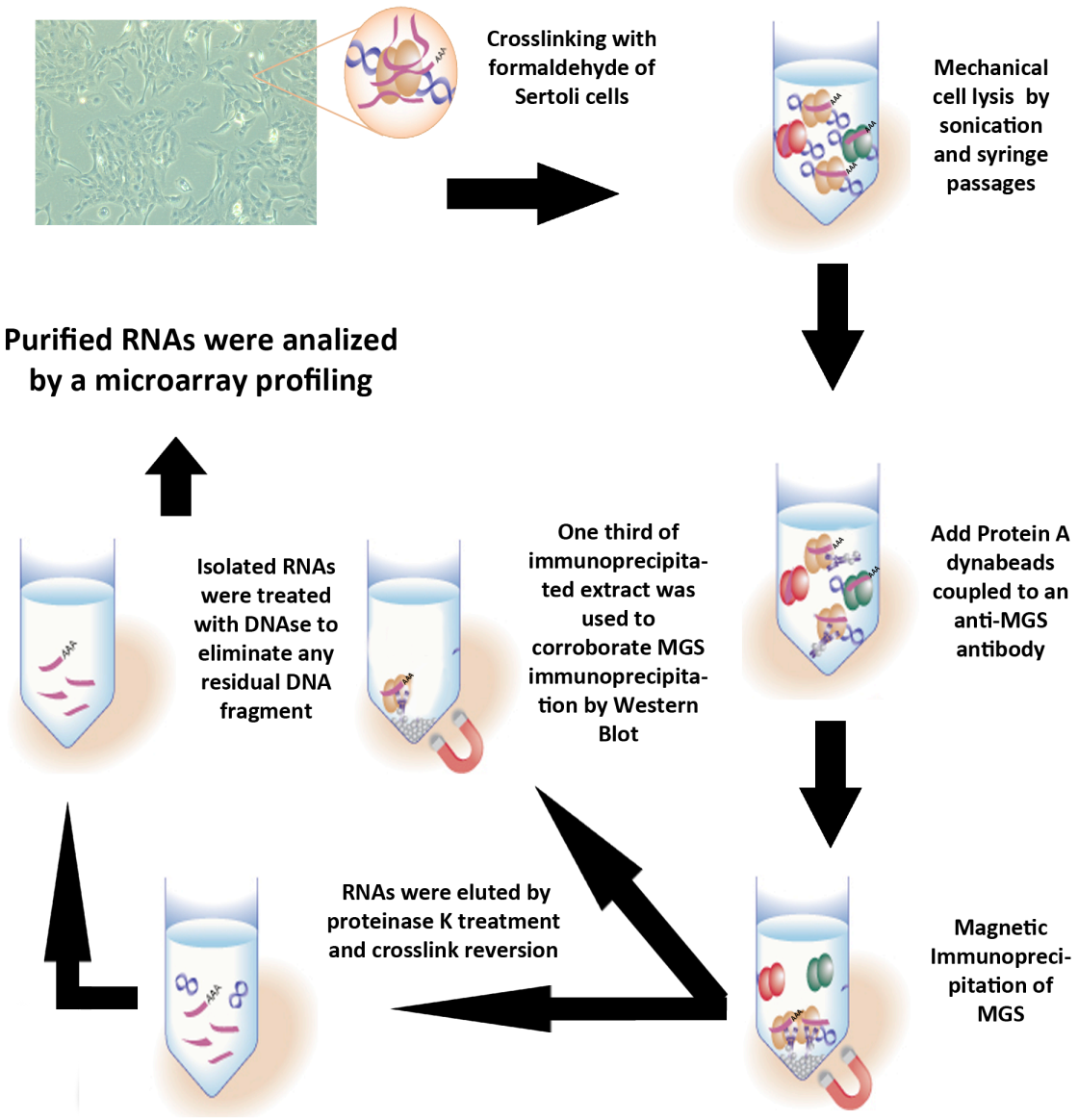
Crosslinking with formaldehyde of Sertoli cells
Mechanical cell lysis by sonication and syringe passages
Add Protein A dynabeads coupled to an anti-MGS antibody
Magnetic Immunopreci-pitation of MGS
RNAs were eluted by proteinase K treatment and crosslink reversion
One third of immunoprecipita-ted extract was used to corroborate MGS immunoprecipita-tion by Western Blot
Isolated RNAs were treated with DNAse to eliminate any residual DNA fragment
Purified RNAs were analized by a microarray profiling

enzyme was performed. An RNA inmunoprecipitation [RIP] assay is described below and schematized in Figure 16.

Several studies have used this experimental procedure to determine, for example, the proteins associated with miRNA-regulated mRNAs and associated mRNAs to a pivotal protein that mediates translational control during cancer progression in adenocarcinomas and glioblastomas (Ortiz-Zapater et al. 2012, Shih et al. 2011). The RNA immunoprecipitation is based in a formaldehyde-induced crosslinking between any primary amino group. Formaldehyde crosslinking occurs between nearby nitrogen atoms in another protein, DNA, or in this case RNA through a $-CH_2-$ linkage. The most relevant consequence of formaldehyde treatment during RIP is that the association between proteins and RNAs molecules are captured as an *in vivo* snapshot inside a cell. After the crosslinking, the cells were lysed and protein extracts were used to immunoprecipitate a protein of interest, in this case the glycogen synthase. Accordingly, the immunoprecipitated extracts were split in two, where one third was used to verify the immunoprecipitation by Western blot and the other two thirds were used to purify RNAs. Prior to RNA purification, the protein components of the IP extracts were digested with Proteinase K and the crosslinking was reverted with temperature as described in **3.2.6.4**. Next, the purified RNAs were treated with DNAse to degrade any remaining contaminant DNA to finally analyse the immunoprecipitated RNAs by a microarray profiling.

For MGS it was already determined that the ctMGS is the best antibody to immunoprecipitate the enzyme by mass spectrometry, as was shown in Figure 12. Thus, crosslinked primary Sertoli cell extracts were used for RNA immunoprecipitation assays with the ctMGS antibody, and also, with a rabbit IgG [Rb IgG] as a negative control for the IP. Additionally, the

Figure 17. MGS pull down confirmation previous to the RNA purification during RIP. MGS immunoprecipitation was confirmed by Western blot analysis using primary Sertoli cell extracts. ctMGS and pS640MGS antibodies were used to pull down the enzyme and a rabbit IgG [RB IgG] was used as the negative control. The immunoprecipitation was firstly detected with the ctMGS antibody during short [1 minute] and long [5 minutes] exposure times [up]. Then, the membrane was "stripped" and re-probed against the pS640MGS and also exposed during short [1 minute] and long times [5 minutes]. In the UB lanes the unbound extracts that do not immunoprecipitate were loaded, while the immunoprecipitated fractions are shown in the IP lanes.

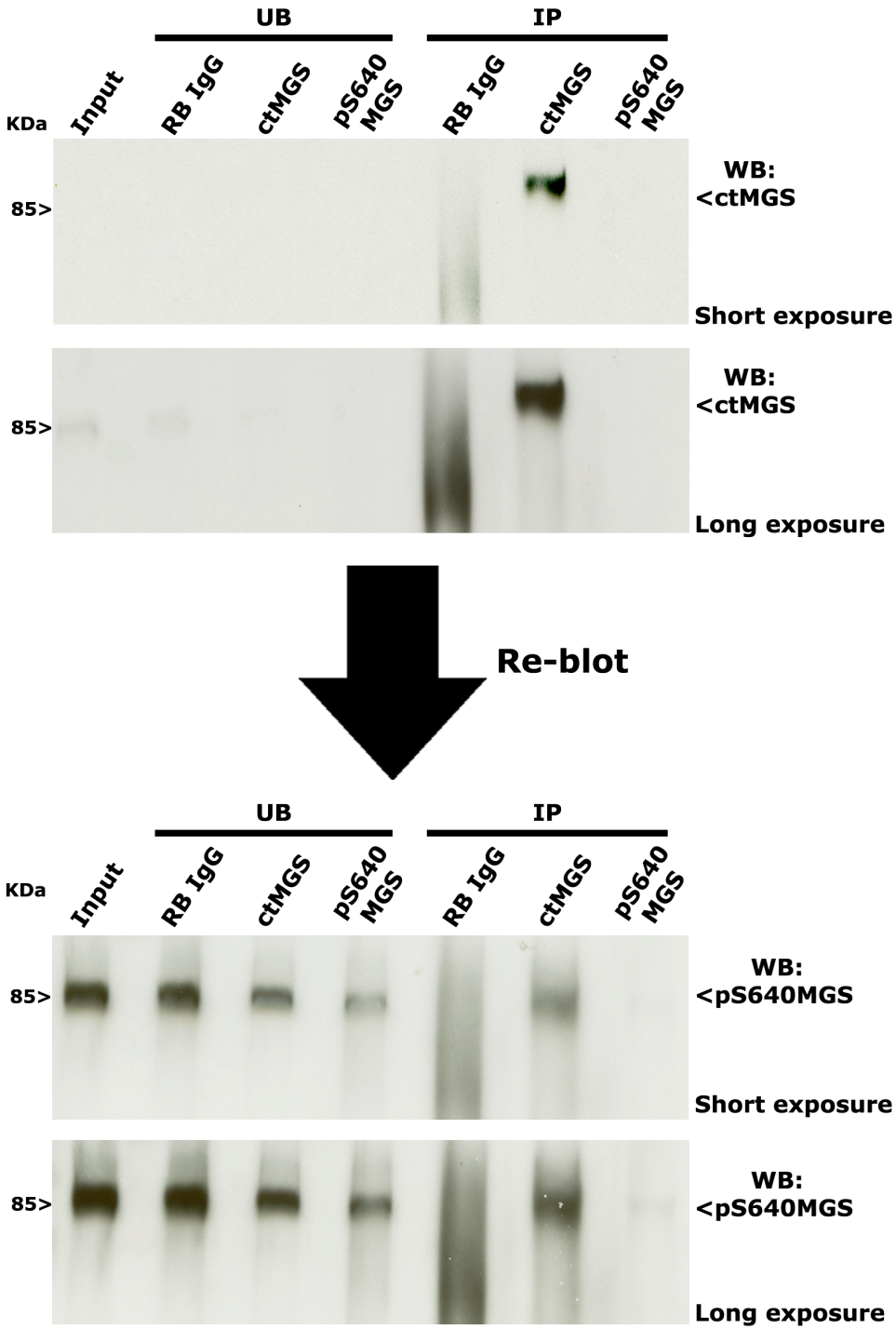
UB
IP
KDa
Input
RB IgG
ctMGS
pS640 MGS
RB IgG
ctMGS
pS640 MGS
85>
WB: <ctMGS
Short exposure
85>
WB: <ctMGS
Long exposure
Re-blot
UB
IP
KDa
Input
RB IgG
ctMGS
pS640 MGS
RB IgG
ctMGS
pS640 MGS
85>
WB: <pS640MGS
Short exposure
85>
WB: <pS640MGS
Long exposure

same experiment with the pS640MGS antibody was performed to analyse the reproducibility of the RIP with different antibodies [Figure 17]. Once the crosslinking and the immunoprecipitation were made, one third of each IP was analysed by Western blot to detect the MGS with the ctMGS antibody.

The blot showed an effective inmunoprecipitation of the enzyme with the ctMGS antibody [Figure 17, up, IP ctMGS lane]. Surprisingly the enzymewas not detected in the Input, UB and pS640MGS IP lanes after a short exposure time of the membrane, and this barely changed after a longer exposure, where faint signals for ctMGS appear [Figure 17, up]. This evidently attracted our attention because of the weak detection of the enzyme, so the membrane was "stripped" and re-blotted, but now against the pS640MGS. Interestingly, the "stripped" membrane showed that pS640MGS was now easily detectable in the Input and UB lanes, and also in the ctMGS IP lane at short exposure times [Figure 17, down, short exposure]. However, under these conditions no IP of the pS640MGS was detectable, so the exposure time was extended and a very weak band for the phosphorylated enzyme was observed in pS640MGS IP lane [Figure 17, down, long exposure]. It is important to highlight that no bands for the ctMGS, nor for the pS640MGS, were observed in the Rb IgG IP lanes, demonstrating that the negative control was successful under our IP conditions. This was very important for this work because this negative control for the IPs [Rb IgG Ip] was the negative control for the microarray data. These results are in agreement with previous observations [Figures 12 and 13] where it was demonstrated that the enzyme immunoprecipitates efficiently with the ctMGS, but the detection by Western blot was better with the pS640MGS antibody in Sertoli cell extracts.

Hence, with the immunoprecipitation of the enzyme complete, the first part of the assay was successful and allows continuing with the RIP analysis.

Figure 18. MGS co-immunoprecipitates with mRNAs. Input and immunoprecipitated primary Sertoli cell extracts, from a single experiment shown in **Figure 18**, were heated to revert the crosslinking and treated with proteinase K to proceed with the RNA purification. Afterwards, the purified RNAs were analysed by mRNA profiling microarray. In **A)** RNA profiles of Input and each immunoprecipitate extract are shown and ploted as concentration in fluorescence units [FU] in function of the RNA length in nucleotides [nt]. Inside the graphs [top right] the concentrations of each extract are shown. The data obtained from the microarray is indicated in **B)**. The enrichment of different quantities of mRNAs in the MGS immunoprecipitated extracts, ctMGS and pS640MGS, in comparison with the negative control are shown in red and green circles for ctMGS and pS640MGS, respectively. The number of enriched mRNAs from both MGS pull downs are depicted in the intersection of the red and green circles.

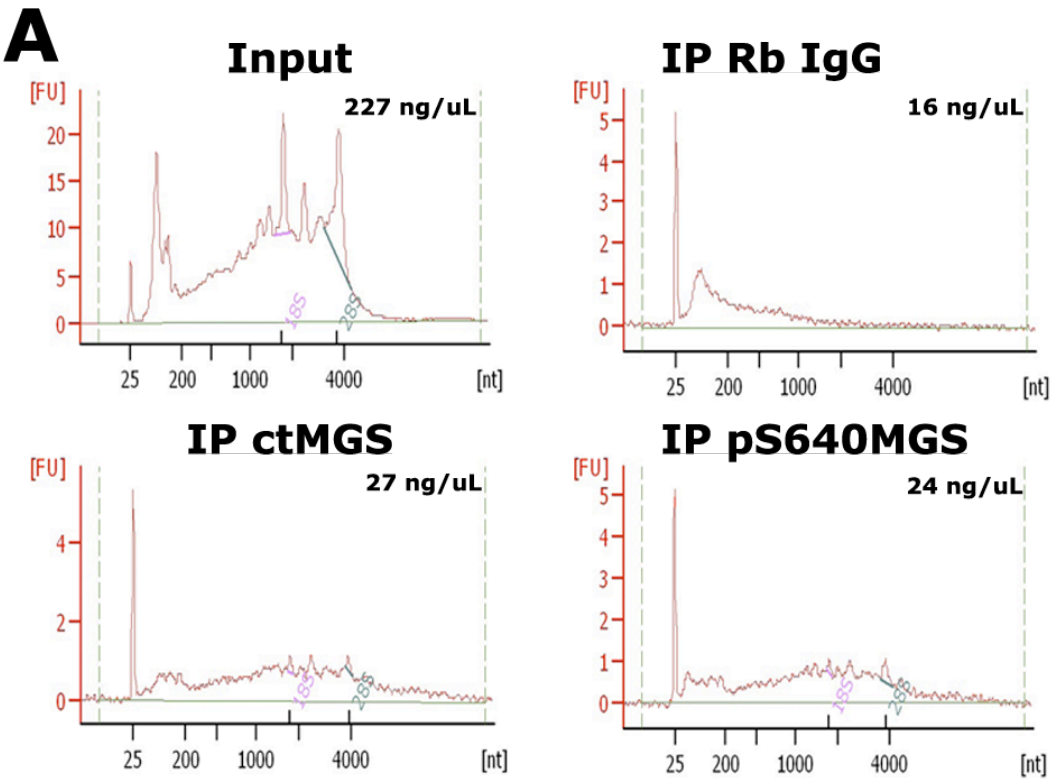
A
Input
227 ng/uL
IP Rb IgG
16 ng/uL
IP ctMGS
27 ng/uL
IP pS640MGS
24 ng/uL
[FU]
[nt]
25
200
1000
4000
18S
28S

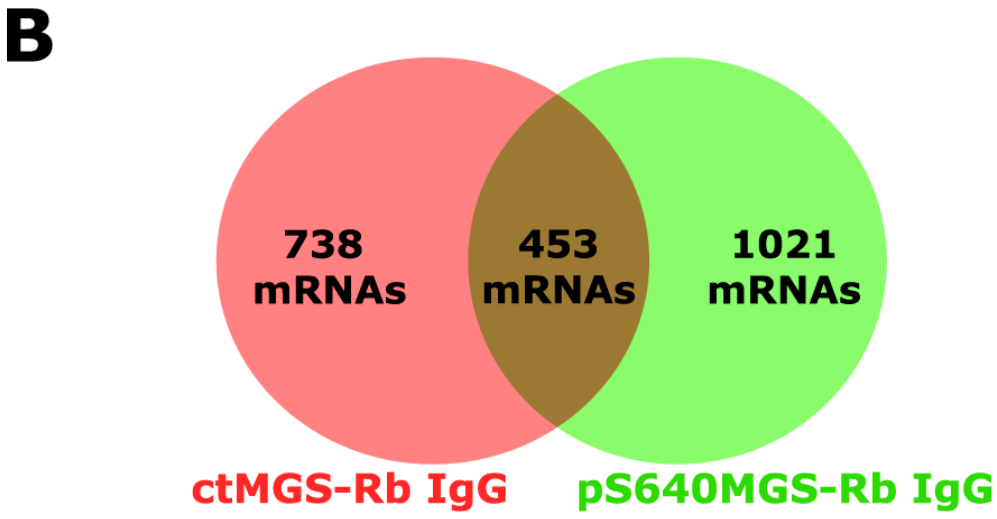
B
738
mRNAs
453
mRNAs
1021
mRNAs
ctMGS-Rb IgG
pS640MGS-Rb IgG

The other two thirds of each IP were used for RNA purification and the samples were assessed to examine the concentration and integrity of the immunoprecipitated RNAs. In this quality control, the obtained concentrations for the RNAs were 227 ng/uL, 16 ng/uL, 27 ng/uL, and 24 ng/uL for the Input, Rb IgG IP, ctMGS IP and pS640MGS IP, respectively [Figure 18A, numbers inside each graph]. The integrity of the RNAs was evaluated by determining the concentration as units of fluorescence, in function of the length in nucleotides of the purified RNAs from each extract [Figure 18A, graphs]. Besides different concentrations of immunoprecipitated RNAs, the graphs showed the presence of two components of the small and large subunits ribosomal RNAs, the 18S and 28S, in the ctMGS and pS640MGS IPs but not in the control IP [Figure 18, graphs]. Additionally, in both MGS RIPs it was observed the presence of RNAs with the average length of an mRNA [1000 to 2000 nucleotides], but not in the Rb IgG IP [Figure 18, graphs]. This was the main clue to make a valid association between the MGS with mRNAs in Sertoli cells.

Later, the identity of those mRNAs was determined by a microarray, from which it was possible to detect the mRNAs in both MGS RIPs in comparison with the control [Figure 18B]. It is important to emphasize at this point that microarray results were obtained as an enrichment of each mRNA in one RIP more than another. In this way, each MGS RIP was compared to the negative control. Analysing the mRNAs enriched in the ctMGS RIP versus the Rb IgG RIP, 1191 mRNAs were found, while the enriched messengers in the pS640MGS RIP versus the Rb IgG RIP were 1474 [Figure 18B, circles]. Both RIPs share 453 mRNAs with a probability of ≈ 1 to be statistically enriched in the MGS RIPs with respect the control [Figure 18B, intersection of the circles].

Subsequently, the shared 453 mRNAs were classified and grouped by function using the bioinformatic tool PANTHER [Protein ANalysis Through Evolutionary Relationships] classification system (Mi et al. 2005, 2013; Thomas et al. 2003). The result of this analysis helped to organize the microarray data according to the molecular function and biological processes [Figure 19, graphs]. From a total of 453 mRNAs encoded genes, 45 of them were not identified, while 408 of them could be associated with different categories. The classification of them by molecular function showed that 163 [40% of the total] genes were related to binding [grey bar upper graph, Figure 19A]. From this 163, almost all are linked to nucleic acid binding and protein binding [yellow and light blue bars respectively, lower graph, Figure 19A]. In the same way, by classifying the genes by their biological function it was observed that 188 [46.1% of the total] genes were associated with a category of metabolic processes [red bar, upper graph, Figure 19B] and also almost all of them, in relationship with primary metabolic processes [orange bar, lower graph, Figure 19B]. It is important to clarify that this latter category was essentially related to protein and nucleobase, nucleoside, nucleotide and nucleic acid metabolic processes where transcription was highly predominant. In brief, these results suggested that MGS is effectively interacting with RNAs, whether rRNA or mRNA.

Figure 19. The MGS interacting mRNAs are mainly associated to primary metabolic processes in Sertoli cells. Bioinformatic classification of the 453 mRNAs that co-immunoprecipitate with the MGS showed in Figure 18. The mRNAs were classified by it molecular function A) and biological process B) using the bioinformatic tool for gene classification PANTHER. For both cases, the terms are associated with colours and bar graphed. The categories with more components indicate the percentage of enrichment over the correspondingly bar. Upper graphs show the enriched category from the total number of analysed mRNAs. Bottom graphs indicate the distribution of each enriched term in the upper graphs.

A

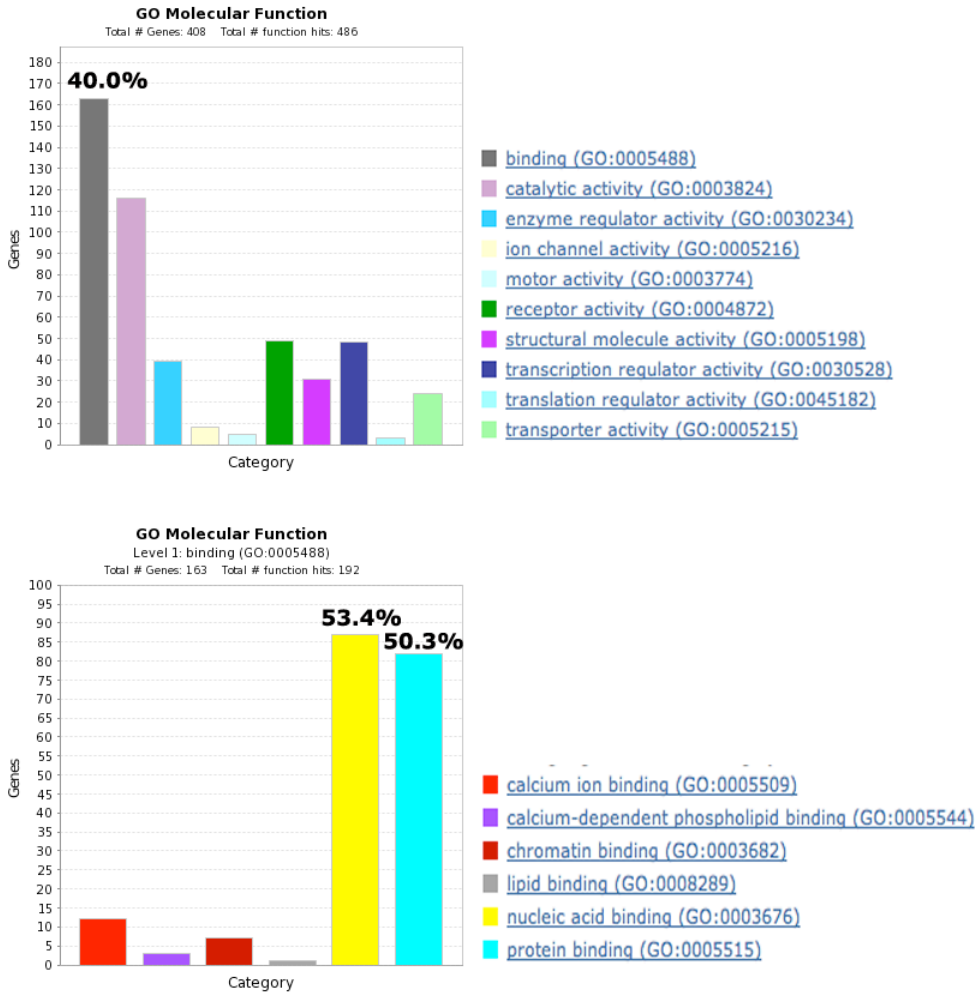
GO Molecular Function
Total # Genes: 408 Total # function hits: 486
40.0%
Genes
Category
binding (GO:0005488)
catalytic activity (GO:0003824)
enzyme regulator activity (GO:0030234)
ion channel activity (GO:0005216)
motor activity (GO:0003774)
receptor activity (GO:0004872)
structural molecule activity (GO:0005198)
transcription regulator activity (GO:0030528)
translation regulator activity (GO:0045182)
transporter activity (GO:0005215)
GO Molecular Function
Level 1: binding (GO:0005488)
Total # Genes: 163 Total # function hits: 192
53.4%
50.3%
Genes
Category
calcium ion binding (GO:0005509)
calcium-dependent phospholipid binding (GO:0005544)
chromatin binding (GO:0003682)
lipid binding (GO:0008289)
nucleic acid binding (GO:0003676)
protein binding (GO:0005515)

B

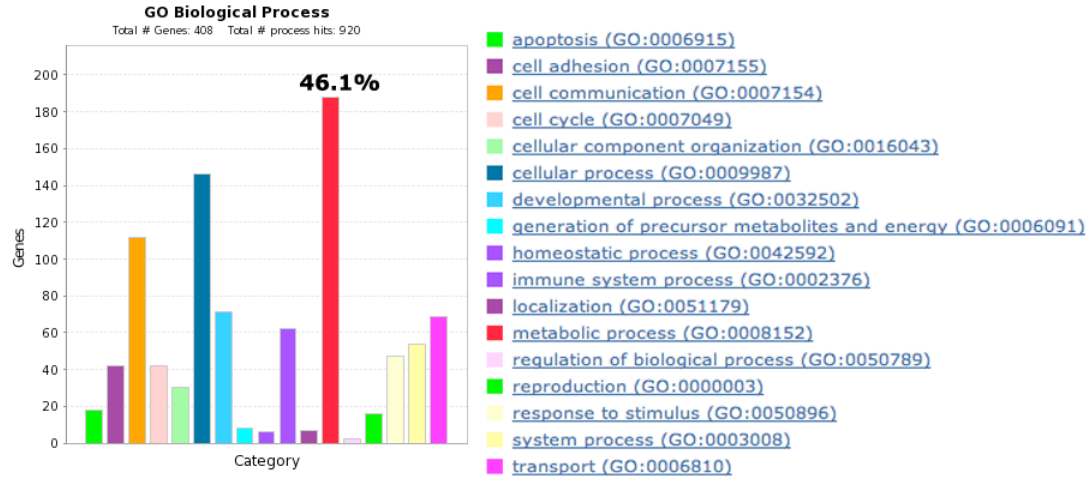
GO Biological Process
Total # Genes: 408 Total # process hits: 920
46.1%
Genes
Category
0
20
40
60
80
100
120
140
160
180
200
apoptosis (GO:0006915)
cell adhesion (GO:0007155)
cell communication (GO:0007154)
cell cycle (GO:0007049)
cellular component organization (GO:0016043)
cellular process (GO:0009987)
developmental process (GO:0032502)
generation of precursor metabolites and energy (GO:0006091)
homeostatic process (GO:0042592)
immune system process (GO:0002376)
localization (GO:0051179)
metabolic process (GO:0008152)
regulation of biological process (GO:0050789)
reproduction (GO:0000003)
response to stimulus (GO:0050896)
system process (GO:0003008)
transport (GO:0006810)

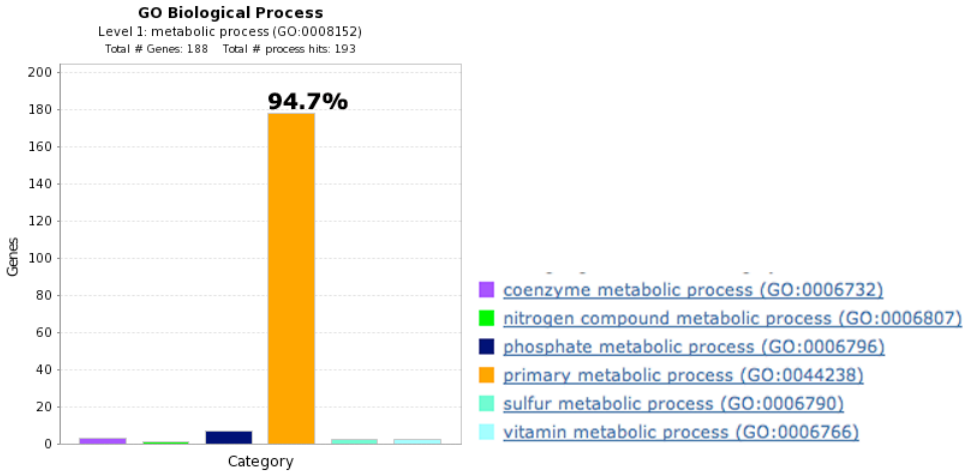
GO Biological Process
Level 1: metabolic process (GO:0008152)
Total # Genes: 188 Total # process hits: 193
94.7%
Genes
Category
0
20
40
60
80
100
120
140
160
180
200
coenzyme metabolic process (GO:0006732)
nitrogen compound metabolic process (GO:0006807)
phosphate metabolic process (GO:0006796)
primary metabolic process (GO:0044238)
sulfur metabolic process (GO:0006790)
vitamin metabolic process (GO:0006766)

5. Discussion

5.1 MGS characterization in Sertoli cells

In this work the functional characterization of muscle glycogen synthase and its possible unknown non-metabolic role in Sertoli cells was studied. By comparing both Sertoli cell types with testicular extracts, some characteristics of the enzyme were identified. MGS mRNA was marginally detectable by RT-PCR in testicular extracts but was clearly expressed in both Sertoli cell types, despite the same amount of RNA load [Figure 3A]. Likewise, this was observed at the protein level where Western blot analyses showed that MGS was almost undetectable in testes in contrast to the levels present in Sertoli cells, and despite the higher protein loading of testicular extracts [Figure 3B]. These results indicate that Sertoli cells are enriched in MGS when compared to other testicular components. Therefore, the reduced amount of the enzyme observed in testicular extracts can be explained by mass dilution. These results agree with what was described in the late 1960s, indicating that testicular glycogen is abundant in prepubertal testes (sexually immature) enriched in Sertoli cells with a few spermatogonia (Fabbrini et al. 1969, Fouquet & Guha 1969). Also, this coincides with a recent publication of our laboratory that showed that Sertoli cells and not germ cells were the main source of testicular glycogen (Villarroel-Espíndola et al. 2013).

The cellular localization of the endogenous enzyme in Sertoli cells was different when compared with the most frequent cellular model of MGS studies, muscle cells. Until now there have been no reports about nuclear localization of the endogenous enzyme; only two of them have demonstrated the nuclear localization of overexpressed MGS in glycogen deprived muscle cells by culturing them in the absence of glucose (Cid et al. 2005, Ferrer et al.

1997). Cellular fractionation and co-immunofluorescence assays [Figures 4A and 4B] revealed for the first time, without disturbing any cellular processes by protein overexpression, that endogenous MGS was located in the nucleus. Specifically, the pS640MGS form was located in sub-nuclear structures named speckles, where the pre-mRNA splicing machinery occurs and the phosphorylated enzyme colocalizes with the splicing factor SC-35 [Figure 4B].

The nuclear localization of the endogenous enzyme in Sertoli cells, without depriving them of glycogen and maintaining the cultures in the presence of glucose, led us to analyse the activation state of MGS. To accomplish this analysis, glycogen synthase activity was measured in primary and 42GPA9 Sertoli cells, indicating for both cases that the enzyme was present but almost in an inactive state [Figure 5]. The activity ratio [–G6P activity/+G6P activity] revealed that the proportion of active enzyme in both cell types was very similar, confirming the cell line 42GPA9 as a good model for MGS studies in Sertoli cells.

The extremely low activity rates of MGS observed in Sertoli cells led us to consider that the enzyme could be present in a high phosphorylated state, and possibly in the Ser640 because it is the main phosphorylation site that inactivates the enzyme (Palm et al. 2013, Skurat et al. 1994). Phospho-Ser 640MGS and total MGS levels were evaluated by phosphatase assays, which suggest that this enzyme could be present in a high-phosphorylated state [Figure 6]. An important point to discuss is how the antibodies can detect the enzyme from Sertoli cell extracts. For both Sertoli cell types, pS640MGS was easily detectable in the absence of phosphatase, but this signal decreased in the presence of the phosphatase indicating the success of the assay. Meanwhile, when total MGS was detected [with the ct-MGS and 3886 MGS antibodies], it was clearly more detectable after the treatment with λ

phosphatase. Thus, these assays helped us to reveal that dephosphorylation could facilitate the exposure of epitopes for total MGS antibodies, which function better when the enzyme is dephosphorylated, and more importantly, is consistent with MGS being present in a highly phosphorylated state in Sertoli cells.

Moreover, the possibility that MGS could be inactive due to high levels of phosphorylation could be sustained by two dimensional gel electrophoresis where some spots to acidic pH [pH 5.55-5.8] were observed for the immunoprecipitated Sertoli MGS [Figure 7, bottom gel]. The more acidic forms of the enzyme suggest that MGS could be phosphorylated in different residues, where muscle and brain MGS are not, because the main covalent post-translational modifications of the enzyme are phosphorylations. MGS has 15 putative sites of phosphorylation where only nine have been established *in vivo* (Poulter et al. 1988) indicating that MGS phosphorylation pattern could differ depending on a cell type, tissue, metabolic state or stimuli. Accordingly, evident differences were observed for Sertoli MGS two dimensional gel electrophoresis pattern, in comparison with the muscle and brain enzyme. The Sertoli MGS pattern showed a set of eight spots to more acidic pH [pH 5,5-6,3], and one spot localized to a more basic pH [pH 7]. The more acidic Sertoli MGS spots [pH 5.55-5.8] were not observed in muscle MGS, but only there is some grade of similarity to the brain MGS. Thus, in summary, these results indicate that endogenous Sertoli MGS is located in the nucleus and cytoplasm, and is present as an almost inactive enzyme possibly due to high levels of phosphorylation.

To demonstrate if the inactive MGS could be susceptible to activation, two already described methods were performed. One, based on Protein Targeting to Glycogen [PTG] overexpression that induces the

dephosphorylation of MGS, and another, established in different publications as an indirect activator of the MGS through the inhibition of GSK3 with lithium salts (Greenberg et al. 2003, MacAulay et al. 2003, Oreña et al. 2000, Vilchez et al. 2007). PTG overexpression by adenovirus infection of Sertoli 42GPA9 cells produced an increase in the intrinsic glycogen synthase activity [-G6P], without changing the total activity [+G6P], meaning that PTG overexpression was effectively activating the enzyme without changing its expression levels. The increment in the activity was evidenced by the activity ratio –G6P/+G6P, reaching values near 0.32 from the 0.024 observed in non-infected Sertoli cells. This ratio indicates the portion of the expressed enzyme that is active, where values below 0.1 correspond to totally inactive enzyme and those over 0.7 denote a totally active enzyme. Sertoli MGS activation was not total, because the activity ratio –G6P/+G6P reached only 0.32 [Figure 8C]. This could be explained by an inefficient infection or using a small number of adenoviral particles. For both Sertoli cell types the same amount of adenoviral particles were used. Nevertheless, the infection efficiency can differ between both Sertoli cell types.

Additionally, the incomplete activation can be due to some mechanism that prevents the over activation of the enzyme by PTG in Sertoli cells. This idea is supported by the observed high levels of pS640MGS and could be sustained by the presence of Malin and Laforin in Sertoli cells (Villarroel-Espíndola et al. 2013), which promotes PTG poli-ubiquitination and proteasome degradation (Worby et al. 2008). Another explanation for the mild activation of MGS by PTG overexpression can be explained by a deficiency in the levels of the allosteric activator [G6P]. During total activity assays, G6P is added to a final concentration of 6.6 mM, while during intrinsic activity measurement the concentration of G6P depends on how much of this

metabolite is present in the cell lysate. Thus, having in mind that Sertoli cells convert more than 95% of the incorporated glucose into lactate via glycolysis, the G6P concentration in these cells could be very low because the equilibrium of the glucose metabolism is shifted to lactate production via glycolysis. For this reason, higher levels of activation were obtained only in total activity assays and not during AdPTG overexpression or intrinsic activity measurements. Despite the mild activation in PTG infected cells, the glycogen content increased more than 30 and 100 times compared to the controls for primary Sertoli and 42GPA9 Sertoli cells, respectively [Figure 8D].

By contrast, the previously described activator of the MGS, lithium chloride, generated a very weak increase in the intrinsic activity and a decrease of the total activity, resulting in a faint rise in the activity ratio –G6P/+G6P with respect to the control [Figure 9A and B]. Likewise, lithium induced the formation of pS640MGS granules and an electrodense glycogen-like structure in the cytoplasm of 42GPA9 Sertoli cells [Figure 10A and B]. It is important to note that the nuclear localization of the phosphorylated enzyme did not change during lithium treatments. In primary Sertoli cells obtained from mice treated with therapeutic doses of lithium, the same cytosolic granule of pS640MGS was observed [Figure 10C]. Hence, lithium effects on Sertoli cells must be examined carefully, because MGS in these cells does not respond as has been described in other models where the enzyme is activated and relocated to a large number of glycogen particles (Oreña et al. 2000, Vilchez et al. 2007). The small increase in the activity ratio –G6P/+G6P during lithium treatments can be explained by a decrease in the total activity in addition with a lesser increase in the intrinsic activity with respect to non-treated cells. Despite this, glycogen content increased 2 and 3 times in primary Sertoli and 42GPA9 Sertoli cells, respectively.

Moreover, the accumulation of the pS640MGS in cytosolic granules in addition to the glycogen-like structure observed in lithium-treated 42GPA9 Sertoli cells could be associated because they are consistent with the glycogen-dependent subcellular localization (Díaz et al. 2011, Wilson et al. 2010). This effect was corroborated in a physiological model of primary Sertoli cells from mice treated with therapeutic doses of lithium, supporting the idea that this particular accumulation of the enzyme is a glycogen granule as a result of the weak activation of the MGS. It is important to highlight that lithium treatments cause stress in testicular cells including Sertoli cells (Zarnescu & Zamfirescu 2006). In the case of Sertoli 42GPA9 cells, 90 mM lithium chloride was added directly to the cell culture medium for 24 hours [acute treatment] provoking an osmotic stress. For primary Sertoli cells, the mice were treated with therapeutic doses of lithium carbonate for 30 days [chronic treatments], which induces the formation of vacuoles. Nevertheless, the viability of treated cells did not decrease [data not shown].

Thus, by comparing both methods for MGS activation, these results indicate that direct dephosphorylation of the enzyme by PP1 through PTG overexpression is a more potent approach to induce the glycogen synthesis in comparison with the inhibition of GSK3 by lithium on Sertoli cells.

5.2 What is the role of MGS in Sertoli cells?

It was described that MGS in Sertoli cells is present as an almost inactive enzyme that cannot be completely activated by two different described methods. Then, why do Sertoli cells present an inactive enzyme? Or more precisely, what could be the function of the MGS in Sertoli cells?

For more than 2 decades, enzymes involved in metabolic processes have been linked to RNAs. Glyceraldehyde-3-phospate dehydrogenase [GAPDH] was the first glycolytic enzyme to be discovered as a transfer RNA [tRNA] binding protein (Ryazanov 1985, Singh & Green 1993). For MGS there is only one published study that associates the enzyme with RNA metabolism, specifically the pS640MGS was discovered co-sedimenting with actively translating ribosomes and its presence regulates the expression of different mRNAs in HeLa cells (Fuchs et al. 2011). Therefore, the latter study guided us to analyse whether ribonuclear particles could interact with MGS in Sertoli cells.

Argonaute-2 [AGO2] is one of the principal components of the RNA processing bodies, and it was highly expressed in Sertoli cells when compared with germ cells. In this study MGS was found in close association with AGO2 and other RNA binding proteins [CPEB1, CPEB4 and DDX6] in Sertoli cells by co-immunofluorescence and co-immunoprecipitation assays [Figure 11, 13 and 14]. Additionally, co-localization of MGS, CPEB1 and Staufen in different zones of the cytoplasm of Sertoli 42GPA9 cells was also visualized [Supplementary figure 1]. Staufen is a double-stranded RNA binding protein acting as an essential factor for mRNA decay in RNA processing bodies and stress granules (Barbee et al. 2006, Eulalio et al. 2007, Moser & Fritzler 2010). Moreover, during cytosolic MGS granules formation by lithium treatments, co-localization of the MGS granules with different components of RNPs like AGO2, GW182, and Staufen was also observed [Supplementary figure 2]. Hence, these co-immunofluorescence experiments showed that under different conditions, some pool of the MGS was always co-localizing with different RBPs components in Sertoli cells.

Co-immunoprecipitation assays corroborated the efficiency of the commercial antibodies to immunoprecipitate MGS from crosslinked Sertoli cell extracts [Figure 12]. The crosslinking was made to emulate the first step and maintain the same conditions of the RNA immunoprecipitation assay. Three MGS antibodies were used to immunoprecipitate the enzyme [ctMGS, 3886 and pS640MGS] from Sertoli cell extracts, being the ctMGS antibody the most successful to pull down the enzyme, which was confirmed by mass spectrometry. In addition to MGS, 33 different proteins were found in the excised band of ≈80-90 KDa [listed alphabetically in Supplementary figure 3A]. These proteins were classified by their class and molecular function using the bioinformatic tool PANTHER [Protein Analysis Through Evolutionary Relationships]. By molecular function, 19 proteins [57.6% of the total] were associated to the category of binding. Inside this category, 14 of them link to nucleic acid binding, 13 proteins to catalytic activity [38.5% of the total], and 7 of them relate to helicase activity [Supplementary figure 3B]. By protein class classification, 14 proteins [42.2% of the total] were associated to nucleic acid binding, and 9 of them specifically to RNA binding [Supplementary figure 3C]. Thus, a large number of the co-immunoprecipitated proteins with the MGS were associated to the category of RNA binding.

Besides MGS, the second protein enriched in the IP extracts was the heat shock protein 90 [HSP90]. This chaperone has been described to be required for the interaction between different components of the RNA-induced silencing complex, like AGO2 and Hiwi with Dicer, through its ATPase activity in HEK293T cells (Tahbaz et al. 2004). In the same way, HSP90 activity mediates the recruitment of AGO2 to p-bodies and stress granules, the assembly of RISC, and the loading of RNA duplexes to AGO2 in mammals, Drosophila, and plants (Iki et al. 2010, Iwasaki et al. 2010,

Makhnevych & Houry 2012, Matsumoto et al. 2011, Meister 2013, Miyoshi et al. 2010, Pare et al. 2009). Moreover, with this analysis, it is possible to discard a cross-reaction of MGS [≈80-90 KDa] and AGO2 [≈95-105 KDa] antibodies, because of the similar molecular weight of them. During pull down assays, AGO2 could not be co-immunoprecipitated after the pull down of MGS with the ctMGS antibody [Figure 13A]. By contrast, pS640MGS could be detected after the immunoprecipitation of AGO2 [Figure 13B].

Both results can be explained by the high levels of phosphorylation of the enzyme, together with the behaviour of the antibodies against the MGS and AGO2 in Sertoli cells. As described in this work, the ct-MGS antibody improved the enzyme detection by Western blot when it was dephosphorylated [phosphatase assays, Figure 6], or when it was highly concentrated [MGS pull down corroboration, Figure 13A], while the pS640MGS antibody efficiently detected the phosphorylated enzyme by Western blot in Sertoli cells, due to high levels of phosphorylation, even if pS640MGS is not concentrated. The latter was observed in the phosphatase assays where despite the dephosphorylation treatments, the pS640MGS antibody could still detect the portion of the enzyme that remained phosphorylated [Figure 6].

Accordingly, when MGS was immunoprecipitated with ctMGS antibody, AGO2 was not detectable possibly because the AGO2 antibody could not detect small amounts of the protein. Nevertheless, when AGO2 was successfully immunoprecipitated, the pS640MGS antibody was able to detect the small quantities of the phosphorylated enzyme in the IP extract. This possible explanation is also useful to the co-IPs of the pS640MGS with the different RBPs, where different levels of the phosphorylated enzyme in each pull down extract was observed in both Sertoli cell types [Figure 14].

Different RBPs interact with other proteins depending on the presence of an RNA molecule like the RNAse DICER and the HIV transcription activator Tat (Bennasser & Jeang 2006). In other cases, the interaction of a known RBP, like the human antigen R [HuR], with myosin IIA is strictly RNA dependent and requires their phosphorylation (Doller et al. 2013). Nevertheless, in this work the interaction of pS640MGS and AGO2 was not dependent on an RNA molecule neither on the MGS activity state [Figure 15]. It seems that the pS640MGS/AGO2 interaction was determined by the phosphorylation of the enzyme, because despite the PTG overexpression, the remaining phosphorylated enzyme was still interacting with AGO2 [Figure 15]. Therefore, it would be interesting to investigate which of the phosphorylation sites/domains of the MGS are essential for this interaction. These could be achieved by the mutation of the phosphorylatable serines [Ser to Ala mutations], by mimicking the phospho-serines [Ser to Asp mutations], or deleting specific regions to prove whether this interaction still occurs.

Considering the interaction of pS640MGS with AGO2 and other RBPs, and that all these RBPs are associated with mRNAs, the interaction of the phosphorylated enzyme with mRNAs was examined. To prove this interaction, RNA inmunoprecipitation assay [RIP] followed by an RNA profiling of the co-immunoprecipitated mRNAs was evaluated. The RIP was performed using the ctMGS and pS640MGS antibodies for the MGS, and an anti rabbit IgG as a negative control for the assay. Both MGS antibodies were used to make a duplicate of the RIP, because the ctMGS antibody should detect the phosphorylated enzyme during the IP, and all the information of the mRNA microarray of the pS640MGS RIP should be found in the ctMGS RIP. Before the mRNA profiling, the success of the MGS IP with both antibodies was corroborated, and as previously mentioned, the ctMGS

antibody was very efficient to immunoprecipitate the enzyme but not to detect it in the blots [Figure 17, up]. In contrast, the pS640MGS was ineffective to pull down the enzyme in comparison with ctMGS, but not to detect the phosphorylated enzyme in the blots as was visualized in the input and unbound lanes [Figure 17, down].

Therefore, after MGS pull down, RNA purification was performed with good yields and RNA integrity in each IP extract. Despite the differences in the MGS pull down observed by Western blot, comparable concentrations of RNA were obtained [27 ng/uL for ctMGS and 24 ng/uL pS640MGS]. Additionally, similar patterns of fluorescence where mean mRNAs in length should be visualized and the presence of the 18S and 28S ribosomal subunits were found in both MGS IPs [Figure 18A]. In the Rb IgG IP less RNA concentration [16 ng/uL] was obtained and practically all concentrated RNAs were of less than 200 nt in length, without detecting the ribosomal subunits. Hence, the detection of small and large ribosomal subunits immunoprecipitating with the MGS are in strong concordance with the observed association of the phosphorylated enzyme with ribosomal subunits in Hela cells (Fuchs et al. 2011).

As pS640MGS IP was notably lower in comparison with ctMGS IP, and taking into account the obtained data of the RNA quality control, it is possible to suggest that there are different populations of the enzyme in Sertoli cells. One portion of the enzyme would be bound to the few observed glycogen amounts, able to be dephosphorylated by PP1-PTG, and able to achieve glycogen synthesis during certain periods or stimulus. This could correspond to a portion of total MGS that is unphosphorylated, in addition to the enzyme that is phosphorylated and accessible to be dephosphorylated. Meanwhile the other portion of the enzyme could have an unknown role by

its interaction with RBPs and RNAs, which would correspond uniquely to the phosphorylated enzyme that is not accessible to be dephosphorylated, because is not bound to glycogen.

The number of mRNAs in each RIP also supports this idea. For the ctMGS RIP a total of 1191 mRNAs were obtained, while for the pS640MGS RIP 1474 mRNAs that had higher fold changes with respect to the negative control, 453 were shared [Figure 18B, ctMGS-Rb IgG and pS640MGS-Rb IgG]. Interestingly, despite the strong immunoprecipitation of the enzyme with the ctMGS in comparison to the pS640MGS, more mRNAs were found after the MGS pull down with the pS640MGS. This suggests that the observed mRNAs in the ct-MGS IP correspond to the mRNAs found in the pS640MGS IP, corroborating the idea that the phosphorylated enzyme is interacting with RNAs.

Mouse cells can transcribe more than 30,000 genes giving at least the same number of mRNAs. For this reason, the shared 453 mRNAs between both MGS RIPs would correspond to a specific population of mRNAs. To find some predominant function associated with these mRNAs, a classification of different categories according to their molecular function or biological process was performed [Figure 19A and B]. Regarding the molecular function, two main categories were obtained, binding [nucleic acid and protein binding] and catalytic activity [Figure 19A]. For the binding category, DNA binding was enriched in comparison with the RNA and protein binding, and was mainly related to transcription factor activity with 48 genes that correspond to 10.5% of the total 453 mRNAs encoded genes. Whereas for the catalytic activity category, no predominant term was observed. Then, the classification by biological process revealed a principal category, metabolic process, with nearly the half of the genes [Figure 19B, up].

Remarkably, this category was almost exclusively constituted by genes related to primary metabolic processes [Figure 19B, down], which in turn, were fundamentally composed by two categories: nucleobase, nucleoside, nucleotide and nucleic acid metabolic process where transcription was the category with the higher number of genes, as was expected by the molecular function classification. The other main category was protein metabolic process where no enriched term was found. After the identification and classification of the mRNAs of both RIPs, it is possible to suggest that pS640MGS is interacting with a population of mRNAs mostly associated with the process of transcription in Sertoli cells.

In this point is important to highlight the fact that MGS was not immunoprecipitated alone during the RIP assays, and that many of the proteins found pulled down with the enzyme are RNA binding proteins. This means that many of the enriched mRNAs found in the IP´s were not uniquely pulled down by the MGS.

To identify the possible role of MGS in Sertoli cells, the association of MGS to RNAs and RBPs was explored. As described earlier, many metabolic enzymes have been related to RNA metabolism and even regulating their own mRNAs. One important feature of some metabolic enzymes that interact with RNAs is the presence of two identical ß-α-ß folds, each one is associated with a nucleotide binding surface called Rossmann fold (Buehner et al. 1973, Singh & Green 1993). This structural domain has been described to bind nucleotides, and specifically nicotinamide adenine dinucleotide [NAD^+] in different glycolytic enzymes. Among them, it is possible to find some dehydrogenases, like lactate dehydrogenase [LDH] and glyceraldehyde-3-phosphate dehydrogenase [GAPDH], and kinases, like phosphoglycerate kinase [PGK] (Nagy et al. 2000, Pioli et al. 2002, Shetty et al. 2004). In the

case of LDH and GAPDH, which have been studied in more detail, NAD^+ inhibits the RNA binding capacity of these proteins by competing with RNAs for the Rossmann fold, making the protein/RNA interaction dependent on NAD^+ concentration (Nagy & Rigby 1995, Nagy et al. 2000, Pioli et al. 2002). Moreover, it is important to highlight that enzymes that bind to mRNA AU-rich elements in the 3`UTR were found associated with polysomes and interacting with cytoskeleton structures (Arnold et al. 1971, Nagy & Rigby 1995, Pioli et al. 2002, Walsh et al. 1989).

MGS localization has been reported to be directed by the remodeling actin filaments in rabbit muscle cells (Prats et al. 2005). Additionally, this enzyme belongs to the family of glycosyltransferases [GT] and specifically to the GT3, because of the use of UDP-glucose as a substrate and its tight regulation by reversible phosphorylation and allosteric effector [G6P]. Glycosyltransfereases contain conserved domains that topologically resembles the Rossmann fold, with two Rossmann domains separated by a large cleft where the catalysis occurs (Buschiazzo et al. 2004, Horcajada et al. 2006, Vrielink et al. 1994). Thus, MGS shares different features with other metabolic enzymes that bind RNA like the association with polysomes, cytoskeleton interaction and the Rossmann fold like topology.

Archaeal glycogen synthase crystallization and human MGS mutational studies have determined that this enzyme has a high affinity glycogen binding site, which is different to the acceptor site in the catalytic cleft and determines the interaction between the enzyme and the polysaccharide (Díaz et al. 2011). This indicates that MGS is anchored to glycogen molecules by the high affinity site, and synthetizing glycogen through the low affinity glycogen-binding site in the catalytic cleft.

Glycogen content in Sertoli cells is very low [≈ 4 ug/mg protein] in comparison with astrocytes [≈40 ug/mg protein] or when the enzyme was partially activated by PTG overexpression [≈740 ug/mg protein]. Additionally, the protein level of MGS is abundant and does not correlate with the low levels of glycogen, leaving the question about where MGS is anchored in Sertoli cells. A possible answer to this question fits well with the previous idea that suggests the presence of different populations of MGS in Sertoli cells. One fraction of the enzyme that is susceptible to be activated for glycogen synthesis should be bound to the small number of glycogen particles through both glycogen-binding sites. The non-catalytic/glycogen high affinity-binding site should be used to position the enzyme for catalysis, while the catalytic/glycogen low affinity-binding site would interact with other glycogen molecules as a primer for the polysaccharide polymerization. On the other hand, another population of the MGS that is not anchored to glycogen particles and cannot be activated must be interacting with other molecules through any of both glycogen-binding sites.

This proposal can be sustained by the two dimensional gel electrophoresis assays, where two different populations of the enzyme were clearly observed. The spot that have a more basic isoelectric point [pH 7] might compose one fraction. The fraction that could correspond to the enzyme that is less [or not] phosphorylated, bound to few molecules of glycogen, susceptible to be dephosphorylated and that achieves glycogen synthesis in Sertoli cells. While the fraction of MGS that has an acidic isoelectric point, could correspond to the enzyme that is more phosphorylated, bound to RNAs and RBPs, cannot be dephosphorylated and is achieving a non-metabolic function in Sertoli cells. In this case it can be suggested that MGS could interact with mRNAs or rRNAs through the

catalytic/glycogen low affinity-binding domain. The catalytic/glycogen low affinity-binding site utilizes UDP-glucose for catalysis, and perhaps the UDP extreme of the nucleotide sugar can be recognized by the catalytic cleft of the enzyme. This idea is also supported by the fact that LDH and GAPDH bind to AU-rich elements in the 3`UTR of the mRNAs (Nagy & Rigby 1995, Pioli et al. 2002). Thus, if the catalytic/glycogen low affinity-binding site could interact with RNA molecules, the non-catalytic/glycogen high affinity-binding site must be kept free, but able to bind glycogen without being activated. This effect could be observed during lithium treatments, where the scarce activation of glycogen synthesis only duplicates the glycogen content. In this way, if small amounts of glycogen are available in the cytoplasm, the free non-catalytic/glycogen high affinity-binding site should interact with it, and the consequence could be the formation of cytosolic granules of the phosphorylated MGS that were still co-localizing with RBPs during lithium treatments.

Sertoli cells achieve a structural function supporting germ cell development through the seminiferous epithelium and as a nutritional supply of lactate for developing germ cells. Sertoli cell metabolism is essential for maintaining the spermatogenic process, and thus, male fertility. Carbohydrate metabolism in Sertoli cells is focused in lactate production through glycolysis, since a high percentage of the incorporated glucose is converted to lactate while less than a 5% is converted to CO_2, lipids and glycogen (Robinson & Fritz 1981). Interestingly, glycogen synthesis was not induced in the presence of insulin (Robinson & Fritz 1981). Even in the absence of glucose, Sertoli cells change their metabolism to maintain the lactate production by the activation of AMP-activated kinase [AMPK] and stimulating catabolic pathways (Riera et al. 2009). Moreover, lipids have been described as the main

source of energy for Sertoli cells via lipid β oxidation, because ATP production decreases only when lipid β oxidation, and not glycolysis, was blocked (Xiong et al. 2009).

In this biological scenario, the presence and the contribution of glycogen to Sertoli cell carbohydrate metabolism is scarce and the results of this study support it. Sertoli cells produce low amounts of glycogen and this agrees with the almost total inactivity of glycogen synthase. A relevant issue is that Sertoli cells used in this work were obtained from sexually mature mice, where Sertoli cells are totally differentiated and their metabolism works as was described above.

Mature Sertoli cells do not proliferate and are fundamental to maintaining spermatogenesis by hormonal control (Alves et al. 2013), while during embryonic stages, pre-Sertoli cells are involved in testes formation through the activation of the master gene *Sry*. Glycogen accumulation and SOX9 expression occurs immediately after the transient activation of *Sry* in pre-Sertoli cells, indicating that testicular cord formation during testiculogenesis needs an energetic support like glycogen (Kanai et al. 2005, Matoba et al. 2005, 2008). Furthermore, in mice lacking the insulin receptor family that usually activates glycogen synthesis, *Sry* activation and SOX9 expression were reduced, indicating that the insulin signalling pathway is essential for pre-Sertoli cells during male sex determination (Nef et al. 2003). This suggests that during testicular organogenesis, glycogen synthase must be activated to synthesize glycogen and maintain the expression of SOX9 after the activation of *Sry* in immature Sertoli cells. For these reasons, it is possible to propose that in immature Sertoli cells, during male sex determination in embryonic stages, glycogen synthase achieves a metabolic role induced by insulin signalling, while in mature Sertoli cells, MGS is not focused on

performing this metabolic role due to the observed small amounts of glycogen and could be accomplishing other functions related to RNA metabolism.

Neurons are other cell models where the glycogen synthesis machinery is present, but in an inactive form (Vilchez et al. 2007). However when the malin-laforin complex is truncated, by mutations in any of their components, the proteasome dependent degradation of PTG is inhibited promoting the glycogen accumulation because of the enforced expression of PTG in neurons (Vilchez et al. 2007). In this work the overexpression of PTG stimulates the dephosphorylation of MGS, and as was presented in this work, the activation of the glycogen synthesis. This suggests that MGS in neurons is maintained inactive and possibly accomplishing the same non-metabolic function similarly to Sertoli cells. In the same way, is important to emphasize the phosphorylation level of MGS, because in this work the observed neuronal apoptosis was due to the dephosphorylation of the enzyme.

In the work of Fuchs et. al. 2011 the enzyme was silenced with siRNAs and the translation of a subset of transcripts related with protein biosynthesis were affected in addition with a loss of polysomes. Interestingly, in GSK3β depleted cells the loss of polysomes was very similar to the observed during MGS depletion, suggesting the relevance of the MGS phosphorylation by GSK3β could be important for this possible new role of the translational regulation of mRNAs expression. Thus, the aforementioned data presented in this study suggest that MGS role in mature Sertoli cells could be associated with the post-transcriptional gene regulation of mRNAs related to transcription.

6. Supplementary Figures

Supplementary figure 1. MGS co-localize with CPEB1 and Staufen in Sertoli cells. Co-immunofluorescence study of fixed and permeabilized Sertoli 42GPA9 cells. The cells were incubated with antibodies against total MGS [green], CPEB1 [red] and Staufen [blue] in a dilution of 1:200, and then with the secondary antibodies Alexa-488 donkey anti mouse IgG, Alexa-568 donkey anti goat IgG and Alexa-633 donkey anti rabbit IgG in a dilution of 1:300. Co-localization of the immunofluorescent signals are shown in MERGE. Scale bars, 20 um.

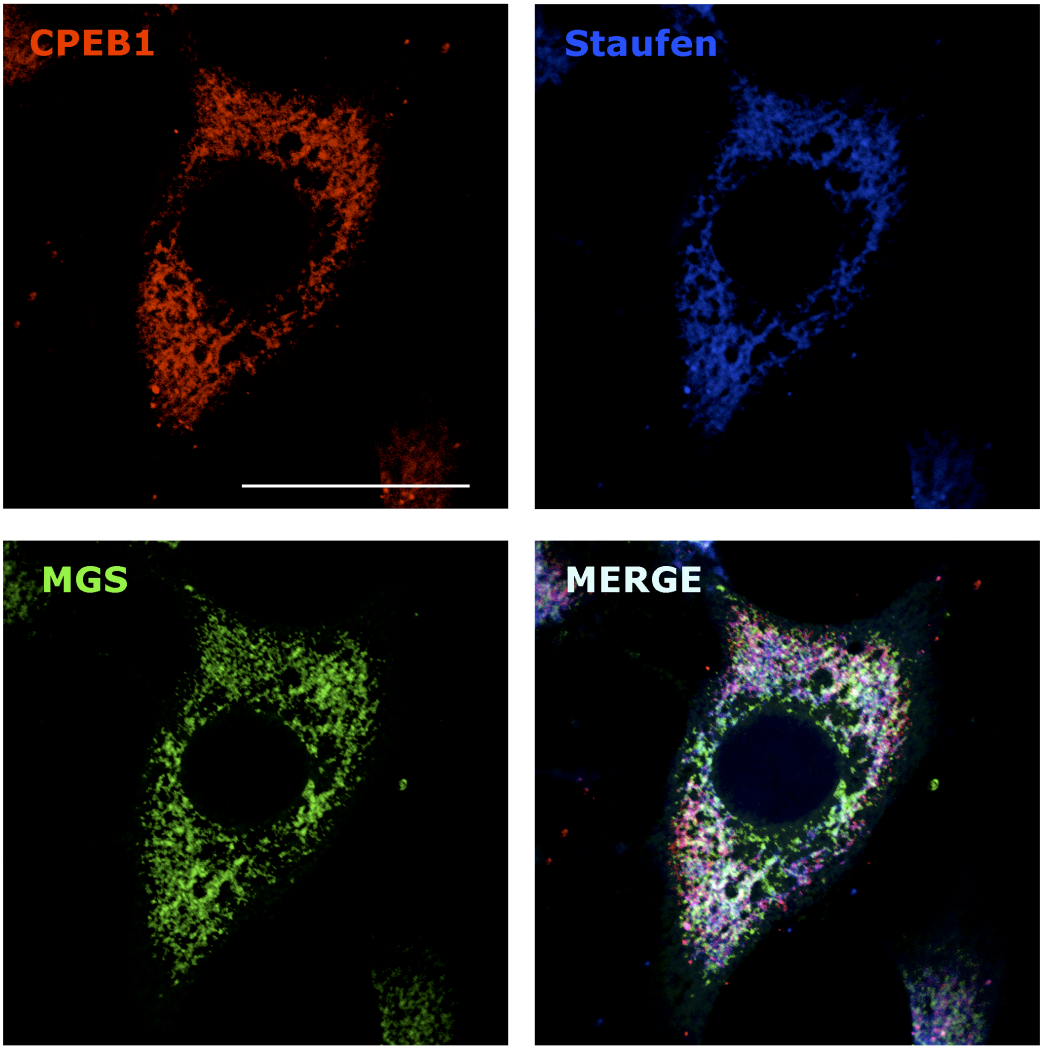
CPEB1
Staufen
MGS
MERGE

Supplementary figure 2. MGS granules co-localize with GW182, AGO2 and Staufen in lithium treated Sertoli cells. Co-immunofluorescence study of fixed and permeabilized Sertoli 42GPA9 cells previously treated with 30mM LiCl for 24 hours. As is shown for each case, the cells were incubated with antibodies against GW182, AGO2, Staufen, total MGS [MGS] and its phosphorylated form in serine 640 [pS640MGS] in a dilution of 1:200. Then the secondary antibodies Alexa-568 donkey anti mouse IgG, Alexa-568 donkey anti goat IgG and Alexa-488 donkey anti rabbit IgG were added in a dilution of 1:300. Co-localization of the fluorescent signals and it zoom are indicated in white squares for each image. Scale bars, 10 um.

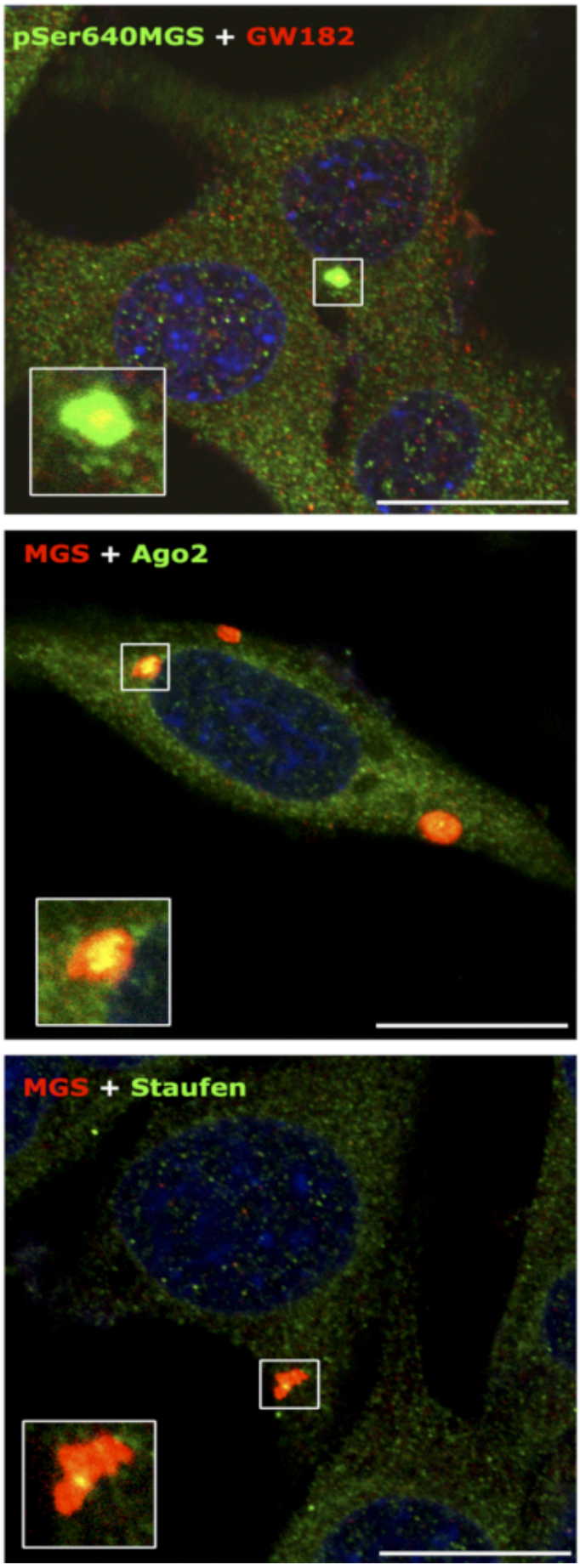
pSer640MGS + GW182
MGS + Ago2
MGS + Staufen

Supplementary Figure 3. MGS interacting proteins are mainly associated to RNA binding in Sertoli cells. MGS was immunoprecipitated using 3 different antibodies and these extracts were loaded and run in 8% SDS-PAGE. The band that corresponds to MGS by size was excised and analysed by mass spectrometry. In A) are listed the proteins that were found additionally to the MGS in the excised band. These proteins were classified by its molecular function B) and protein class C) using the bioinformatic tool for gene classification PANTHER. For both cases, the terms are associated with colours. The categories with more components are highlighted in yellow and the correspondingly piece of the pie graph is detached. Black arrows indicate the distribution of each enriched term with another pie graph.

A

1.- 60S ribosomal protein L4
2.- ATP-dependent RNA helicase DDX1
3.- ATP-dependent RNA helicase DDX50
5.- Coatomer subunit gamma-1
6.- DDB1- and CUL4-associated factor 8
7.- DNA replication licensing factor MCM5
8.- DNA replication licensing factor MCM7
9.- DNA topoisomerase 3-beta-1
10.- DnaJ homolog subfamily C member 10
11.- FACT complex subunit SSRP1
12.- Heat shock protein HSP 90-alpha
13.- Heat shock protein HSP 90-beta
14.- Heterogeneous nuclear ribonucleo-protein U
15.- Keratin, type I cytoskeletal 10
16.- Keratin, type I cytoskeletal 15
17.- Keratin, type II cytoskeletal 1
18.- Keratin, type II cytoskeletal 73
19.- Myosin-10
20.- Myosin-9
21.- Nuclear pore complex protein Nup93
22.- Nucleolar RNA helicase 2
23.- Polycomb protein Suz12
24.- Polyubiquitin-B
25.- Probable ATP-dependent RNA heli-case DDX27
26.- Putative pre-mRNA-splicing factor ATP-dependent RNA helicase DHX15
27.- Putative rRNA methyltransferase 3
28.- Ribosomal RNA processing protein 1 homolog B
29.- Semaphorin-3C
30.- Testis-expressed sequence 10 pro-tein
31.- Translocation protein SEC63 homo-log
32.- Transportin-3
33.- U4/U6 small nuclear ribonucleopro-tein Prp3

B

Molecular Function Classification

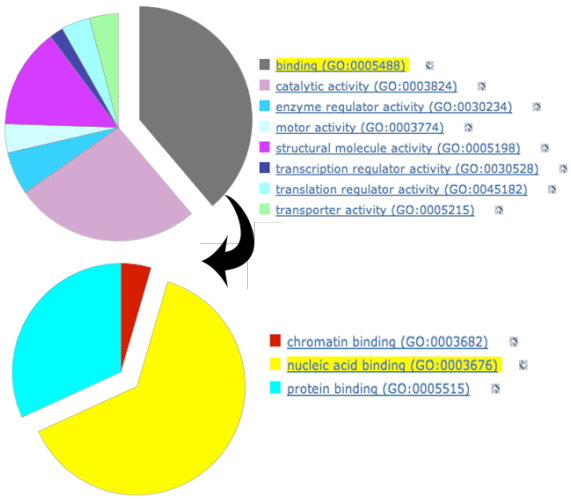

C

Protein Class Classification

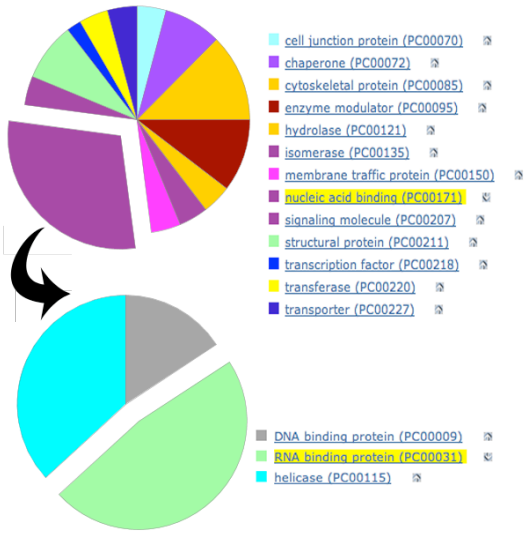

7. Bibliography

Aggen J, Nairn A, Chamberlin R. 2000. Regulation of protein phosphatase-1. *Chem. Biol.* 7(1):R13–23

Al-Azemi M, Omu FE, Kehinde EO, Anim JT, Oriowo M a, Omu AE. 2010. Lithium protects against toxic effects of cadmium in the rat testes. *J. Assist. Reprod. Genet.* 27(8):469–76

Alves MG, Rato L, Carvalho R a, Moreira PI, Socorro S, Oliveira PF. 2013. Hormonal control of sertoli cell metabolism regulates spermatogenesis. *Cell. Mol. Life Sci.* 70(5):777–93

Angulo C, Castro M a, Rivas CI, Segretain D, Maldonado R, et al. 2008. Molecular identification and functional characterization of the vitamin c transporters expressed by sertoli cells. *J. Cell. Physiol.* 217(3):708–16

Anway MD, Folmer J, Wright WW, Zirkin BR. 2002. Isolation of sertoli cells from adult rat testes: an approach to ex vivo studies of sertoli cell function. *Biol. Reprod.* 68(3):996–1002

Arnold H, Henning R, Pette D. 1971. Quantitative comparison of the binding of various glycolytic enzymes to f-actin and the interaction of aldolase with g-actin. *Eur. J. Biochem.* 22(1):121–26

Bajpai M, Gupta G, Setty BS. 1998. Changes in carbohydrate metabolism of testicular germ cells during meiosis in the rat. *Eur. J. Endocrinol.* 138(3):322–27

Banerji TK, Maitra SK, Dey M, Hawkins HK. 2001. Gametogenic responses of the testis in spotted munia (lonchura punctulata; aves) to oral administration of lithium chloride. *Endocr. Res.* 27(3):345–56

Barbee S a, Estes PS, Cziko A-M, Hillebrand J, Luedeman R a, et al. 2006. Staufen- and fmrp-containing neuronal rnps are structurally and functionally related to somatic p bodies. *Neuron.* 52(6):997–1009

Beinert H, Kennedy MC. 1993. Aconitase, a two-faced protein: enzyme and iron regulatory factor. *FASEB J.* 7(15):1442–49

Bennasser Y, Jeang K-T. 2006. Hiv-1 tat interaction with dicer: requirement for rna. *Retrovirology*. 3:95

Bourdon V, Lablack a, Abbe P, Segretain D, Pointis G. 1998. Characterization of a clonal sertoli cell line using adult pylt transgenic mice. *Biol. Reprod.* 58(2):591–99

Bouskila M, Hunter R, Ibrahim A, Delattre L, Peggie M, et al. 2010. Allosteric regulation of glycogen synthase controls glycogen synthesis in muscle. *Cell Metab.* 12(5):456–66

Boussouar F, Benahmed M. 2004. Lactate and energy metabolism in male germ cells. *Trends Endocrinol. Metab.* 15(7):345–50

Brady MJ, Printen JA, Mastick CC, Saltiel AR. 1997. Role of protein targeting to glycogen (ptg) in the regulation of protein phosphatase-1 activity. *J. Biol. Chem.* 272(32):20198–204

Buehner M, Ford GC, Moras D, Olsen KW, Rossmannt MG. 1973. D-glyceraldehyde-3-phosphate dehydrogenase: three-dimensional structure and evolutionary significance. *Proc. Natl. Acad. Sci. U. S. A.* 70(11):3052–54

Buschiazzo A, Ugalde JE, Guerin ME, Shepard W, Ugalde R a, Alzari PM. 2004. Crystal structure of glycogen synthase: homologous enzymes catalyze glycogen synthesis and degradation. *EMBO J.* 23(16):3196–3205

Carosa E, Radico C, Giansante N, Rossi S, D'Adamo F, et al. 2005. Ontogenetic profile and thyroid hormone regulation of type-1 and type-8 glucose transporters in rat sertoli cells. *Int. J. Androl.* 28(2):99–106

Castello A, Fischer B, Eichelbaum K, Horos R, Beckmann BM, et al. 2012a. Insights into rna biology from an atlas of mammalian mrna-binding proteins. *Cell.* 149(6):1393–1406

Castello A, Fischer B, Eichelbaum K, Horos R, Beckmann BM, et al. 2012b. Insights into rna biology from an atlas of mammalian mrna-binding proteins. *Cell*, pp. 1–14

Chan TM, Exton JH. 1976. A rapid method for the determination of glycogen content and radioactivity in small quantities of tissue or isolated hepatocytes. *Anal. Biochem.* 71(1):96–105

Cheng CY, Mruk DD. 2012. The blood-testis barrier and its implications for male contraception. *Pharmacol Rev.* 64(1):16–64

Chu E, Allegra CJ. 1996. The role of thymidylate synthase as an rna binding protein. *Bioessays.* 18(3):191–98

Chu E, Koeller DM, Casey JL, Drake JC, Chabner BA, et al. 1991. Autoregulation of human thymidylate synthase messenger rna translation by thymidylate synthase. *Proc. Natl. Acad. Sci. U. S. A.* 88(20):8977–81

Chu E, Takimoto CH, Voeller D, Grem JL, Allegra CJ. 1993. Specific binding of human dihydrofolate reductase protein to dihydrofolate reductase messenger rna in vitro. *Biochemistry.* 32(18):4756–60

Cid E, Cifuentes D, Baqué S, Ferrer JC, Guinovart JJ. 2005. Determinants of the nucleocytoplasmic shuttling of muscle glycogen synthase. *FEBS J.* 272(12):3197–3213

Cieśla J. 2006. Metabolic enzymes that bind rna: yet another level of cellular regulatory network? *Acta Biochim. Pol.* 53(1):11–32

Courtens JL, Plöen L. 1999. Improvement of spermatogenesis in adult cryptorchid rat testis by intratesticular infusion of lactate. *Biol. Reprod.* 61(1):154–61

De BP, Gupta S, Zhao H, Drazba JA, Banerjee AK. 1996. Specific interaction in vitro and in vivo of glyceraldehyde-3-phosphate dehydrogenase and la protein with cis-acting rnas of human parainfluenza virus type 3. *J. Biol. Chem.* 271(40):24728–35

De Kretser DM, Catt KJ, Dufau ML, Hudson B. 1971. Studies on rat testicular cells in tissue culture. *J. Reprod. Fertil.* 24(3):311–18

De Rooij DG, Russell LD. All you wanted to know about spermatogonia but were afraid to ask. *J. Androl.* 21(6):776–98

Díaz A, Martínez-Pons C, Fita I, Ferrer JC, Guinovart JJ. 2011. Processivity and subcellular localization of glycogen synthase depend on a non-

catalytic high affinity glycogen-binding site. *J. Biol. Chem.* 286(21):18505–14

Doller A, Schulz S, Pfeilschifter J, Eberhardt W. 2013. Rna-dependent association with myosin iia promotes f-actin-guided trafficking of the elav-like protein hur to polysomes. *Nucleic Acids Res.* 1:1–16

Erkkilä K, Aito H, Aalto K, Pentikäinen V, Dunkel L. 2002. Lactate inhibits germ cell apoptosis in the human testis. *Mol. Hum. Reprod.* 8(2):109–17

Eulalio A, Behm-Ansmant I, Izaurralde E. 2007. P bodies: at the crossroads of post-transcriptional pathways. *Nat. Rev. Mol. Cell Biol.* 8(1):9–22

Fabbrini a, Re M, Conti C. 1969. Glycogen in the normal human testis: a histochemical and histoenzymatic study. *J. Endocrinol.* 43(4):499–506

Fernández-Novell JM, Bellido D, Vilaró S, Guinovart JJ. 1997. Glucose induces the translocation of glycogen synthase to the cell cortex in rat hepatocytes. *Biochem. J.* 321 (Pt 1:227–31

Ferrer JC, Baqué S, Guinovart JJ. 1997. Muscle glycogen synthase translocates from the cell nucleus to the cytosol in response to glucose. *FEBS Lett.* 415(3):249–52

Fouquet JP, Guha S. 1969. Glycogen, phosphorylase and glycogen synthase in hamster testis during postnatal development. *J. Reprod. Fertil.*, pp. 455–64

Friedman DL, Larner J. 1963. Studies on udpg-alpha-glucan transglucosylase iii. interconversion of two forms of muscle udpg-alpha-glucan transglucosylase by a phosphorylation-dephosphoylation reaction sequence. *Biochemistry*, pp. 669–75

Fuchs G, Diges C, Kohlstaedt L a, Wehner K a, Sarnow P. 2011. Proteomic analysis of ribosomes: translational control of mrna populations by glycogen synthase gys1. *J. Mol. Biol.* 410(1):118–30

Fugassa E, Palmero S, Gallo G. 1987. Triiodothyronine decreases the production of androgen binding protein by rat sertoli cells. *Biochem. Biophys. Res. Commun.* 143(1):241–47

Fukuda T, Hedinger C, Groscurth P. 1975. Ultrastructure of developing germ cells in the fetal human testis. *Cell Tissue Res.* 161(1):55–70

Galardo MN, Riera MF, Pellizzari EH, Cigorraga SB, Meroni SB. 2007. The amp-activated protein kinase activator, 5-aminoimidazole-4-carboxamide-1-b-d-ribonucleoside, regulates lactate production in rat sertoli cells. *J. Mol. Endocrinol.* 39(4):279–88

Galardo MN, Riera MF, Pellizzari EH, Sobarzo C, Scarcelli R, et al. 2010. Adenosine regulates sertoli cell function by activating ampk. *Mol. Cell. Endocrinol.* 330(1-2):49–58

Ganesh S, Agarwala KL, Ueda K, Akagi T, Shoda K, et al. 2000. Laforin, defective in the progressive myoclonus epilepsy of lafora type, is a dual-specificity phosphatase associated with polyribosomes. *Hum. Mol. Genet.* 9(15):2251–61

Gentleman RC, Carey VJ, Bates DM, Bolstad B, Dettling M, et al. 2004. Bioconductor: open software development for computational biology and bioinformatics. *Genome Biol.* 5(10):R80

González-González E, López-Casas PP, del Mazo J. 2008. The expression patterns of genes involved in the rnai pathways are tissue-dependent and differ in the germ and somatic cells of mouse testis. *Biochim. Biophys. Acta.* 1779(5):306–11

Greenberg CC, Meredith KN, Yan L, Brady MJ. 2003. Protein targeting to glycogen overexpression results in the specific enhancement of glycogen storage in 3t3-l1 adipocytes. *J. Biol. Chem.* 278(33):30835–42

Guinovart JJ, Salavert a, Massagué J, Ciudad CJ, Salsas E, Itarte E. 1979. Glycogen synthase: a new activity ratio assay expressing a high sensitivity to the phosphorylation state. *FEBS Lett.* 106(2):284–88

Gunaga KP, Chitra Rao M, Sheth AR, Rao SS. 1972. The role of glycogen during the development of the rat testis and prostate. *J. Reprod. Fertil.*, pp. 157–62

Guo TB, Chan KC, Hakovirta H, Xiao Y, Toppari J, et al. 2003. Evidence for a role of glycogen synthase kinase-3 beta in rodent spermatogenesis. *J. Androl.* 24(3):332–42

Halse R, Fryer LGD, McCormack JG, Carling D, Yeaman SJ. 2003. Regulation of glycogen synthase by glucose and glycogen: a possible role for amp-activated protein kinase. *Diabetes*. 52(1):9–15

Hanashiro I, Roach PJ. 2002. Mutations of muscle glycogen synthase that disable activation by glucose 6-phosphate. *Arch. Biochem. Biophys.* 397(2):286–92

Hárkómen M, Kormano M. 1970. Energy metabolism of the normal and cryptorchid rat testis. *J. Reprod. Fertil.* 25(1):29–39

Hentze MW, Kuhnt LC. 1996. Molecular control of vertebrate iron metabolism : mrna-based regulatory circuits operated by iron , nitric oxide , and oxidative stress. . 93(August):8175–82

Hentze MW, Preiss T. 2010. The rem phase of gene regulation. *Trends Biochem. Sci.* 35(8):423–26

Hess RA, Renato de Franca L. 2008. Spermatogenesis and cycle of the seminiferous epithelium. *Adv. Exp. Med. Biol.* 636:1–15

Holstein A-F, Schulze W, Davidoff M. 2003. Understanding spermatogenesis is a prerequisite for treatment. *Reprod. Biol. Endocrinol.* 1:107

Horcajada C, Guinovart JJ, Fita I, Ferrer JC. 2006. Crystal structure of an archaeal glycogen synthase: insights into oligomerization and substrate binding of eukaryotic glycogen synthases. *J. Biol. Chem.* 281(5):2923–31

Hubbard MJ, Cohen P. 1991. Targeting subunits for protein phosphatases. *Methods Enzymol.* 201:414–27

Iki T, Yoshikawa M, Nishikiori M, Jaudal MC, Matsumoto-Yokoyama E, et al. 2010. In vitro assembly of plant rna-induced silencing complexes facilitated by molecular chaperone hsp90. *Mol. Cell.* 39(2):282–91

Irizarry R a, Hobbs B, Collin F, Beazer-Barclay YD, Antonellis KJ, et al. 2003. Exploration, normalization, and summaries of high density oligonucleotide array probe level data. *Biostatistics*. 4(2):249–64

Iwasaki S, Kobayashi M, Yoda M, Sakaguchi Y, Katsuma S, et al. 2010. Hsc70/hsp90 chaperone machinery mediates atp-dependent risc loading of small rna duplexes. *Mol. Cell.* 39(2):292–99

Jensen J, Jebens E, Brennesvik EO, Ruzzin J, Soos MA, et al. 2006. Muscle glycogen inharmoniously regulates glycogen synthase activity, glucose uptake, and proximal insulin signaling. *Am. J. Physiol. Endocrinol. Metab.* 290(1):E154–E162

Jutte NH, Eikvar L, Levy FO, Hansson V. 1985. Metabolism of palmitate in cultured rat sertoli cells. *J. Reprod. Fertil.* 73(2):497–503

Jutte NH, Grootegoed JA, Rommerts FF, van der Molen HJ. 1981. Exogenous lactate is essential for metabolic activities in isolated rat spermatocytes and spermatids. *J. Reprod. Fertil.* 62(2):399–405

Kaiser G, Monteiro SC, Gelain DP, Souza LF, Perry MLS, Bernard EA. 2005. Metabolism of amino acids by cultured rat sertoli cells. *Metabolism.* 54(4):515–21

Kanai Y, Hiramatsu R, Matoba S, Kidokoro T. 2005. From sry to sox9: mammalian testis differentiation. *J. Biochem.* 138(1):13–19

Kaptain S, Downey WE, Tang C, Philpott C, Haile D, et al. 1991. A regulated rna binding protein also possesses aconitase activity. *Proc. Natl. Acad. Sci. U. S. A.* 88(22):10109–13

Karpel RL, Burchard AC. 1981. A basic isozyme of yeast glyceraldehyde-3-phosphate dehydrogenase with nucleic acid helix-destabilizing activity. *Biochim. Biophys. Acta.* 654(2):256–67

Kim J, Dang C. 2005. Multifaceted roles of glycolytic enzymes. *Trends Biochem. Sci.* 30(3):142–50

Kuramori C, Hase Y, Hoshikawa K, Watanabe K, Nishi T, et al. 2009. Mono-(2-ethylhexyl) phthalate targets glycogen debranching enzyme and affects glycogen metabolism in rat testis. *Toxicol. Sci.* 109(1):143–51

Leiderman B, Mancini RE. 1969. Glycogen content in the rat testis from postnatal to adult ages. *Endocrinology.* 85(3):607–9

Lie PPY, Cheng CY, Mruk DD. 2009. Coordinating cellular events during spermatogenesis: a biochemical model. *Trends Biochem. Sci.* 34(7):366–73

Liu J, Carmell MA, Rivas F V, Mardsen CG, Thomson JM, et al. 2004. Argonaute2 is the catalytic engine of mammalian rnai. *Science (80-.).* 3(305):1437–41

Liu J, Schmitz JC, Lin X, Tai N, Yan W, et al. 2002. Thymidylate synthase as a translational regulator of cellular gene expression. *Biochim. Biophys. Acta.* 1587(2-3):174–82

Liu X, Reig B, Nasrallah IM, Stover PJ. 2000. Human cytoplasmic serine hydroxymethyltransferase is an mrna binding protein. *Biochemistry.* 39(38):11523–31

MacAulay K, Hajduch E, Blair AS, Coghlan MP, Smith S a., Hundal HS. 2003. Use of lithium and sb-415286 to explore the role of glycogen synthase kinase-3 in the regulation of glucose transport and glycogen synthase. *Eur. J. Biochem.* 270(18):3829–38

Makhnevych T, Houry W a. 2012. The role of hsp90 in protein complex assembly. *Biochim. Biophys. Acta.* 1823(3):674–82

Matoba S, Hiramatsu R, Kanai-Azuma M, Tsunekawa N, Harikae K, et al. 2008. Establishment of testis-specific sox9 activation requires high-glucose metabolism in mouse sex differentiation. *Dev. Biol.* 324(1):76–87

Matoba S, Kanai Y, Kidokoro T, Kanai-Azuma M, Kawakami H, et al. 2005. A novel sry-downstream cellular event which preserves the readily available energy source of glycogen in mouse sex differentiation. *J. Cell Sci.* 118(Pt 7):1449–59

Matsumoto K, Minami M, Shinozaki F, Suzuki Y, Abe K, et al. 2011. Hsp90 is involved in the formation of p-bodies and stress granules. *Biochem. Biophys. Res. Commun.* 407(4):720–24

McGowan K, Pekala PH. 1996. Dehydrogenase binding to the 3'-untranslated region of glut1 mrna. *Biochem. Biophys. Res. Commun.* 221(1):42–45

Meister G. 2013. Argonaute proteins: functional insights and emerging roles. *Nat. Rev. Genet.* 14(7):447–59

Meister G, Landthaler M, Patkaniowska A, Dorsett Y, Teng G, Tuschl T. 2004. Human argonaute2 mediates rna cleavage targeted by mirnas and sirnas. *Mol. Cell.* 15(2):185–97

Meroni SB, Riera MF, Pellizzari EH, Galardo MN, Cigorraga SB. 2004. Fsh activates phosphatidylinositol 3-kinase/protein kinase b signaling pathway in 20-day-old sertoli cells independently of igf-i. *J. Endocrinol.* 180(2):257–65

Meyer-Siegler K, Mauro DJ, Seal G, Wurzer J, deRiel JK, Sirover MA. 1991. A human nuclear uracil dna glycosylase is the 37-kda subunit of glyceraldehyde-3-phosphate dehydrogenase. *Proc. Natl. Acad. Sci. U. S. A.* 88(19):8460–64

Mi H, Lazareva-Ulitsky B, Loo R, Kejariwal A, Vandergriff J, et al. 2005. The panther database of protein families, subfamilies, functions and pathways. *Nucleic Acids Res.* 33(Database issue):D284–8

Mi H, Muruganujan A, Thomas PD. 2013. Panther in 2013: modeling the evolution of gene function, and other gene attributes, in the context of phylogenetic trees. *Nucleic Acids Res.* 41(Database issue):D377–86

Miyoshi T, Takeuchi A, Siomi H, Siomi MC. 2010. A direct role for hsp90 in pre-risc formation in drosophila. *Nat. Struct. Mol. Biol.* 17(8):1024–26

Morais da Silva S, Hacker A, Harley V, Goodfellow P, Swain A, Lovell-Badge R. 1996. Sox9 expression during gonadal development implies a conserved role for the gene in testis differentiation in mammals and birds. *Nat. Genet.* 14:62–68

Moser JJ, Fritzler MJ. 2010. Cytoplasmic ribonucleoprotein (rnp) bodies and their relationship to gw/p bodies. *Int. J. Biochem. Cell Biol.* 42(6):828–43

Nagy E, Henics T, Eckert M, Miseta A, Lightowlers RN, Kellermayer M. 2000. Identification of the nad(+)-binding fold of glyceraldehyde-3-phosphate dehydrogenase as a novel rna-binding domain. *Biochem. Biophys. Res. Commun.* 275(2):253–60

Nagy E, Rigby W. 1995. Glyceraldehyde-3-phosphate dehydrogenase selectively binds au-rich rna in the nad-binding region (rossmann fold).pdf. *J. Biol. Chem.* 270:2755–63

Nakanishi Y, Shiratsuchi A. 2004. Phagocytic removal of apoptotic spermatogenic cells by sertoli cells: mechanisms and consequences. *Biol. Pharm. Bull.* 27(1):13–16

Nef S, Verma-Kurvari S, Merenmies J, Vassalli J-D, Efstratiadis A, et al. 2003. Testis determination requires insulin receptor family function in mice. *Nature*. 426(6964):291–95

Nehar D, Mauduit C, Boussouar F, Benahmed M. 1998. Interleukin 1-alpha stimulates lactate dehydrogenase a expression and lactate production in cultured porcine sertoli cells. *Biol. Reprod.* 59(6):1425–32

Nuttall FQ, Gannon MC. 1993. Allosteric regulation of glycogen synthase in liver. a physiological dilemma. *J. Biol. Chem.* 268(18):13286–90

Oliveira PF, Alves MG, Rato L, Laurentino S, Silva J, et al. 2012. Effect of insulin deprivation on metabolism and metabolism-associated gene transcript levels of in vitro cultured human sertoli cells. *Biochim. Biophys. Acta*. 1820(2):84–89

Oliveira PF, Alves MG, Rato L, Silva J, Sá R, et al. 2011. Influence of 5α-dihydrotestosterone and 17β-estradiol on human sertoli cells metabolism. *Int. J. Androl.* 34(6 Pt 2):e612–20

Oonk RB, Jansen R, Grootegoed JA. 1989. Differential effects of follicle-stimulating hormone, insulin, and insulin-like growth factor i on hexose uptake and lactate production by rat sertoli cells. *J. Cell. Physiol.* 139(1):210–18

Oreña SJ, Torchia a J, Garofalo RS. 2000. Inhibition of glycogen-synthase kinase 3 stimulates glycogen synthase and glucose transport by distinct mechanisms in 3t3-l1 adipocytes. *J. Biol. Chem.* 275(21):15765–72

Ortiz-Zapater E, Pineda D, Martínez-Bosch N, Fernández-Miranda G, Iglesias M, et al. 2012. Key contribution of cpeb4-mediated translational control to cancer progression. *Nat. Med.* 18(1):83–90

Palm DC, Rohwer JM, Hofmeyr J-HS. 2013. Regulation of glycogen synthase from mammalian skeletal muscle--a unifying view of allosteric and covalent regulation. *FEBS J.* 280(1):2–27

Papaioannou MD, Pitetti J-L, Ro S, Park C, Aubry F, et al. 2009. Sertoli cell dicer is essential for spermatogenesis in mice. *Dev. Biol.* 326(1):250–59

Pare J, Tahbaz N, López-Orozco J, Lapointe P, Lasko P, Hobman TC. 2009. Hsp90 regulates the function of argonaute 2 and its recruitment to stress granules and p-bodies. *Mol. Biol. Cell.* 20:3273–84

Perucho M, Salas J, Salas ML. 1977. Identification of the mammalian dna-binding protein p8 as glyceraldehyde-3-phosphate dehydrogenase. *Eur. J. Biochem.* 81(3):557–62

Pioli P a, Hamilton BJ, Connolly JE, Brewer G, Rigby WFC. 2002. Lactate dehydrogenase is an au-rich element-binding protein that directly interacts with auf1. *J. Biol. Chem.* 277(38):35738–45

Poulter L, Ang S-G, Gibson B, Williams D, Holmes C, et al. 1988. Analysis of the in vivo phosphorylation state of rabbit skeletal muscle glycogen synthase by fast-atom-bombardment mass spectrometry. *Eur. J. Biochem.* 175:497–510

Prats C, Cadefau J a, Cussó R, Qvortrup K, Nielsen JN, et al. 2005. Phosphorylation-dependent translocation of glycogen synthase to a novel structure during glycogen resynthesis. *J. Biol. Chem.* 280(24):23165–72

Printen JA, Brady MJ, Saltiel AR. 1997. Ptg, a protein phosphatase 1-binding protein with a role in glycogen metabolism. *Science.* 275(5305):1475–78

Raoof NT, Pearson RM, Turner P. 1989. Lithium inhibits human sperm motility in vitro. *Br. J. Clin. Pharmacol.* 28(6):715–17

Rato L, Alves MG, Socorro S, Carvalho RA, Cavaco JE, Oliveira PF. 2012a. Metabolic modulation induced by oestradiol and dht in immature rat sertoli cells cultured in vitro. *Biosci. Rep.* 32(1):61–69

Rato L, Alves MG, Socorro S, Duarte AI, Cavaco JE, Oliveira PF. 2012b. Metabolic regulation is important for spermatogenesis. *Nat. Rev. Urol.* 9(6):330–38

Rentzsch F, Hobmayer B, Holstein TW. 2005. Glycogen synthase kinase 3 has a proapoptotic function in hydra gametogenesis. *Dev. Biol.* 278(1):1–12

Riera MF, Galardo MN, Pellizzari EH, Meroni SB, Cigorraga SB. 2009. Molecular mechanisms involved in sertoli cell adaptation to glucose deprivation. *Am. J. Physiol. Endocrinol. Metab.* 297(4):E907–14

Roach PJ. 1990. Control of glycogen synthase by hierarchal protein phosphorylation. *FASEB J.* 4(12):2961–68

Robinson R, Fritz IB. 1981. Metabolsim of glucose by sertoli in culture. *Biol. Reprod.* 24:1032–41

Rossell D, Guerra R, Scott C. 2008. Semi-parametric differential expression analysis via partial mixture estimation. *Stat. Appl. Genet. Mol. Biol.* 7(1):Article15

Rüdel S, Flatley A, Weinmann L, Kremmer E, Meister G. 2008. A multifunctional human argonaute2-specific monoclonal antibody. *RNA.* 14(6):1244–53

Russell L. 1977. Movement of spermatocytes from the basal to the adluminal compartment of the rat testis. *Am. J. Anat.* 148(3):313–28

Russell LD, Ren HP, Sinha Hikim I, Schulze W, Sinha Hikim AP. 1990. A comparative study in twelve mammalian species of volume densities, volumes, and numerical densities of selected testis components, emphasizing those related to the sertoli cell. *Am. J. Anat.* 188(1):21–30

Ryazanov AG. 1985. Glyceraldehyde-3-phosphate dehydrogenase is one of the three major rna-binding proteins of rabbit reticulocytes. . 192(1):1–4

Ryves WJ, Harwood AJ. 2001. Lithium inhibits glycogen synthase kinase-3 by competition for magnesium. *Biochem. Biophys. Res. Commun.* 725:720–25

Schmahl J, Capel B. 2003. Cell proliferation is necessary for the determination of male fate in the gonad. *Dev. Biol.* 258(2):264–76

Schteingart HF, Meroni SB, Cánepa DF, Pellizzari EH, Cigorraga SB. 1999. Effects of basic fibroblast growth factor and nerve growth factor on lactate production, gamma-glutamyl transpeptidase and aromatase activities in cultured sertoli cells. *Eur. J. Endocrinol.* 141(5):539–45

Seilicovich a, Pérez Lloret a. 1973. Glycogen and related enzymes in normal and cryptorchid human testes: a cytochemical study. *J. Reprod. Fertil.* 33(3):379–83

Setchell BP. 2004. Hormones: what the testis really sees. *Reprod. Fertil. Dev.* 16(5):535–45

Sharpe RM, McKinnell C, Kivlin C, Fisher JS. 2003. Proliferation and functional maturation of sertoli cells, and their relevance to disorders of testis function in adulthood. *Reproduction*. 125(6):769–84

Shetty S, Muniyappa H, Halady PKS, Idell S. 2004. Regulation of urokinase receptor expression by phosphoglycerate kinase. *Am. J. Respir. Cell Mol. Biol.* 31(1):100–106

Shih JD, Waks Z, Kedersha N, Silver P a. 2011. Visualization of single mrnas reveals temporal association of proteins with microrna-regulated mrna. *Nucleic Acids Res.* 39(17):7740–49

Shulman RG, Bloch G, Rothman DL. 1995. In vivo regulation of muscle glycogen synthase and the control of glycogen synthesis. *Proc. Natl. Acad. Sci. U. S. A.* 92(19):8535–42

Singh R, Green MR. 1993. Sequence-specific binding of transfer rna by glyceraldehyde-3-phosphate dehydrogenase. *Science (80-.).* 259:365–68

Singh S, Singh PK, Bhadauriya P, Ganesh S. 2012. Lafora disease e3 ubiquitin ligase malin is recruited to the processing bodies and regulates the microrna-mediated gene silencing process via the decapping enzyme dcp1a. *RNA Biol.* 9(12):1440–49

Skurat A V, Wang Y, Roach PJ. 1994. Rabbit skeletal muscle glycogen synthase expressed in cos cells. identification of regulatory phosphorylation sites. *J. Biol. Chem.* 269(41):25534–42

Slaughter GR, Means AR. 1983. Follicle-stimulating hormone activation of glycogen phosphorylase in the sertoli cell-enriched rat testis. *Endocrinology*. 113(4):1476–85

Song Y, Jiang Y, Ying W, Gong Y, Yan Y, et al. 2010. Quantitative proteomic survey of endoplasmic reticulum in mouse liver. *J. Proteome Res.* 9:1195–1202

Sultan Sheriff D. 1984. Further studies on testicular lipids and glycogen in human patients with unilateral varicocele. *Andrologia.* 16(5):442–45

Tahbaz N, Kolb F a, Zhang H, Jaronczyk K, Filipowicz W, Hobman TC. 2004. Characterization of the interactions between mammalian paz piwi domain proteins and dicer. *EMBO Rep.* 5(2):189–94

Tarulli G, Stanton P, Meachem S. 2012. Is the adult sertoli cell terminally differentiated? *Biol. Reprod.* 87(1):13, 1–11

Thakur SC, Thakur SS, Chaube SK, Singh SP. 2003. Subchronic supplementation of lithium carbonate induces reproductive system toxicity in male rat. *Reprod. Toxicol.* 17(6):683–90

Thomas JA, Schlender KK, Larner J. 1968. A rapid filter paper assay for udpglucose-glycogen glucosyltransferase, including an improved biosynthesis of udp-14c-glucose. *Anal. Biochem.* 25(1):486–99

Thomas PD, Campbell MJ, Kejariwal A, Mi H, Karlak B, et al. 2003. Panther: a library of protein families and subfamilies indexed by function. *Genome Res.* 13(9):2129–41

Tilmann C, Capel B. 1999. Mesonephric cell migration induces testis cord formation and sertoli cell differentiation in the mammalian gonad. *Development.* 126(13):2883–90

Vilchez D, Ros S, Cifuentes D, Pujadas L, Vallès J, et al. 2007. Mechanism suppressing glycogen synthesis in neurons and its demise in progressive myoclonus epilepsy. *Nat. Neurosci.* 10(11):1407–13

Villarroel-Espíndola F, Maldonado R, Mancilla H, Vander Stelt K, Acuña A, et al. 2013. Muscle glycogen synthase isoform is responsible for testicular glycogen synthesis: glycogen overproduction induces apoptosis in male germ cells. *J. Cell. Biochem.* 114:1653–64

Vrielink a, Rüger W, Driessen HP, Freemont PS. 1994. Crystal structure of the dna modifying enzyme beta-glucosyltransferase in the presence and

absence of the substrate uridine diphosphoglucose. *EMBO J.* 13(15):3413–22

Waites GM, Gladwell RT. 1982. Physiological significance of fluid secretion in the testis and blood-testis barrier. *Physiol. Rev.* 62(2):624–71

Wallander ML, Leibold EA, Eisenstein RS. 2006. Molecular control of vertebrate iron homeostasis by iron regulatory proteins. *Biochim. Biophys. Acta.* 1763(7):668–89

Walsh JL, Keith TJ, Knull HR. 1989. Glycolytic enzyme interactions with tubulin and microtubules. *Biochim. Biophys. Acta.* 999(1):64–70

Weber JE, Russell LD, Wong V, Peterson RN. 1983. Three-dimensional reconstruction of a rat stage v sertoli cell: ii. morphometry of sertoli--sertoli and sertoli--germ-cell relationships. *Am. J. Anat.* 167(2):163–79

Wenger RH, Katschinski DM. 2005. The hypoxic testis and post-meiotic expression of pas domain proteins. *Semin. Cell Dev. Biol.* 16(4-5):547–53

Wilson WA, Boyer MP, Davis KD, Burke M, Roach PJ. 2010. The sucellular localization of yeast glycogen synthase is dependent upon glycogen content. *Can J Microbiol.* 56(5):408–20

Worby C a, Gentry MS, Dixon JE. 2008. Malin decreases glycogen accumulation by promoting the degradation of protein targeting to glycogen (ptg). *J. Biol. Chem.* 283(7):4069–76

Xiong W, Wang H, Wu H, Chen Y, Han D. 2009. Apoptotic spermatogenic cells can be energy sources for sertoli cells. *Reproduction.* 137(3):469–79

Younger ST, Corey DR. 2011. Transcriptional gene silencing in mammalian cells by mirna mimics that target gene promoters. *Nucleic Acids Res.* 39(13):5682–91

Zarnescu O, Zamfirescu G. 2006. Effects of lithium carbonate on rat seminiferous tubules: an ultrastructural study. *Int. J. Androl.* 29(6):576–82

Zibrova D, Grempler R, Streicher R, Kauschke SG. 2008. Inhibition of the interaction between protein phosphatase 1 glycogen-targeting subunit and glycogen phosphorylase increases glycogen synthesis in primary rat hepatocytes. *Biochem. J.* 412(2):359–66

Zysk JR, Bushway AA, Whistler RL, Carlton WW. 1974. Temporary sterility in male mice by 5-thio-d-glucose. *J. Reprod. Fertil.*, pp. 69–72